

Engineering Design and Void Characterisation of Thick Composites

A Thesis

submitted to the University of Manchester for the degree of

Master of Philosophy

in the Faculty of Engineering and Physical Sciences

2015

YUAN CHAI

School of Materials

Contents

Contents	2
List of Figures	6
List of Tables	11
Abstract	13
Declaration	13
Copyright	15
Acknowledgements	16
1. Introduction	17
1.1. Background	17
1.2. Aims and Objectives	19
1.3. Structure of Thesis	19
2. Literature Review	21
2.1. Composites	21
2.1.1. Fibre Reinforced Composites	21
2.1.2. Fabrication Methods of Composite Materials	23
2.1.3. Vacuum Assisted Resin Infusion	24
2.2. Voids in Composite Materials	26
2.2.1. Effect of Voids on Mechanical Properties of Composite Materials	26
2.2.2. The Formation of Voids in Liquid Composite Moulding	27
2.2.2.1. Resin Flow	27
2.2.2.2. The Mechanisms of Void Formation	30
2.2.3. Strategies for Void Reduction	36
2.3. Void Characterisation in Composite Materials	38
2.3.1. Void Characterisation by Conventional Techniques	38

2.3.1.1. Density Method	38
2.3.1.2. Microscopy Method (Metallography).....	40
2.3.1.3. Water Absorption.....	42
2.3.2. Void Characterisation by Non-destructive Testing (NDT) techniques.....	44
2.3.2.1. Ultrasonic Test.....	46
2.3.2.2. X-Ray Computed Tomography (CT).....	47
2.4. X-ray CT and its Application in Void Characterisation	48
2.4.1. X-ray Computed Tomography	48
2.4.2. X-ray Absorption Physics	49
2.4.3. Reconstruction	50
2.4.4. Artefacts	51
2.4.5. X-ray CT Study on Voids	54
2.4.5.1. Quantification of Voids	55
2.4.5.2. Morphology and Spatial Distribution of Voids	57
3. Preliminary Study	61
3.1. Introduction.....	61
3.2. Experimental Investigation	61
3.2.1. Manufacturing of Thick Composite Panel	61
3.2.2. X-ray CT testing.....	62
3.3. Results and Discussion	64
3.4. Chapter Summary	66
4. Experimental	67
4.1. Selection of Materials	67
4.1.1. Fabrics	67
4.1.2. Resin System.....	68
4.2. Fabrication of Thick Composite Panels.....	69
4.2.1. Conventional Vacuuming Bagging Resin Infusion Method	69
4.2.1.1. Preparation of the Mould	69
4.2.1.2. Lay-up of the Fabrics.....	70

4.2.1.3. Setting-up the Vacuum Bagging System	70
4.2.1.4. Resin Infusion	72
4.2.1.5. Curing Cycle	74
4.2.1.6. Demoulding and Trimming of the Panel	74
4.2.2. Modified Vacuuming Bagging Resin Infusion Method.....	74
4.2.2.1. Inlet Tube Position in Resin	75
4.2.2.2. Double Meshes	76
4.2.2.3. Double Outlets	77
4.2.3. Overview of the Panels Manufactured.....	79
4.3. Characterisation Techniques.....	80
4.3.1. Specimen Preparation.....	80
4.3.2. Ultrasonic C-Scan	80
4.3.3. X-ray CT	83
4.3.3.1. X-ray System Overview	83
4.3.3.2. Sample Set-up.....	84
4.3.3.3. X-ray CT Machine Set-up and Data Acquisition.....	85
4.3.3.4. X-ray CT Data Reconstruction	87
4.3.3.5. Segmentation and Visualisation of the X-ray CT Data	88
4.3.3.6. Data Analysis Using MATLAB®	92
5. Results and Discussion.....	93
5.1. Voids in Composite Panels.....	93
5.1.1. Effect of Thresholding on the Determination of Voids	93
5.1.2. Morphology of Voids.....	96
5.1.2.1. Spherical Voids.....	96
5.1.2.2. Elongated Voids.....	98
5.1.3. Void Content in the Composite Panels	100
5.1.4. Void Distribution in the Composite Panels.....	101
5.2. Effect of Textile Reinforcement on Composite Panel Quality	110
5.2.1. Effect of the Number of Fabric Layers	110
5.2.2. Effect of Fabric Linear Density.....	111

5.3.	Effect of Modified VARI Methods on Thick Composite Panel Quality	112
5.3.1.	Effect of Top and Bottom Meshes	112
5.3.2.	Effect of Two Outlets.....	114
5.3.3.	Effect of Resin Level in the Inlet Tube.....	117
5.4.	Validation of the CT Results by Ultrasonic C-Scan	118
6.	Conclusions and Future Work Recommendations	121
6.1.	Conclusions.....	121
6.2.	Future Work Recommendations	122
	References	124
	Appendix	130

Word Count: 27166

List of Figures

Figure 2.1: F-22 Raptor. (Courtesy of Boeing Defense).....	22
Figure 2.2: Schematic illustration of VARI process (Goren and Atas, 2008).	25
Figure 2.3: The formation of macroscopic and microscopic voids during resin infusion and their relation to the flow velocity and the Ca. The intersect point corresponds to an optimum Ca with minimum void. (Leclerc and Ruiz, 2008).....	31
Figure 2.4: A typical Macro-void between fibre yarns. (Rudd <i>et al.</i> , 1997).....	32
Figure 2.5: Flow mechanisms for macro-void formation. (Rudd <i>et al.</i> , 1997).....	33
Figure 2.6: A typical micro-void within the fibre yarn. (Rudd <i>et al.</i> , 1997).....	34
Figure 2.7: Schematic diagram of the resin flow front shape causing micro-voids. (Rudd <i>et al.</i> , 1997)	35
Figure 2.8: The in-mould pressure sensor placed through the vacuum bag (Leonard, 2008).	36
Figure 2.9: C-scan images for different plates with voids. (Kas and Kaynak, 2005)	47
Figure 2.10: Schematic illustration of X-ray CT technique. (Landis and Keane, 2010)	48
Figure 2.11: Illustration of different X-ray CT acquisition configurations: a. fan beam, b. cone beam, and c. parallel beam (Landis and Keane, 2010).....	49
Figure 2.12: An example of ring artefacts. (Baruchel <i>et al.</i> , 2000)	53
Figure 2.13: An example of centring error with features appearing doubled (Davis and Elliott, 2006; Stock, 1999).	54
Figure 2.14: Demonstration of the selected voids contoured in red. (Nikishkov <i>et al.</i> , 2013)	57

Figure 2.15: X-ray CT slice images of CFRP samples with various porosity (a: ~0 vol%, b: ~0,15%, c: ~0.35 %, d: ~0.9 %, e: ~4.50 %, f: ~10 %) (Kastner <i>et al.</i> , 2010).	58
Figure 2.16: 3-D volume rendering of voids in a CFRP sample (Little <i>et al.</i> , 2009).	59
Figure 2.17: 3D renderings of void content evolution during processing (Centea and Hubert, 2011).	60
Figure 3.1: The sample set-up for the CT scan.	63
Figure 3.2: Typical XY slice images of a) T1 20 layers b) T2 30 layers c) T3 50 layers....	64
Figure 3.3: The difficulty in identifying void regions by differences in grayscale value. (a) XY slice image of T3 with two highlighted lines, (b) grayscale value change along the first line, and (c) grayscale value change along the second line.....	65
Figure 4.1: Schematic diagram of the vacuum bagging system in the VARI method (side view).....	71
Figure 4.2: Schematic diagram of the set-up of the conventional VARI method (top view).	71
Figure 4.3: (a) Schematic diagram of the inlet tube position in conventional VARI method. (b) Schematic diagram of the modified inlet tube position. The tube was cut under the resin surface, so that no air remained in the tube when infusion started.	76
Figure 4.4: Schematic diagram of the modified VARI method with a second layer of mesh under the bottom peel ply.....	77
Figure 4.5: Schematic diagram of the modified VARI method with a second resin outlet positioned symmetrically to the first outlet.....	78
Figure 4.6: Image of a full panel with markers labelling the cutting guidelines. The full panel was cut into 9 small squares using a diamond saw. The cutting wheel was 2.5mm thick, so the panel cannot be perfectly recovered after cutting.	80

Figure 4.7: Schematic diagram of ultrasonic B- and C-scans of an internal defect. (Geier, 1994)	81
Figure 4.8: The sample set-up for ultrasonic C-scan testing.....	82
Figure 4.9: Schematic diagram of the moving route of the probe in ultrasonic C-scan. The grid size and index step are defined as the width and height of the grid, respectively.	83
Figure 4.10: The Nikon XT H 225 X-ray CT imaging system. The source, sample stage and detector are highlighted.....	84
Figure 4.11: Schematic diagram of the sample set-up for the CT scan. A stack of specimens were scanned at one time. Blu-Tack™ was used between the specimens, holding them stable during the scan. A piece of tacky tape was used as the marker to identify the specimens in the CT data.	85
Figure 4.12: Schematic diagram of the scan set-up to make sure the sample is in the field of view during the scan. The source-sample and sample-detector distance are limited by the sample size.	86
Figure 4.13: A typical previewed cross-sectional slice image of the sample. (a) before beam hardening correction and the line profile, and (b) after beam hardening correction and the line profile.	87
Figure 4.14: Schematic diagram showing the axes of specimens in the reconstructed CT data. The X direction points to the top surface of the panel.	88
Figure 4.15: A typical slice image (a) before filtering, and (b) after smoothing using the anisotropic diffusion filter.....	90
Figure 4.16: Histogram of a typical X-ray CT volume, with three peaks representing voids, composite material and Blu-Tack™, respectively.	91
Figure 5.1: A typical XY slice image of the composite specimen with voids. The void region	

is segmented using three different threshold ranges and highlighted in red. The grey value range is (a) 0 to 12, (b) 0 to 15 and (c) 0 to 18, respectively.	93
Figure 5.2: Extracted volume of the typical segmented voids. One spherical void is highlighted in blue, and the other surrounding voids are shown in red. Views of (a) XY, (b) XZ, and (c) YZ planes are shown.	98
Figure 5.3: XY view of extracted volumes of the typical segmented voids. The elongated voids are highlighted in red, lying in (a) the Y direction, (b) the Z direction and (c) at 45 ° to the Y direction.....	99
Figure 5.4: The YZ view porosity map of sample A.	102
Figure 5.5: The YZ view porosity map of sample B.	103
Figure 5.6: The YZ view porosity map of sample C.	104
Figure 5.7: The YZ view porosity map of sample D.	105
Figure 5.8: The YZ view porosity map of sample E.....	106
Figure 5.9: The YZ view porosity map of sample F.....	107
Figure 5.10: The YZ view porosity map of sample G.	108
Figure 5.11: The YZ view porosity map of sample H.	109
Figure 5.12: XZ view porosity maps of part 8 in (a) sample A and (b) sample B, showing the void distribution through the panel thickness. Meshes are demonstrated as the orange layer on the sample surfaces.	114
Figure 5.13: The image of the panel and the outlet tubes in the infusion stage. Air bubbles came out of the two outlet tubes simultaneously.	116
Figure 5.14: Ultrasonic C-scan images of three specimens from sample F and the colour spectrum of the dB losses. The set range is 20-105dB.	118

Figure 5.15: The projected porosity map calculated based on segmented X-ray CT volumes.
The number of void voxels is displayed in different colours.....119

List of Tables

Table 2.1: The application of NDT techniques to examine various defects in composite materials. (Adapted from Baker <i>et al.</i> (2015)).....	44
Table 2.2: Comparison of different methods for void content measurement. X-ray CT is a non-destructive technique and seems to possess the highest accuracy. (Kastner <i>et al.</i> , 2010)	56
Table 2.3: Comparison of microscopy-based and CT scan-based measurements for the voids in a unidirectional Carbon/Epoxy specimen. (Nikishkov <i>et al.</i> , 2013).....	57
Table 3.1: List of panels manufactured.....	62
Table 3.2: X-ray CT scanning parameters of the panels.....	63
Table 4.1: Properties of Araldite® LY 564 epoxy resin and Aradur® 3486 hardener from datasheet.....	69
Table 4.2: Parameters used for calculating the amount of the resin system.	73
Table 4.3: Summary of the panels manufactured using different processing parameters (in red).	79
Table 4.4: Scanning parameters of the downsized aramid fibre-epoxy composite panels.	86
Table 5.1: Void content of the composite panels measured using the CT data.	100
Table 5.2: Properties of samples for the study of the effect of the number of fabric layers.	110
Table 5.3: Properties of samples for the study of the effect of fabric properties.....	111
Table 5.4: Properties of samples for the study of the effect of additional mesh.....	113
Table 5.5: Properties of samples for the study of the effect of additional outlet.	115

Table 5.6: Properties of samples for the study of the effect of cutting the inlet tube in resin.

.....117

Abstract

The University of Manchester

Yuan Chai

Master of Philosophy

Engineering Design and Void Characterisation of Thick Composites

April, 2015

Voids are defects that are difficult to completely eliminate during the manufacturing process of composite materials. With the increase of void content (i.e. porosity), the mechanical properties and service life of the composite materials will be significantly affected. It is thus of vital importance to improve the quality of composite materials and avoid the formation of voids. In this project, military-use Twaron[®]-epoxy thick composite panels have been manufactured and non-destructive testing (NDT) techniques have been used to assess the voids in the panels. Three modification suggestions to the vacuum assisted resin infusion (VARI) composite fabrication method have been proposed in order to improve the quality of the composite panels.

X-ray computed tomography (CT) has been employed to assess the voids in composite panels, which enables the void content, the morphology and distribution of the voids to be examined in three dimensional views. The void content is found in a range from 0.39% to 1.75% in different composite panels. In composite panels with different thickness, the results show that the porosity increases with an increasing number of fabric layers. Moreover, the threading density and the linear density of the yarns used to weave the fabrics are shown to affect the impregnation process. The void content in the composite panels consisting of coarse fabrics is less than that in the panel made of fine fabrics. Ultrasonic C-scan is also used in this research to study the void distribution from a qualitative perspective, showing a good agreement with the X-ray CT results.

The effect of three modifications to the VARI method has been studied. Firstly, cutting the resin inlet tube under the resin surface can effectively eliminate the air remaining in the tube and reduce the air drawn into the vacuum bagging system, and this will reduce the voidage from 1.62% to 0.91%. Moreover, double meshes have been used as the resin flow media in the infusion process, which can enhance the through-thickness resin flow. Compared with the panel made by the conventional VARI method, the voids are fewer and more localised in the panel made with double meshes. In addition, a second outlet has been used, which can alleviate the non-homogenous expulsion of voids and can avoid air being accumulated and trapped in the fabric. It has been observed that the quality in the central part of the panel has been improved using symmetrical outlets.

In this research, the non-destructive characterisation capability of X-ray CT has been confirmed and the voids in the composite materials have been visualised in three dimensions. Based on the investigation into the distribution of voids in the composite panel and the formation mechanisms involved, the idea of modifying manufacturing techniques has been proposed to improve the quality of composite materials. The three-dimensional visualisation of the size, shape and distribution of voids can provide useful information for the modelling and numerical studies of void formation and highlights the effect of voids on mechanical properties.

Declaration

I declare that no portion of the work referred to in the thesis has been submitted in support of an application for another degree or qualification of this or any other university or other institute of learning.

Copyright

- i.** The author of this thesis (including any appendices and/or schedules to this thesis) owns certain copyright or related rights in it (the “Copyright”) and s/he has given The University of Manchester certain rights to use such Copyright, including for administrative purposes.
- ii.** Copies of this thesis, either in full or in extracts and whether in hard or electronic copy, may be made **only** in accordance with the Copyright, Designs and Patents Act 1988 (as amended) and regulations issued under it or, where appropriate, in accordance with licensing agreements which the University has from time to time. This page must form part of any such copies made.
- iii.** The ownership of certain Copyright, patents, designs, trade marks and other intellectual property (the “Intellectual Property”) and any reproductions of copyright works in the thesis, for example graphs and tables (“Reproductions”), which may be described in this thesis, may not be owned by the author and may be owned by third parties. Such Intellectual Property and Reproductions cannot and must not be made available for use without the prior written permission of the owner(s) of the relevant Intellectual Property and/or Reproductions.
- iv.** Further information on the conditions under which disclosure, publication and commercialisation of this thesis, the Copyright and any Intellectual Property and/or Reproductions described in it may take place is available in the University IP Policy (see <http://documents.manchester.ac.uk/DocuInfo.aspx?DocID=487>), in any relevant Thesis restriction declarations deposited in the University Library, The University Library’s regulations (see <http://www.manchester.ac.uk/library/aboutus/regulations>) and in The University’s policy on presentation of Theses.

Acknowledgements

I would like to express my gratitude to all the people who have helped me in any way in this project.

Firstly, I would like to sincerely express my gratitude to my supervisor Dr. Xiaogang Chen and it is my privilege to work with him. His immense knowledge, support and encouragement motivated me throughout this project.

I am truly grateful to Dr. Sree Shankhachur Roy, Mayank Gautam, Edward Godwin based at the Northwest Composites Centre in the University of Manchester. Particularly I would like to extend special thanks to Dr. Alan Nesbitt, who gave me invaluable advice on how to manufacture high-quality composites.

Particular thanks to Dr. Fabien Léonard, Dr. Julia Behnsen, Dr. Tristan Lowe and Dr. Sam McDonald based at the Henry Moseley X-ray Imaging Facility in the University of Manchester for their expert advice and assistance on CT imaging. I would like to express my special thanks to Prof. Philip Withers who provided the X-ray facilities and imaging analysis workstation for my research.

My deepest appreciation and thanks to my friends and colleagues, especially Shengnan Min and Dr. Yanyan Chu, who have made valuable suggestions through my entire study, the discussion with them inspired me a lot. In addition, the help in programming from Haibo Ni and Xun Zhang is deeply appreciated. Special thanks to Ying Wang for her support and help at all times.

Last but not the least, my gratitude to my parents for their unceasing encouragement, support and care is beyond my words. They have taught me to have faith and determination in whatever I do. This thesis would not have been possible without their support.

1. Introduction

1.1. Background

Advanced composite materials have been extensively used in military equipment, aerospace and the aircraft industry because of their remarkable mechanical properties, high designability, lightweight and fatigue resistance. As composite materials are applied to more fields, the market demand is expanding, thus it is of great interest to reduce manufacturing cost and improve quality.

High quality composite components should have high fibre volume fraction, uniform consolidation, low residual stress and low void content, and in these materials defects such as buckling should be avoided. Any unexpected internal defects will affect the properties of the composite material, and bring uncertainty to the service life and safety of the components. Therefore, the causes of defects and the solutions aimed at reducing defects have received great attention.

Void content is an important index character to assess the quality of composite materials (Nikishkov *et al.*, 2013; Little *et al.*, 2009). Many studies have suggested that porosity will significantly affect the mechanical properties of composite materials. For example, the interlaminar shear property of composites will decrease by 5-15% with a 1% increase in void content (Ghiorse, 1991; Bowles and Frimpong, 1992). Many analytical and numerical models have been established to study the resin infusion process, but the void content and distribution are difficult to predict because of the complexity of the composite materials.

Over the last few decades, non-destructive testing (NDT) techniques have been employed to characterise the internal defects without damaging the composite materials. Ultrasonic C-scan is frequently used to assess voids in composite parts, but there is no standardised procedures to characterise different composite materials which makes the results differ when they are measured in different facilities for the same sample. In addition, it is required that the composite materials used in the aerospace and aircraft industries should have their void content less than 2-2.5% for safety reasons (Schnars and Henrich, 2006). The small void

content is difficult to measure precisely using conventional techniques. Recently, X-ray computed tomography (CT), a promising 3-D NDT technique, has been increasingly used to characterise internal defects and damage in carbon fibre and glass fibre reinforced composites.

The quality control of the raw materials of composites is essential to ensure the quality of composite materials, whilst the quality control of the processing techniques is vital to manufacture reliable composite components. The manufacturing of polymeric composite components is a complicated process in which the materials and the components are fabricated and moulded simultaneously, thus many factors will affect the quality of the composites especially for the void content.

The vacuum assisted resin infusion (VARI) method, one of the liquid moulding techniques, is a frequently used manufacturing method to fabricate polymeric matrix composites. The VARI method has the advantages of low manufacturing cost and excellent properties of the products, and it can be adapted to manufacture large and complex structures. In the VARI method, fabrics are impregnated with resin flow aided by vacuum and then the fully infused panel is cured into composite parts. The quality of the manufacturing process is dependent on the conditions of the raw materials, the conditions of the machines, humidity, temperature and pressure, making the precise control of all the factors far more difficult.

In this project, a military-use Twaron[®] fibre/epoxy composite system is chosen as the material. Considering all the aspects mentioned above, this project is aimed to use NDT techniques to characterise the voids in composite panels manufactured using the VARI method. Furthermore, based on the characterisation results and the understanding of the formation mechanisms of voids, modifications will be proposed to the conventional processing techniques in the VARI method in order to obtain high quality composite panels.

1.2. Aims and Objectives

Aims

- Understand the manufacturing process of thick composites.
- Understand the void distribution in thick aramid fibre reinforced composite panels made using the VARI method.
- Improve the quality of the composite panels by reducing the void content.

Objectives

1. Characterisation of the void content and distribution in composite panels using X-ray CT.
2. Compare the void distribution obtained using ultrasonic C-scan with X-ray CT data.
3. Study the effect of variation in panel thickness and fabric type on void distribution.
4. Propose modifications on the VARI method to reduce voids.
5. Study the effect of the modifications on void distribution.

1.3. Structure of Thesis

Chapter 2 reviews the manufacturing methods of composite materials and the causes and mechanism of void formation in the manufacturing process. The influence of voids on the properties of composite materials and the methods for reducing voids are discussed. This chapter also discusses methods to characterise and analyse voids. Other than destructive methods, NDT techniques including X-ray CT and ultrasonic C-scan and their application to assess voids are reviewed.

Chapter 3 presents the preliminary studies at the initial stage of the project, including the manufacturing and characterization of the first three panels, the preliminary analysis of void

distribution.

The experimental methods used in this project are presented in Chapter 4 in three aspects, including the experimental design (materials and comparison groups), the manufacturing of panels, and the assessment of voids in three-dimensions. The details of the processing parameters of the samples and the design of several comparison experiments are presented. Furthermore, the manufacturing process of Twaron-epoxy composite panels by the VARI method, and the modified VARI methods aiming to improve the quality of the composite panels are presented. Finally, the characterisation techniques and the methods used to analyse voids are also discussed in detail.

Chapter 5 discusses the experimental results obtained for the void content and void distribution, and the samples are grouped for comparing different processing parameters and techniques. Based on the void distribution in the samples and the study of void formation mechanisms, the effect of the structure and properties of the reinforcement on the formation of voids and the effect of the modifications made to the conventional manufacturing process are discussed.

Chapter 6 presents the main conclusions drawn from the studies in this project and the future recommendations are proposed based on the experience and findings in this process.

2. Literature Review

2.1. Composites

Over the last few decades, the field of composite materials has been rapidly evolving and with their unique properties composite materials are replacing conventional materials in a variety of cutting-edge fields, such as aerospace, aircraft, medical and military applications, and they have also been widely used in civil engineering, transportation and sports (Gloria *et al.*, 2010; Gay, 2014). The capability of manufacturing composites is considered as an important factor reflecting the high technology level of a country (Hahn and Tsai, 1980).

2.1.1. Fibre Reinforced Composites

Among various composite materials, fibre reinforced composites (FRC) are most extensively and intensively used. Fibre reinforced composite material is termed as a type of material with high strength fibres dispersed in matrix material (Hull and Clyne, 1996).

In the automotive industry, FRC materials are gradually taking over from metallic materials. They have been applied to load bearing structures, such as leaf spring and drive shaft, because of their relatively light weight and high strength. In addition, due to their high-temperature resistance and high energy absorption capability, FRCs are considered ideal materials for automotive bonnets and bumpers. The adaption of FRC materials, with better mechanical properties than steels and alloys, can reduce the weight of an automotive body by 40 to 60%. For a given kinetic energy, the energy transfer efficiency and the performance of the automobile can be improved, which leads to a breakthrough in making full use of the kinetic energy. In addition, FRCs are playing an important role in the safety systems in cars. The tensile strength of FRC materials is generally above 3500MPa, about 7 to 9 times that of steel. Although the strength along the fibre direction is much higher than the transverse direction due to the anisotropy in material properties, FRCs can meet the demands in safety performance with lighter-weight structures. Other than the ability to withstand temperatures higher than 2000°C, FRCs, especially carbon fibre reinforced composite materials, are far more resistant to corrosion and radiation. Moreover, lubricant,

which is troublesome to deal with in the use of metals, is not required when using FRC materials.

Due to the particular advantage of composite materials in weight reduction and ease of moulding, the use of composite materials in the aircraft industry has also dramatically increased. For example, 23% by weight of the materials used in the Airbus A380 are composite materials, and the usage of composite materials in the Boeing 787 is 50%. The weight fraction of composite parts in the fourth generation of military aircraft is 27 to 28%. Particularly, in the F-22 Raptor as seen in Figure 2.1, 25% of the materials used are fibre reinforced composite materials (Mouritz, 2012).



Figure 2.1: F-22 Raptor. (Courtesy of Boeing Defense)

In addition to the advantages stated above, the manufacturing cost of structures made from FRC materials is far less than that of conventional materials, although the cost of fabricating fabrics is higher than that of metals (Rudd *et al.*, 1997). The distinguished ease of moulding FRCs into complex shaped components contributed to the cost reduction. For example 40 to 60% is saved in the manufacturing cost of part tooling for FRC components (Long, 2005).

2.1.2. Fabrication Methods of Composite Materials

Compared with the fabrication of polymers and metals, the manufacture of composite materials and components have the following features.

- The fabrication of the composite materials and the manufacture of the composite components are completed simultaneously.
- Constituent materials with different properties, processing characteristics and cost can be used to manufacture composite materials.
- The properties and geometry of composite components are directly affected by the processing procedures. In this case, in order to manufacture qualified composites with limited cost, the moulding technique and process route should be determined as early as possible.

Once the processing route is determined, not only the geometry and properties of the composite are set, but also the production efficiency and cost are affected, so it is of vital importance to choose appropriate manufacturing methods according to the expected features of the composite parts.

The manufacturing process for composite materials can be generally categorised into open moulding, closed moulding and continuous moulding (e.g. pultrusion). In recent years, liquid composite moulding (LCM), in a closed moulding process, is one of the most widely used manufacturing techniques in the aerospace and military industries. The difference between LCM and traditional techniques is that the reinforcement is not wetted before lay-up. For thermosetting resin, liquid resin is injected into the closed mould with the fabrics; for thermoplastic resin, the solid resin in the mould will melt and flow at elevated temperature, wetting the fabrics. The wetting process is followed by curing. Although there are many parameters affecting the LCM process, the design of an LCM manufacturing process generally concerns the fabric lay-up system, the resin transferring system, the mould matching and closing systems and the air and resin flow control system (Stover, 1990).

As a rising advanced composite manufacturing technique, LCM possesses several important features. On one hand, the manufacturing cost is relatively low while the fibre volume fraction of the final composite component is relatively high. On the other hand, a wide range of sizes and shapes of components can be manufactured using LCM. Both large-scaled structural parts and sophisticated minor parts can be fabricated, and it is suitable for mass production of complex shaped components. Typical LCM techniques include resin transfer moulding, resin injection moulding, resin film infusion and vacuum infusion moulding process.

2.1.3. Vacuum Assisted Resin Infusion

The VARI method is a low cost LCM technique, which has gained popularity in the manufacture of high quality composite materials used for wind turbines, ships, aircraft and military applications over the last twenty years (Tzetzis and Hogg, 2008). It is interesting that in research literature VARI is interpreted using various acronyms (Ragondet, 2005), such as VARTM-Vacuum Assisted Resin Transfer Moulding (Koefoed, 2003; Correia *et al.*, 2004), VBRTM-Vacuum Bag Resin Transfer Moulding (Kang *et al.*, 2000), VARIM-Vacuum Assisted Resin Infusion Moulding (Khattab, 2006), SCRIMP™-Seemann Composites Resin Infusion Moulding Process (Boh *et al.*, 2005). In spite of the different terms, the processes in these methods are generally very similar; approaches by which resin is infused into dry fabric preforms.

Figure 2.2 shows the schematic of a VARI process. In the typical VARI process the closed mould is composed of a stiff bottom mould and a flexible vacuum bag. With the aid of vacuum, the air within the reinforcement materials can be expelled. In the resin infusion process, resin flows under the pressure gradient between the inlet and the outlet and wets out the fabrics. Finally the composite is cured under room temperature or elevated temperature.

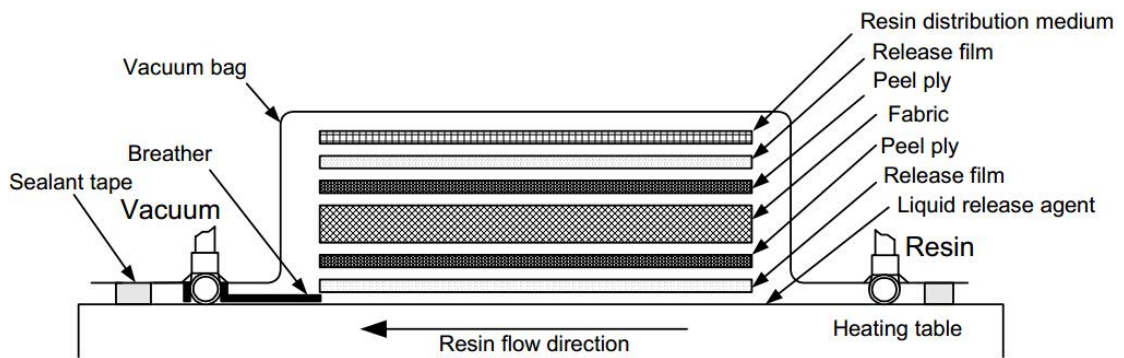


Figure 2.2: Schematic illustration of VARI process (Goren and Atas, 2008).

The VARI method has the following features:

- good flexibility of the mould, which enables a high fibre volume fraction and good product properties;
- good repeatability, which ensures stable product quality;
- easy processing procedures, which is suitable for the manufacture of thick and large sized structures;
- as in the VARI method one solid mould is used, only one surface of the manufactured composite is smooth, which limits the application;
- the thickness of the product is not uniform.

2.2. Voids in Composite Materials

The occurrence of voidage is inevitable in the manufacturing process for composite materials, especially in regions of complex structure, regardless of the types of resin and fibre used or the fibre surface treatment. In this section, the effect of voids on composite properties, the mechanisms in void formation and the methods to reduce voids are discussed.

2.2.1. Effect of Voids on Mechanical Properties of Composite Materials

Over the last few decades, efforts have been made both theoretically and experimentally by many researchers to explain the effect of voids on composite materials from different perspectives. However, the results are generally largely scattered and irreproducible, in which case even for composites having the same void content, the extent of influence of voids on the properties is highly likely to be varied. This is partly due to the inadequate consideration of the shape and distribution of voids, which is not easily observed with conventional characterisation techniques.

Composites are extensively used because of their outstanding mechanical properties, but the existence of voids brings an uncertainty in the real-time performance, which is unacceptable in high-tech applications. It is noted that voids tend to have detrimental influence on the tensile, compressive, shear and flexural strength and also the fatigue life of composite materials (Judd, 1978; Bowles and Frimpong, 1992; de Almeida and Neto, 1994; Goodwin *et al.*, 1997; Chambers *et al.*, 2006; Costa *et al.*, 2001). The interlaminar shear strength of composites is mostly affected by the void content, with a 7% decrease induced by a 1% increase in void content (Goodwin *et al.*, 1997). Moreover, the existence of voids makes the composite more susceptible to water absorption, high temperature and other environmental conditions (Costa *et al.*, 2001). Voids can cause weaker interfaces which resulted from poor adhesion, more abrasion between fibres, and an easier path for crack propagation because of the coalescence of voids (Saidpour, 1991), which are the essential damage mechanisms which downgrade the properties of composite materials.

2.2.2. The Formation of Voids in Liquid Composite Moulding

As composite properties are affected by internal voids, it is essential to reveal the cause of void formation and the distribution of voids in FRP composites with the investigation into the manufacturing techniques, which is of great importance to ascertain the reliability of composite structures and avoid unexpected failure in use. In this project, the VARI method is used to manufacture military-use bullet-proof composite materials and the features and distribution of voids are assessed, and the relations between manufacture processing parameters and voids are investigated.

The development of voids in the moulding process is a complicated area in the studies of composite materials because the manufacturing process of composite materials is associated with issues such as the transfer of heat, momentum and mass, the chemical reactions in the multi-phase system and the time-dependent material properties and boundary conditions. The mechanisms of void formation are similar in all the liquid composite moulding (LCM) manufacturing methods.

2.2.2.1. Resin Flow

In LCM manufacturing processes, the fabric reinforcements are laid in the sealed mould before resin infusion, so resin has to spread all over the mould and fully wet-out the fabric before the resin starts to gel and its viscosity increases. Although the vacuum pump can assist the removal of air from the mould, air-pockets are still common defects found in the composites manufactured by the LCM method, due to the limitation in the vacuum level and the gas produced in the gel process.

In the infusion process where resin flows in the mould, reinforcing fabrics can be treated as anisotropic porous media. In 1856, Henry Darcy proposed the well-known Darcy's law based on experiments on the flow of water through sand (Darcy, 1856). In the liquid moulding manufacturing of composite materials, Darcy's law is regarded as the most important theoretical model for defining the flow of resin in reinforcing fabrics. In this model, it is assumed that the fabric preform is rigid and will not deform when the resin flows.

With factors such as inertia, gravity, surface tension and the capillary effect being unconsidered, he established the following formula,

Equation 2.1

$$Q = K \frac{A \Delta P}{\eta S}$$

where Q (m^3/s) is the volume flow through a constant cross-section of the sample; K (m^2) is the permeability tensor of the fabric preform; A (m^2 , perpendicular to the flow direction) is the cross-sectional area; ΔP (Pa) is the pressure gradient in the flow length of S ; η ($Pa \cdot s$) is the viscosity of the flow; S (mm) is the distance from the flow front.

In his theory, the flow behaviour of Newtonian fluid in porous media has been elaborated. Through a unit area, the flow speed is proportional to the pressure gradient, and the permeability of the reinforcing material is the ratio between them. In Darcy's law, however, the micro-scale fluid mechanics of flow behaviour was not included. Using the macro-scale statistical average method, the interaction between fabric and resin can be associated with permeability, which is a coefficient representing the permeable characteristics of the fabric. Permeability can be used to characterise the level of difficulty for resin to flow through porous fabric, where a higher value indicates a lower resistance when the resin flows through the fabric. The permeability of reinforcing materials is normally anisotropic, and the permeability along each of the three directions of the laminate is different. The permeability unit is the darcy, as

$$1 \text{ darcy} \approx 10^{-12} m^2$$

Darcy's law can be extended to various forms in different dimensions.

For the one dimensional case,

Equation 2.2

$$u_x = \frac{Q}{A} = -\frac{KdP}{\eta dx}$$

For the two dimensional case,

Equation 2.3

$$\begin{bmatrix} u_x \\ u_y \end{bmatrix} = -\frac{1}{\eta} \begin{bmatrix} K_{xx} & K_{xy} \\ K_{yx} & K_{yy} \end{bmatrix} \begin{bmatrix} \frac{\partial P}{\partial x} \\ \frac{\partial P}{\partial y} \end{bmatrix}$$

For the three dimensional case

Equation 2.4

$$\begin{bmatrix} u_x \\ u_y \\ u_z \end{bmatrix} = -\frac{1}{\eta} \begin{bmatrix} K_{xx} & K_{xy} & K_{xz} \\ K_{yx} & K_{yy} & K_{yz} \\ K_{zx} & K_{zy} & K_{zz} \end{bmatrix} \begin{bmatrix} \frac{\partial P}{\partial x} \\ \frac{\partial P}{\partial y} \\ \frac{\partial P}{\partial z} \end{bmatrix}$$

where K (m^2) is the permeability tensor of the fabric preform; u is the velocity of resin flow (m/s); u_x , u_y and u_z are velocity vectors and; $\frac{dp}{dx}$, $\frac{\partial p}{\partial x}$, $\frac{\partial p}{\partial y}$ and $\frac{\partial p}{\partial z}$ are the pressure gradients.

In the LCM manufacturing process, the typical fabric preform is made from fibrous yarns, and each yarn consists of thousands of individual fibres. In recent years, with further investigation into the pore structure of porous media, researchers tend to employ mathematical methods to understand the correlations between permeability and the microscopic structures of porous media by underpinning the physical insights and this leads to more accurate modelling for the geometry of the fibrous yarns. However, theoretical and numerical methods have been limited by the fact that only in fabrics satisfying specific assumptions can the permeability be predicted, while the actual flow conditions in fabrics

with complex structure are far more complicated. Therefore, theoretical models and simulations should be appropriately used when studying the permeability and resin flow in composite manufacturing.

2.2.2.2. The Mechanisms of Void Formation

In resin fusion, the flow modes of resin fall into two types: 1. Macro-flow along the gap between yarns, and 2. Micro-flow between individual fibres. Considering the local resin flow condition, the competing of the two modes of flow can result in two types of voids – macro-voids and micro-voids. Macro-voids are larger voids formed between fibrous yarns, while micro-voids refer to the small voids formed between individual fibres or in the surface cracks of the fibres.

In the mould filling process, the main driving forces for resin flow inside fabric reinforcements are the pressure gradient and the capillary effect (Rudd *et al.*, 1997). In fabric reinforced composites, the pressure gradient mostly determines the wet-through or the flow velocity of the macroscopic front; while capillary pressure and surface tension govern the wet-out or the flow velocity of the microscopic front (inside fibrous yarns). If the two driving forces are different at certain locations in the preform, the manner of resin flow will be directly influenced and the shape of the flow front will change. The variation in the flow speed will result in the advance or delay of resin flow, known as the fingering effect because of the resulting pattern (Gourichon *et al.*, 2006; Gourichon *et al.*, 2008; Kuentzer *et al.*, 2007; Schell *et al.*, 2007).

According to the experimental results by Br éard *et al.* (2003) and Patel and Lee (1996), it is known that the percentage of macro-voids or micro-voids resembles a logarithmic function of the flow rate, and in Figure 2.3 the estimated logarithmic relations have been plotted. In order to understand the influence of viscous force and surface tension in the formation of voids, a dimensionless parameter, capillary number (Ca), has been defined as follows (Leclerc and Ruiz, 2008),

Equation 2.5

$$C_a = \frac{\eta v}{\gamma}$$

where η is the viscosity of the fluid, γ is the surface tension at the air/resin interface and v is the fluid velocity.

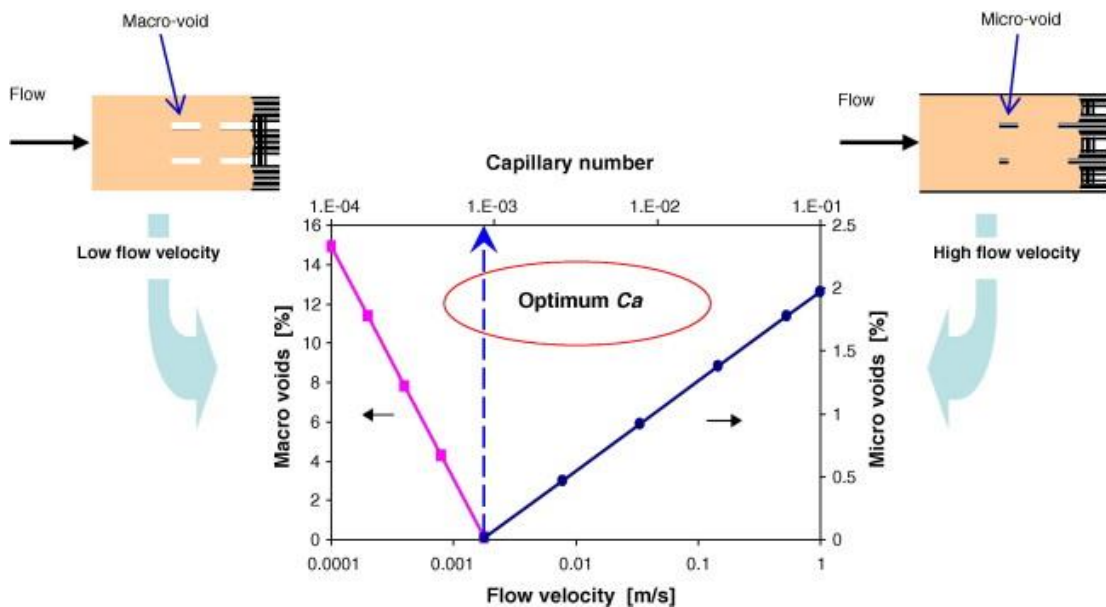


Figure 2.3: The formation of macroscopic and microscopic voids during resin infusion and their relation to the flow velocity and the Ca. The intersect point corresponds to an optimum Ca with minimum void. (Leclerc and Ruiz, 2008)

Consequently, the logarithmic relation between void percentage and Ca can be derived, as shown in Figure 2.3. Leclerc and Ruiz (2008) proposed that at the intersection point of the two lines representing macro- and micro-voids respectively, the Ca and flow velocity for minimum void volume can be obtained. Therefore, the parameters in the manufacturing process, such as resin viscosity, moulding temperature and the resin injection rate, should be tailored so that the Ca or flow velocity can be kept around the optimised value for fewer voids. The two macro- and micro-voids are detailed in the following paragraphs.

Macro-voids

As mentioned previously, when the capillary effect is greater than the pressure force, the flow rate within yarns exceeds that between yarns. This is the main cause of macro-voids as seen in Figure 2.4, and the formation of these large voids is shown in Figure 2.5.

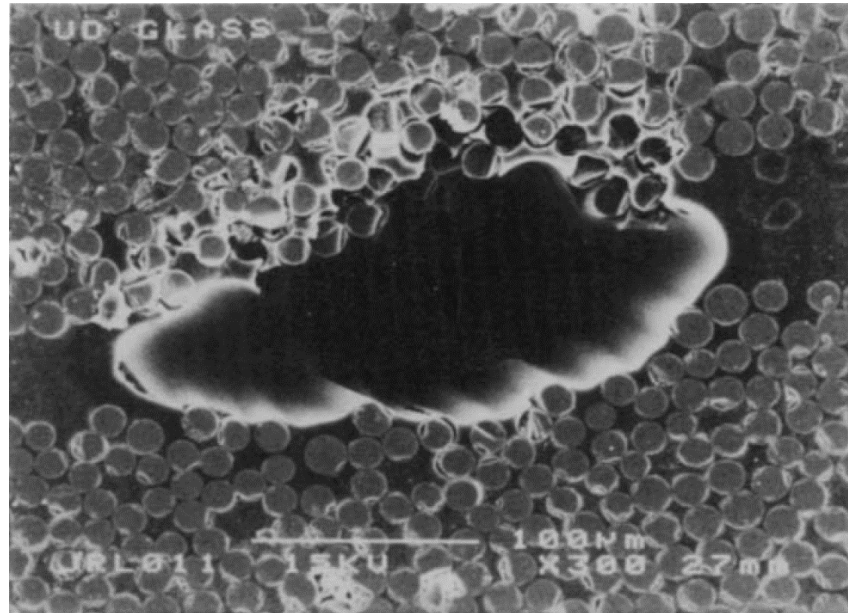


Figure 2.4: A typical Macro-void between fibre yarns. (Rudd *et al.*, 1997)

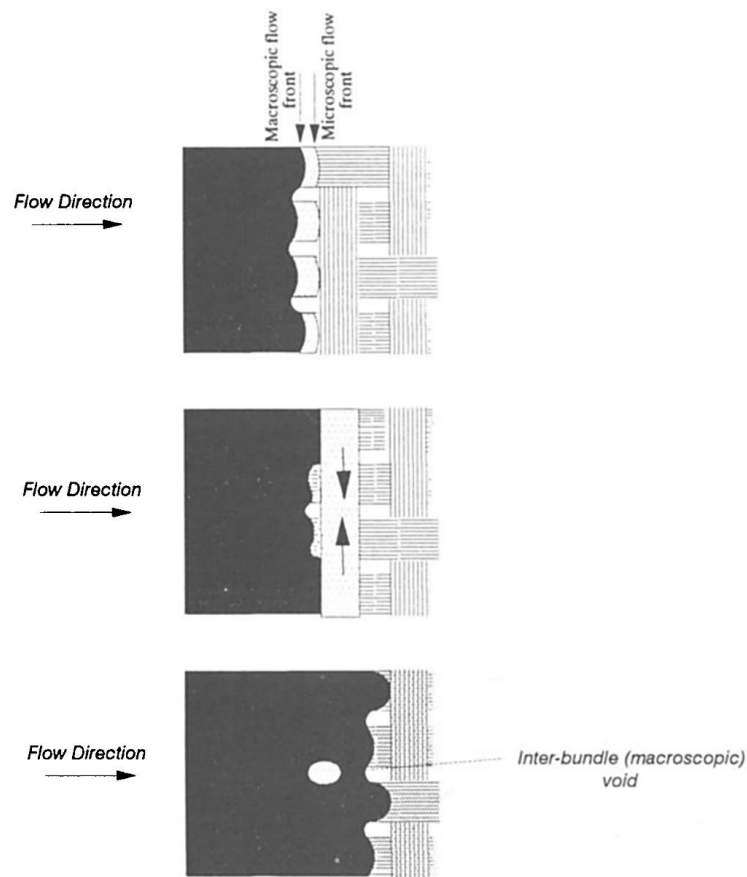


Figure 2.5: Flow mechanisms for macro-void formation. (Rudd *et al.*, 1997)

At a certain temperature, when the injection pressure is relatively low, the capillary effect within fibrous yarns dominates, resulting in the fluid flow front shaped as in Figure 2.5, and the fluid inside the fibre yarns will move into the gap between the fibrous yarns. If the flow front lagging behind between yarns has not arrived at the position where the fluid within the yarns spreads into the gaps between yarns as expected, air tends to be entrapped between the yarns, leading to large cavity.

Macro voids also tend to form between layers of fabrics. Resin flows at different rates in the fibre direction and along the transverse direction, giving rise to variation of in-plane permeability and through-thickness transverse permeability of the fabrics. Usually, the in-plane permeability is greater than the transverse permeability. At the onset of the mould filling process, the resin flows simultaneously in the fibre direction and transversely, but faster in the fibre direction, so the intra-laminar flow front exceeds the inter-laminar advance front. In the region between the two fronts, the resin flows transversely along the thickness

direction at the same time, so it is highly possible to trap air in between layers, and it is similar to the formation of large voids between yarns.

When the injection pressure is determined while the temperature is relatively higher, large voids also tend to form. The main reason is that the mobility of resin becomes higher at elevated temperatures, in which case the viscosity of the resin reduces and the flow accelerates. Under the combined action of injecting pressure and capillary effect, the flow in a small space exceeds the flow in larger gaps. The mechanism of void formation under such circumstance resembles that at a similar temperature but with lower pressure, and the shape of the resin flow front is also similar.

Micro-voids

If the pressure gradient dominates the capillary effect, the resin flow rate between yarns will be high. This is the main cause of the micro-void as shown in Figure 2.6.

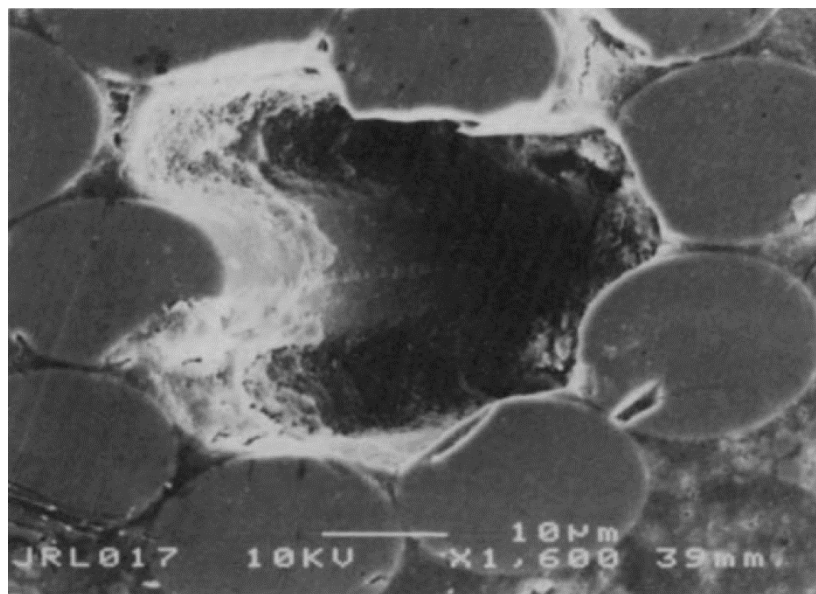


Figure 2.6: A typical micro-void within the fibre yarn. (Rudd *et al.*, 1997)

At a certain temperature, if the injection pressure is relatively high, the capillary effect within yarns is weaker than the effect of the pressure gradient, so resin flow is governed by the pressure difference. Figure 2.7 shows a front shape for such a flow. In this case, the advanced resin flow between yarns will spread into the yarns. If this occurs before the arrival

of the flow front within the yarns, which is left behind, then the air within the yarns in this region will be wrapped by the resin from the gapping channels and will form micro-voids.

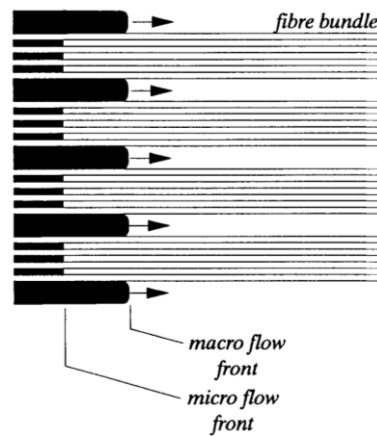


Figure 2.7: Schematic diagram of the resin flow front shape causing micro-voids. (Rudd *et al.*, 1997)

In general, the causes and factors affecting the formation of voids are complicated, and the common factors include:

- entrapped air in the mould (failed to be removed);
- the vapouration mould release agent (organic solution);
- dissolvable gases and vapourising chemicals (the moisture absorbed when stored);
- curing process (volatile organic compounds, injection pressure, environmental parameters);
- properties of the resin (viscosity and surface tension);
- properties of the reinforcements (fibre type, isotropy and surface treatment);
- contact angle between resin and fibres.

In addition, the characteristics of the reinforcement architecture are also key factors influencing the development of voids, as the geometry, structure and lay-up sequence of the reinforcing fabrics may directly induce the formation of voids. In the voids caused by chemical reactions, the moisture emitted from the reaction is a major cause (Shim *et al.*, 1994).

2.2.3. Strategies for Void Reduction

In order to improve the quality of the composites and avoid the formation of voids, some studies have been conducted on making improvements to the VARI method, focussing on the preparation of the resin system and the real-time control of the infusion process.

The resin preparation is an important process in the manufacture of large composite parts, where a large quantity of resin is required. If the epoxy resin and the hardener cannot be uniformly mixed the properties of the resin system will be dramatically reduced. In addition, when mixing a large amount of epoxy resin, much heat will be released from the exothermic reaction, which will result in serious consequence if not properly dealt with. The Princess Yachts Company proposed a solution to this problem (Leonard, 2008). They developed a meter-mixing technology system to automatically mix resin. The system can be connected to the resin containers and automatically mix the resins with the required ratio, which eliminates the problems introduced by human handling.



Figure 2.8: The in-mould pressure sensor placed through the vacuum bag (Leonard, 2008).

The infusion process is another important stage in determining the quality of composites. Leonard (2008) reported a control system with in-mould pressure sensors placed into the vacuum bag at different locations, as shown in Figure 2.8. Thus the local pressure at these points can be derived during the infusion process, facilitating the optimisation of the infusion. Kikuchi *et al.* (1995) and Kosaka *et al.* (2004) also developed similar monitoring systems for the infusion process.

Johnson and Pitchumani (2008) proposed a local heating strategy in the infusion process to aid resin flow in the regions with low permeability due to the non-uniformity of the fabric structure. It should be noted that a balance needs to be made between the reduction of local viscosity and the accelerated increase of overall viscosity due to the heating. Using their technique, void content is reduced in the manufactured composite.

2.3. Void Characterisation in Composite Materials

Composite material is a complex structural system composed of different phases, which provoke a lot of uncertainties, such as in the purchase of raw materials, the fabrication of intermediate materials, and the final stage of the manufacturing process of the composites, so that it is difficult to avoid manufacturing defects and unexpected failure from internal damage. Moreover, advanced composite components are generally used in the aircraft, aerospace and military fields, where reliability and safety are the key factors of an appropriate structural design, so it is of great importance to examine the internal defects and damage in composite materials.

With the employment of scientific and effective testing methods and evaluation system, the properties of the composite components can be accurately and specifically revealed, which is of positive effect on the progress in the manufacture and development of composites. The characteristics of the composite materials can be investigated and evaluated from different aspects using a range of testing and characterisation methods.

2.3.1. Void Characterisation by Conventional Techniques

Some traditional methods are still widely used nowadays for measuring the void content of composite materials. These include the density method, the optical microscopy method and the water absorption method.

2.3.1.1. Density Method

The most basic method to measure the amount of voidage is the density method (ASTM D3171) (Green 1991). In this method, the density of fibre, resin and the composite, and the weight fraction of fibres and resin are determined first, and then the void content can be approximated by the following formula:

Equation 2.6

$$V_v = 100 - \left[\left(m_f * \frac{\rho_c}{\rho_f} \right) + (100 - m_f) * \frac{\rho_c}{\rho_m} \right]$$

where V_v is the void content, m_f is the weight fraction of the fibre, ρ_f is the density of the fibre, ρ_m is the density of the resin and ρ_c is the density of the composite.

To measure the above values, the conventional techniques that are used can be acid digestion or resin burning-off, depending on the properties of the fibre and the resin in the composite material.

Acid digestion

Acid digestion is a destructive method, and is often used to measure the parameters for void content calculation. It is still considered as one of the most widely used and effective methods. Its main procedures are as follows: the polymer matrix will be digested with an acid solution without damaging the fibres, and the fibres which remain will be washed, dried and then weighed. Referring to the original weight of the composite tested together with the fibre and the resin densities, the volume fraction of the fibre and the resin can be calculated. Therefore the volume fraction of voids in the composite sample before testing can be obtained. In this technique, concentrated nitric acid and sulphuric acid are most frequently chosen to dissolve the resin matrix, depending on the fibre type (ASTM D3171).

Resin Burning-off Method

The resin burn-off method is very similar to acid digestion, and is commonly used for glass fibre reinforced composites (Geier, 1994). In this process, the composite will be burned at certain temperature, which will be controlled so that the fibres are kept stable and intact while the resin burns. The remaining fibres will be weighed, and then the void content can be calculated based on these values.

Although the processing technique is different in the above two methods, the final goal is the

same, which is to extract the fibres in the composite in order to obtain the weight for calculation of the void content. These methods, in which void content is computed based on the densities, are achieved by measuring and calculating the volume fraction of voids in a composite sample. The processing techniques and operations required are relatively easy and no expensive instrumentation is needed with these methods, so they have been extensively used in industrial and research areas. However, these methods possess limitations in that the size, shape and distribution of voids cannot be revealed. With regard to the accuracy of measurement, the error resulting from some other inherent defects in the composite materials, and the mass loss from the oxidisation of fibres in the process of removing the polymer matrix will affect the void content measured. Therefore, the accuracy of measurement using these methods is relatively low, with an error no less than 0.5%, which will inhibit the use of these methods in composites with low void content to a certain extent (ISO 1172:2002; ASTM D3171).

2.3.1.2. Microscopy Method (Metallography)

The void content of composite materials can also be determined by examining the cross-section of ground and polished samples. This measurement technique is based on the statistical analysis of microscopic images, and the procedures can be roughly described as follows: firstly samples of the composite material need to be cut off from the component, followed by grinding and polishing the cross-section of the sample potted in cold setting resin. This method is similar to the metallographic inspection and analysis of metal materials. After sample preparation, the cross-section will be examined on an optical microscope under an ocular with narrow grid lines. The images with the best contrast will be captured through adjusting the magnification and brightness difference. Nevertheless, it should be noted that it is very difficult to polish carbon fibre reinforced composite materials, because carbon fibres are brittle and are easy to pull out locally (Geier, 1994).

Manual method

The manual method is to count and analyse the information on images taken using optical

microscopy (NFT 57 109:1979; ISO 7822:1990). Transparent gridded paper can be used in the counting process, and how the observed voids distribute among the fine grids will be recorded accordingly. The grids locating in the void area will be recorded, and for the boundary area the methods of recording are varied, depending on the precision requirement of the measurement. For example, if 1/4 of a grid is considered as the minimum unit area, then the area occupying more than a quarter of a grid is counted as 1/2; the area larger than 1/2 will be recorded as 3/4; and one will be counted for area larger than 3/4 of a grid. The ratio of the total area of voids to the area of the microscopic image is the area void content (Geier, 1994), as given by

Equation 2.7

$$V_v = \frac{n}{N}$$

Where N is the total number of grids in the image, and n is the number of grids with voids. Optical microscopes with higher magnification or finer gridded papers can be employed in order to optimise the results and improve the accuracy of measurement.

Automatic Method

After the development of the manual method, with the advancing of computing techniques, the use of computer software to aid the automatic analysis of information in images and statistical measurement has been realised. In the image processing software Photoshop®, the function of ‘show grid’ can be used to replace the traditional transparent grid paper, and the gap between grid lines and the size of sub-grids can be easily adjusted according to the required precision. The ImageTool software has made the work even easier, relieving operators from counting manually, by using an ‘area’ function. When dragging the mouse along the outline of voids, the area inside the closed outline will be regarded as the area of voids, and the value will be automatically shown in the ‘result’. Thus, the void content is the area of voids divided by the total area. In addition, the measurement can be conducted in

MATLAB[®]. Firstly, the image will be processed into a binary image with only black and white regions, and the pixels having white or black colour will be counted, with the black pixels representing voids. The void content is obtained by dividing the number of black pixels by the total number of pixels in the image. In the process of changing a grey-scale image into a binary image, the choice of threshold will directly affect the detection of the edges of voids, which will affect the measurement of void content. Therefore, it is essential to systematically compare the results obtained using different thresholds before determining the final value to threshold the image. This value should be appropriately chosen based on the actual image in order to get the correct void content.

Generally, using the methods based on microscopic images to measure void content is straightforward to find the type, shape, size and distribution of voids with a relatively high accuracy. However, the void content is an area-based value measured from certain cross-sections and the void content of the 3-D volume can only be obtained using statistical methods, so this method has its limitations and should be used cooperatively with other techniques

2.3.1.3. Water Absorption

The water absorption method, also known as the water take-up method, is a reliable method for porosity measurement (Olster, 1972). The basic principle of this method is to measure the volume of water absorbed by the composite sample when it is saturated after being immersed in water for a certain period of time, thus the void content in the composite material can be derived. It should be noted that the diffusion of water in the bulk matrix resin has been considered, so the first step of this test is to measure the amount of water taken-up by the same resin via diffusion. A resin sample (with the same weight of the resin in the composite sample) without voids is immersed in water, equilibrium will be attained when the water diffusion in the sample is saturated. The surface of the sample should be thoroughly cleaned before weighing, and the difference in weight before and after water take-up is considered to be the water absorbed by the resin sample. During the water absorbing process, if necessary, the water can be heated and kept boiling. Then, the water

absorbed by the composite sample should be tested following the same procedures as testing the resin sample. Thus, the weight difference between water absorbed by the composite sample and that of the resin sample is the amount of water absorbed due to filling the voids. Based on the water absorption in the non-voided resin sample and the composite sample at equilibrium, the porosity can be estimated using the following formula:

Equation 2.8

$$V_v = (W_c - W_r) / (\rho_w V_c)$$

Where V_v is the void content, W_r is the amount of water absorbed by the resin, W_c is the amount of water absorbed by the composite, V_c is the volume of the composite sample, and ρ_w is the density of water.

Using this method, the void volume fraction of the composite component can be derived, but it is still impossible to reveal the local density of voids. The accuracy of measurement by water absorption is similar to that of the density method. Water is mostly employed as the soaking media, but it is not the only choice. The soaking media should possess low viscosity and high fluidity, and it must not react with or dissolve the fibre or the resin, so that the sample can be well wetted. The time to attain equilibrium is varied for different types of resin, and is widely ranged. In some of the studies, the sample was immersed in boiling water for as long as 300 hours, so this method is not as widely used as the density method (Cilley *et al.*, 1974).

The three testing methods described above are traditional methods to measure the porosity in composite materials. Because of the advantages that these methods are easy to perform and no complex equipment is needed, they are still used nowadays to assess the properties of materials or to act as a comparison technique for reference. However, the composite parts will be damaged and not usable after the tests, so the use of these methods in the assessment of defects in the entire component is limited. In practical applications, due to the complexity of the inner structure in composite materials, it is very difficult, costly and even impossible to avoid defects by tailoring the processing techniques. In the meantime, the results derived

from samples of the composite material are often not representative of the macroscopic quality of the composite component. Therefore, it is essential to develop and study the NDT characterisation of defects in composite materials.

2.3.2. Void Characterisation by Non-destructive Testing (NDT) techniques

The use of techniques to characterise the properties and features of materials without damaging the material or influencing the component performance are known as non-destructive testing (NDT) or non-destructive evaluation (NDE) or non-destructive inspection (NDI). It has been extensively and intensively applied in various areas, such as industrial manufacturing and scientific research. It is a credible technique to examine product quality, assure the safety and extend the service life of materials. In the area of composite materials, Table 2.1 lists some examples of frequently used NDT techniques.

Table 2.1: The application of NDT techniques to examine various defects in composite materials. (Adapted from Baker *et al.* (2015))

NDT for FRP Composite	State of Cure	Porosity (Voids)	Moisture	Fibre Orientation	Fibre Debonding	Delamination	Cracking	Global Inspection	Proof Tests	Strain Measurement
Radiography										
White Light										
Coherent Light										
Thermography										
Microwave										
Eddy Current										
Dielectric										
Electric										
Spectroscopy										
Ultrasonics										
Acoustic Emission										
Vibration										

As shown in Table 2.1, the examination by NDT covers many aspects of the properties. They can comprehensively assess the shape, size, location, orientation, distribution and content of voids. Moreover, the examination will not cause any damage to a new component or a used

part for maintenance check. The scope of application and the predominance of each technique is varied, so in real-life applications the technique should be determined according to the requirements of characterisation. Generally speaking, The NDT can be divided into two categories: the qualitative methods and the quantitative methods (Geier, 1994; Centea and Hubert, 2011).

Qualitative tests:

- visual observation and dye penetration;
- photometry;
- ultrasonics (echography, US);
- X-rays, γ -rays and neutron radiography;
- IR (infrared radiation) thermography;
- vibrothermography;
- laser holographic interferometry;
- eddy currents;
- the analysis of light impacts (tapping).

Quantitative tests:

There is a variety of qualitative examination techniques and many of them are similar to the methods detailed in the previous section, whereas these techniques are used correlatively with image processing to derive quantitative information (Birt and Smith, 2004).

- ultrasonics (echography, US);
- X-rays, γ -rays and neutron radiography;
- IR thermography;
- laser interferometry;
- eddy currents;
- microwaves.

Conventional mechanical and physical characterisation techniques lack the capability to

detect the internal defects without damaging the material. Therefore, in the present project, advanced non-destructive scanning techniques, including ultrasonic C-Scan and X-ray CT, have been used to analyse the global distribution and local features of voids.

2.3.2.1. Ultrasonic Test

Ultrasound is the sound wave with a frequency much higher than the range of human hearing that is from 20Hz to 20KHz. Low-frequency ultrasound in the range of 0.2-15MHz can propagate through composite materials (Geier, 1994). Ultrasound needs to be transmitted in media, and at the interface between different media the transmission speed of the ultrasound will change and energy degradation will also occur because of the reflection and transmission phenomena. Therefore, if there are voids or other defects in the composite material, the void content can be estimated according to the change in amplitude and speed of the returned ultrasound wave. The ultrasonic technique has become one of the most widely used NDT methods to inspect composite materials because of the advantages of outstanding penetration capability, directionality, sensitivity and harmlessness to the human body.

Ultrasonic inspection has been extensively applied in the void characterisation in composite materials. Stone and Clarke (1975) investigated the relationship of the porosity in FRC materials with the speed and attenuation of ultrasound. The study on unidirectional composite panels with constant thickness showed that the ultrasonic attenuation is in a bi-linear relationship with the void content. Moreover, it was also found that the interlaminar strength decreased with increasing void content. In the aspect of characterising the void morphology, it was noted that when the porosity was less than 1.5%, the voids were generally sphere shaped with a diameter of 5-20 μ m, which was caused by the volatiles, and the size of the voids will increase with increasing porosity; while when the porosity was more than 1.5%, the entrapped air between layers started to dominate and these voids are flat and elongated along the fibre direction, with a size much larger than that of the voids caused by volatiles.

Kas and Kaynak (2005) used the ultrasonic C-scan technique to investigate the RTM manufacturing process, especially on the influence of injection pressure. Panels manufactured at the injection pressure of 2 atmospheres were found to have the best mechanical properties. The results showed that if the injection pressure was larger than 2 atm, the number of voids (100 to 1000 μm) increased, which reduced the mechanical properties. This could be explained by the change in the flow rates between fibrous yarns and within fibrous yarns. At higher injection pressure, the macroscopic flow between fibrous yarns starts to predominate, resulting in voids induced by uneven flow fronts. Figure 2.9 shows the C-scan image of composite panels with voids.

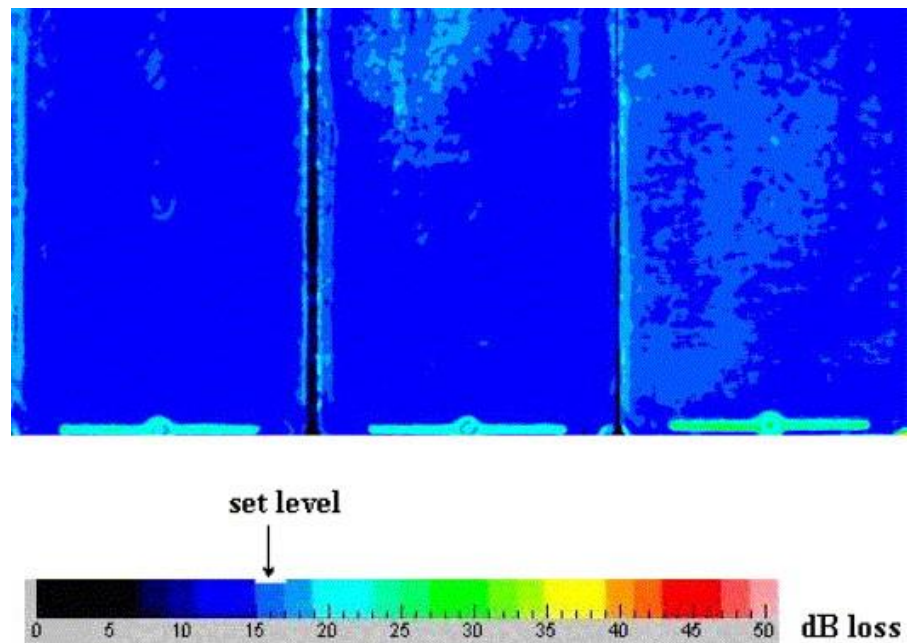


Figure 2.9: C-scan images for different plates with voids. (Kas and Kaynak, 2005)

2.3.2.2. X-Ray Computed Tomography (CT)

The X-ray computed tomography (X-ray CT) technique is the main NDT technique used in this project. The X-ray CT technique and the use of X-ray CT on void characterisation are reviewed in the next section.

2.4. X-ray CT and its Application in Void Characterisation

X-ray CT is a radiographic imaging technique which is capable of showing the three-dimensional internal structure of objects. X-ray CT has been mainly employed in the medical field since the 1970s. It has now gained popularity as a NDT technique to characterise the three-dimensional (3-D) microstructure of materials and components, especially defects and internal damage, to a high accuracy.

2.4.1. X-ray Computed Tomography

When a penetrating X-ray beam passes an object, a projection of the transmitted beam is obtained on the detector. A series of projections will be taken of the object when it is rotated over either 180° or 360°. After being processed with a reconstruction algorithm, the two-dimensional (2-D) projections will be converted into a 3-D volume composed of 2-D cross-sections of the object, and different grey scale level represents different materials. The general process is illustrated in Figure 2.10.

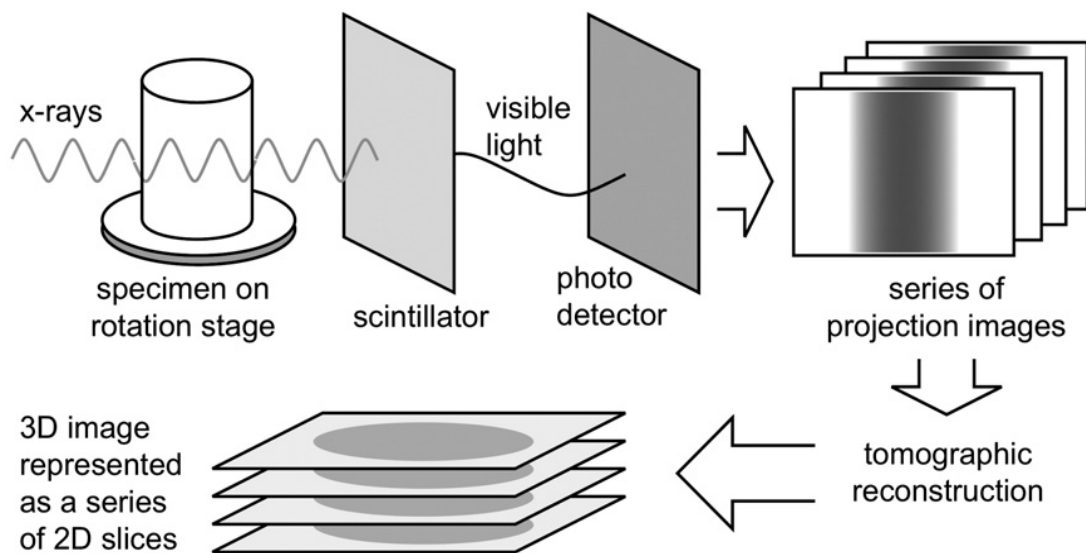


Figure 2.10: Schematic illustration of X-ray CT technique. (Landis and Keane, 2010)

The X-ray CT instrumentation has advanced steadily to achieve faster acquisition at higher resolution. In the first-generation X-ray CT systems, a narrow pencil beam and a single sensitive element were used and during acquisition successive translation and rotation was required, resulting in very long scan time (Hounsfield, 1973). In the scanners using a fan

beam and a linear array of photodetectors as illustrated in Figure 2.11a, complete linear information can be acquired in each projection, shortening the scan time. Subsequent use of a cone beam along with 2-D detectors as seen in Figure 2.11b, which allowed the acquisition of 2-D projection images, so scanning is considerably faster. At the moment, cone-beam sources are most extensively applied in lab-based X-ray CT instruments. However, in synchrotron radiation, a parallel beam with a narrow energy band with as shown in Figure 2.11c is used, enhancing the imaging capability by largely reducing beam-induced artefacts and scan time.

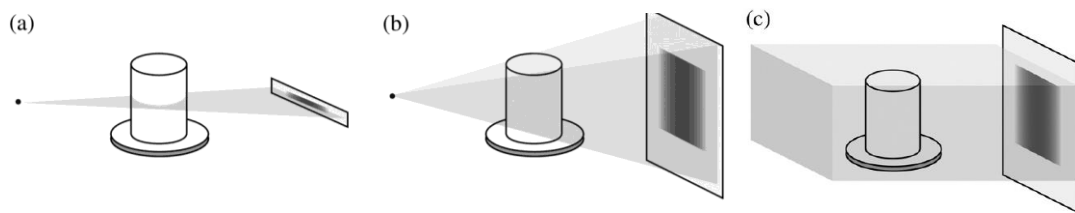


Figure 2.11: Illustration of different X-ray CT acquisition configurations: a. fan beam, b. cone beam, and c. parallel beam (Landis and Keane, 2010).

2.4.2. X-ray Absorption Physics

The basic physical principles involved in X-ray CT imaging are the X-ray absorption physics. The amount of absorption of an entering beam is a logarithmic function of the attenuation coefficient of the object and the travelling distance passing through the object. The attenuation coefficient of a certain material is determined by the density of the material, its effective atomic number and the X-ray beam energy (Baruchel *et al.*, 2000). The attenuation coefficients of aramid fibre and epoxy resin are similar, which results in low contrast and difficulty to distinguish between them. However, the voids have a much lower attenuation coefficient than the composite, so X-ray CT is considered a suitable technique to examine voids in the bulk composite. The X-ray CT technique is based on the Beer-Lambert law, which is the basis for the reconstruction of X-ray CT data into 3-D volumes. The formula is as follows,

Equation 2.9

$$I = I_0 \exp(-\mu x)$$

where I_0 is the intensity of the incident X-ray beam, and I is the intensity after it travels a distance of x in the material with a linear attenuation coefficient μ . The more general form for a non-homogenous material can be obtained by integrating the increments of attenuation along the X-ray propagation path,

Equation 2.10

$$I = I_0 \exp \left[- \int_s f(x, y) ds \right]$$

where $f(x,y)$ is the attenuation coefficient at position (x, y) along the X-ray path.

2.4.3. Reconstruction

The intention of using the X-ray CT technique is to visualise the 3-D inner structure of an object. After a series of radiographs being taken, the next step is to reconstruct a 3-D map of X-ray absorption of each point in the volume, which will be presented as a series of 2-D slice images. In 1917, Radon reconstructed a function from its line integrals (Radon, 1917) and later this became the basic mathematical formulation for reconstruction of X-ray CT data. Since then, a variety of reconstructing methods have been developed by considering the efficiency in reducing noise, artefacts computational complexity, and increasing spatial resolution, and flexibility. Among the various reconstruction algorithms proposed, the following are most extensively used: the filtered back projection (FBP) algorithm (Herman, 1979) and the algebraic reconstruction technique (ART) for a parallel beam, and the Feldkamp-Davis-Kress (FDK) algorithm (Feldkamp *et al.*, 1984) for small angle cone-beam geometry. Back-projection and filtering are the main two steps in the algorithms (Nesterets and Gureyev, 2009). In the back projection process, the ray integrals will be projected back

across the object, and then interact in regions where the attenuation coefficient is different. The back-projected result gives an approximated presentation of the original object, but needs to be further filtered to remove any blurring. This is normally processed in the frequency domain, using the Fourier slice theorem, and the details were discussed by Kak and Slaney (1988).

The FDK algorithm was developed based on the FBP algorithm, and is an algorithm specific for cone beam reconstruction. The result is approximate because of insufficient sampling taken from the cone shaped beam. In Radon space, or Fourier space, there is a conical volume with no value in each spatial region in the object, which is referred to as the missing cone, and the cone angle is the angle of the cone beam. In this case, the FDK algorithm works well for small angled cone beam systems.

ART is an iterative method of reconstruction and has gained more popularity recently. It begins with an estimate of the object and the approach to the solution is by a series of iterative projection-correction steps (Pan *et al.*, 2009), which has a better tolerance for noise or missing projections. ART proves to be very effective in eliminating imaging artefacts and improving image quality, but it is time-consuming and expensive to run.

Considering all the advantages and disadvantages of the algorithms, FBP based algorithms are still dominant in X-ray CT systems because of their straightforward implementation and computational efficiency.

2.4.4. Artefacts

Artefacts are any features in a reconstructed volume that do not exist in the object scanned. A variety of artefacts can result from specific set-up geometry and the material scanned, thereby degrading the image quality of CT data. Typical artefacts and the solutions to minimise their effects are discussed in the following section.

The beam-hardening artefact is caused by the polychromatic X-ray beam in lab-based

instruments. When a polychromatic X-ray beam crosses an object, photons with lower energy tend to be absorbed first, and the beam gradually becomes harder (more penetrating) as it travels further. This gives rise to increasing mean beam energy along the X-ray travel path (Brooks and Di Chiro, 1976). Beam hardening will result in cupping, shading, or streaking features in the reconstructed images. Beam hardening artefacts can be reduced by filtering the incident beam and calibration correction of the source.

Ring artefacts are generally shaped as circles in the reconstructed images and the centre of the circles is the rotation axis (Shepp and Stein, 1977), as shown in Figure 2.12. The signal delivered by every sensitive cell of the detector must be linearly spread between the offset level and the gain level. The detector should be calibrated so that the signal delivered is linearly spaced between the offset and gain levels of the elements. Uncalibrated detector or non-linear signal levels will lead to ring artefacts. There are two methods to minimise ring artefacts when acquiring projections. The first is to carefully re-calibrate the detector before scanning. The second is to make the object drift with small and known movements during the scan, eliminating the effect of broken detector elements.

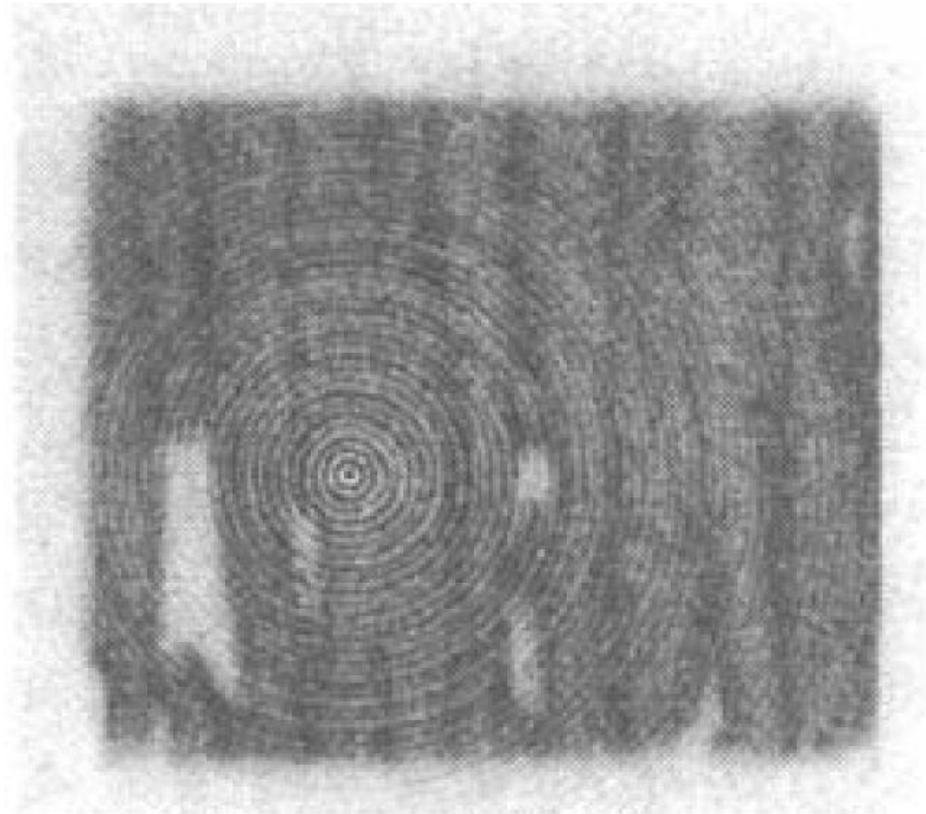


Figure 2.12: An example of ring artefacts. (Baruchel *et al.*, 2000)

The centring artefact is also a common problem, induced by the errors made when determining the centre of rotation of the object in the scan. Incorrect choice of the centre will result in distortions in the reconstructed image, as shown in Figure 2.13. The centring artefact can be eliminated in the data acquiring software and reconstructing software either during the scan set-up stage or during the reconstruction stage.

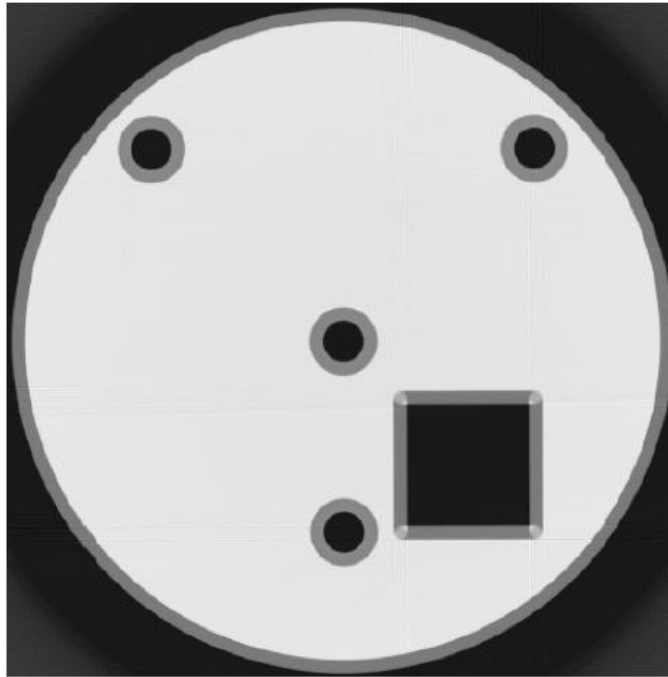


Figure 2.13: An example of centring error with features appearing doubled (Davis and Elliott, 2006; Stock, 1999).

2.4.5. X-ray CT Study on Voids

X-ray CT has been used to solve a variety of problems in materials science in a review by Stock (1999). In fibre reinforced polymer matrix composite materials, X-ray CT has been used to observe internal features that have good contrast with the bulk composite material, including voids (Centea and Hubert, 2011) and damage (Moffat *et al.*, 2008; Wright *et al.*, 2008).

As discussed previously, manufacturing defects often lead to considerable degradation of structural behaviour of composite components. The use of non-destructive X-ray CT on the examination of defects aids quantification and mapping of the voids to a high accuracy not attainable using any other technique. In addition, the better understanding of the amount, geometry and distribution of voids will give some idea of the optimisation of manufacturing techniques.

2.4.5.1. Quantification of Voids

Many studies have been reported on the quantification of voids in carbon-carbon and glass fibre-epoxy composites (Douarche *et al.*, 2001; Martin-Herrero and Germain, 2007; Weber *et al.*, 2010; Kastner *et al.*, 2010; Little *et al.*, 2009; Centea and Hubert, 2011; Tiseanu *et al.*, 2011; Nikishkov *et al.*, 2013), but few have investigated this problem in aramid fibre reinforced composites. However, the principle of using X-ray CT to measure porosity is the same regardless of the material; the bulk material should have good attenuation contrast with air or other gases generated in the gel process, so that voids can be segmented according to the difference in grayscale.

The precision of quantification in X-ray CT data is always a challenge because of the artefacts and the inherent anisotropic nature of composite materials. Martin-Herrero and Germain (2007) developed a labelling algorithm to process carbon-carbon composite data obtained using phase contrast. The labelling process includes filtering, refining and cleaning of the X-ray CT data. They concluded that with appropriate image processing, the true microstructure can be obtained.

Kastner *et al.* (2010) did a comprehensive study of porosity in carbon fibre reinforced plastics (CFRP) materials using X-ray CT. They confirmed the repeatability of measurements by X-ray CT and validated the consistency of porosity values compared with standard methods (e.g. ultrasonic attenuation and acid digestion). The repeatability of the measured porosity value is better than other conventional techniques. The absolute standard deviation for four measurements of the sample with 4.6 % porosity was ± 0.043 of a percentage point, which seemed much less than the error using other techniques, as illustrated in Table 2.2. It has also been noted that if appropriate segmentation method is applied, the obtained porosity value shows small dependency on voxel size and other CT scanning parameters.

Table 2.2: Comparison of different methods for void content measurement. X-ray CT is a non-destructive technique and seems to offer the highest accuracy. (Kastner *et al.*, 2010)

Method	Measurement principle	Accuracy in percentage points	Replicability	Time	Costs	Limitations	
Ultrasonic testing	Absorption of ultrasonic waves	± 1 % (if the material is well known ± 0.5 %)	o	+	+	Influence of pore-geometry and orientation, sample-geometry	non-destructive
Acid digestion	Gravimetry	± 1 % (if the material is well known ± 0.5 %)	destructive	-	o	Influence of analysed volume and material properties	destructive
Materialography - microscopy	Analysis of optical pictures	± 1 %	destructive	+ ... - (Depending on number of micro sections)	+ ... - (Depending on number of micro sections)	Influence of grinding, small analyse volume	destructive
Computed Tomography	Absorption of X-Rays	<0.5 %	+	o	-	Samples must be small for a good resolution	non-destructive

Nikishkov *et al.* (2013) questioned about the accuracy of voidage quantification using X-ray CT. In order to minimise the error in voidage measurement, they designed a density-based contouring method to segment voids to the sub-pixel resolution (an example of void segmentation using this method is demonstrated in Figure 2.14), and the results from X-ray CT and optical microscopy showed good agreement in carbon fibre-epoxy systems. Due to the 3-D nature of manufacturing defects, the measurement of the dimensions of voids is not reliable using 2-D techniques. As shown in Table 2.3, the limitation of measurement in optical microscopy images and X-ray CT slice images was addressed because of their 2-D nature, thereby the advantage of 3-D X-ray CT analysis was demonstrated.

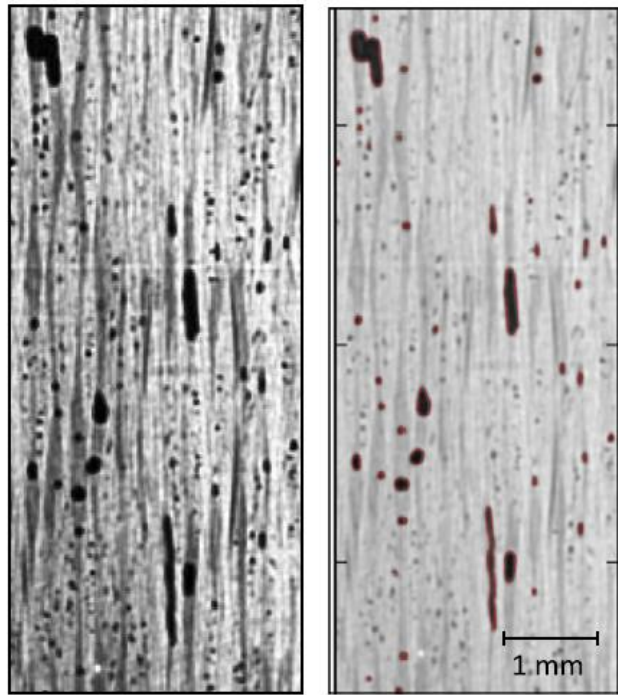


Figure 2.14: Demonstration of the selected voids contoured in red. (Nikishkov *et al.*, 2013)

Table 2.3: Comparison of microscopy-based and CT scan-based measurements for the voids in a unidirectional Carbon/Epoxy specimen. (Nikishkov *et al.*, 2013)

Void no	Microscope		CT scan, single section		CT scan, 3D analysis	
	Length (mm)	Width (mm)	Length (mm)	Width (mm)	Length (mm)	Width (mm)
1	2.86	0.044	2.77	0.046	3.93	0.056
2	2.24	0.056	2.37	0.049	2.42	0.052
3	1.78	0.067	1.40	0.048	1.81	0.075
4	2.28	0.063	1.62	0.042	2.36	0.068

2.4.5.2. Morphology and Spatial Distribution of Voids

A great deal of work has been done to visualise the morphology and distribution of voids by 3-D volume rendering of the segmented void volume in cured CFRP composites (Little *et al.*, 2009; Centea and Hubert, 2011; Reh *et al.*, 2012). However, hardly any work has been done on Kevlar composites, and also the relationship between the processing parameters during

manufacture, and the shape and distribution of voids in the final composite samples have not yet been established, which is the main topic in this project.

Kastner *et al.* (2010) observed that in CFRP samples with relatively low void content the voids were mostly spherical, whereas in high-porosity (>3 %) samples the voids tended to be flat and larger. Moreover, the voids were not evenly distributed in the sample, with many voids localised in certain layers. The X-ray CT slice images for samples with different void content are shown in Figure 2.15. Little *et al.* (2009) also found that with the increase of void content, the shape of the large voids changed and became more elongated with small spherical voids distributed throughout the sample, as can be seen in Figure 2.16.

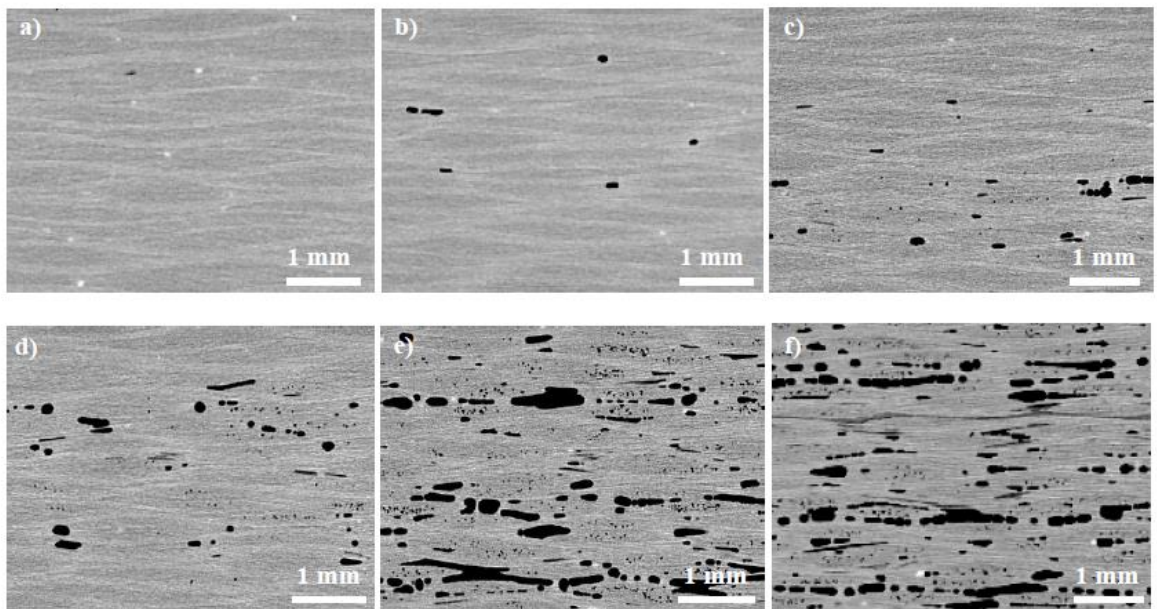


Figure 2.15: X-ray CT slice images of CFRP samples with various porosity (a: ~0 vol%, b: ~0,15%, c: ~0.35 %, d: ~0.9 %, e: ~4.50 %, f: ~10 %) (Kastner *et al.*, 2010).

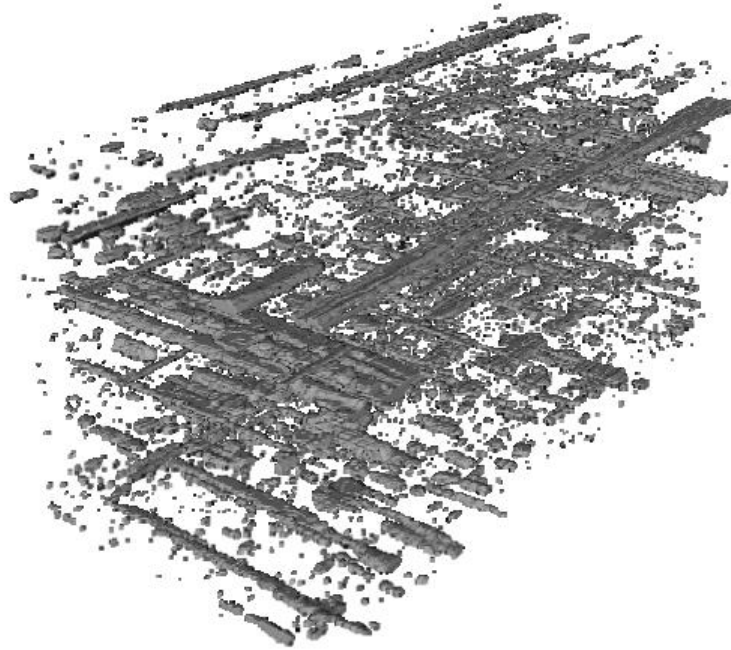
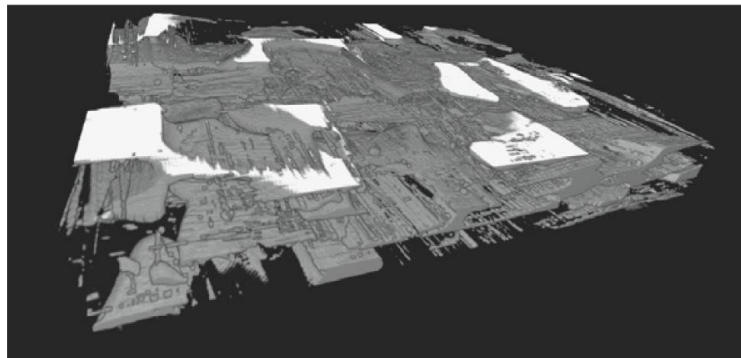
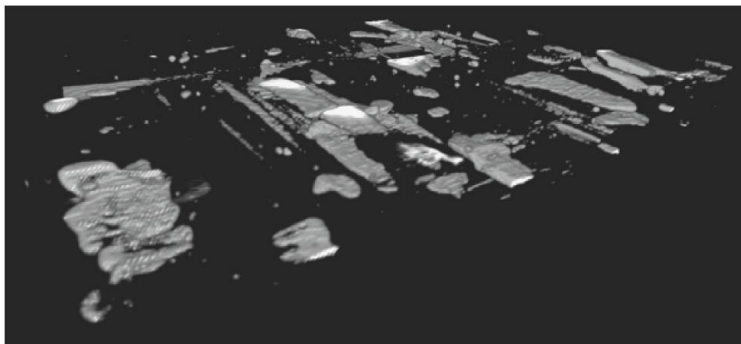


Figure 2.16: 3-D volume rendering of voids in a CFRP sample (Little *et al.*, 2009).

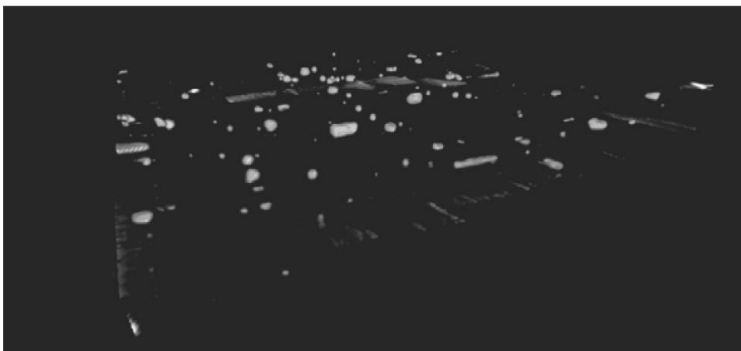
Some progress has been made to reveal the void formation during the manufacture of composites from preregs. The work by Centea and Hubert (2011) demonstrated the use of X-ray tomography to observe the evolution of voids in out-of-autoclave cured CFRP. They made a composite panel from woven pre-impregnated materials, and interrupted the curing cycle at various stages. In their work the changes in volume and distribution of voids during the curing cycle were presented. Figure 2.17 shows a volume rendering of the sample at different curing stages, where ellipsoid ‘bubble’ shaped voids were found in the final cured sample. However, it is still difficult to study the evolution of voids in the LCM manufacturing process. Such a topic has been focused on by researchers in Southampton (Streeter *et al.*, 2007). Unfortunately, no significant findings from their study have been published so far.



(a)



(b)



(c)

Figure 2.17: 3D renderings of void content evolution during processing (Centea and Hubert, 2011).

3. Preliminary Study

This chapter discusses early-stage studies into the project, including the objectives of the project, the study of the manufacturing process, the design of experiments and the problems encountered.

3.1. Introduction

The preliminary studies aimed to achieve the following objectives:

- getting familiar with manufacturing thick textile composite panels by the VARI method;
- understanding the capability of X-ray CT in the characterisation of voids formed in thick composites;
- having a basic knowledge of the characteristics of porosity in thick composites;
- having a basic knowledge of the void distribution in thick composites;
- proposing modifications to the VARI processing technique based on the preliminary results.

3.2. Experimental Investigation

3.2.1. Manufacturing of Thick Composite Panel

Three aramid-epoxy composite panels with different thicknesses were fabricated. Twaron[®] fabrics were employed as the aramid reinforcement. The amount of fabric was limited at the initial stage of the project, so the dimensions of the samples were varied and determined according to the size of available fabrics. Table 3.1 shows the details of the panels manufactured. The three panels were made from 20, 30 and 50 layers of fabrics, and were labelled as T1, T2 and T3, respectively. As the initial studies were about learning the manufacturing process and the NDT techniques, the variation in panel size was not an issue. For the detailed VARI manufacturing process, please refer to Section 4.2.1.

Table 3.1: List of panels manufactured.

Panel	Fabric Characteristics	Number of layers	Size of the flat panels (mm)
T1	Linear mass density: 168 Tex	20	160 x 130 x 7.9
T2	Thread density: 8.5 ends/cm	30	170 x 140 x 11.6
T3	Structure: Plain weave	50	120 x 100 x 18.1

3.2.2. X-ray CT testing

As mentioned previously, X-ray CT can be used to characterise composite materials non-destructively. The internal structures, different components and defects of the composite materials can be directly and precisely visualised. The initial scans were performed on the Nikon Metrology Custom Bay in the Henry Moseley X-ray Imaging Facility (HMXIF). The X-ray CT results were used to study the features and distribution of the internal porosity.



Figure 3.1: The sample set-up for the CT scan.

Because of the imaging physics (which will be discussed in detail later, in Section 4.3.3.2), the result of scanning three panels at a time was better than that of scanning a single panel. Figure 3.1 shows such a scanning set-up, where the three flat panels were held together by tapes and vertically placed on a polystyrene foam block. Then the foam was placed and secured on the rotating sample stage to avoid any unwanted movement during the scan. The scanning parameters are shown in Table 3.2.

Table 3.2: X-ray CT scanning parameters of the panels.

Target material	Tungsten
Voltage	300kV
Current	2.3mA
Exposure time	0.1s
Number of projections	721
Voxel size	100 μ m

3.3. Results and Discussion

In the process of manufacturing thick composite panels using the conventional VARI method (a modified liquid composite moulding (LCM) technique), it was found that the resin wetting-out time was longer in thicker composite panels. Since the permeability of the reinforcement, the viscosity of the resin and the shape and dimensions of the composite parts vary in composite systems used under different conditions, there is no standardised infusion time. The infusion time, along with the factors mentioned above, should be carefully controlled to improve the panel quality and reduce voids. Considering the practical operational process and the preliminary characterisation results, several modifications in the processing technique will be discussed in Chapter 4.

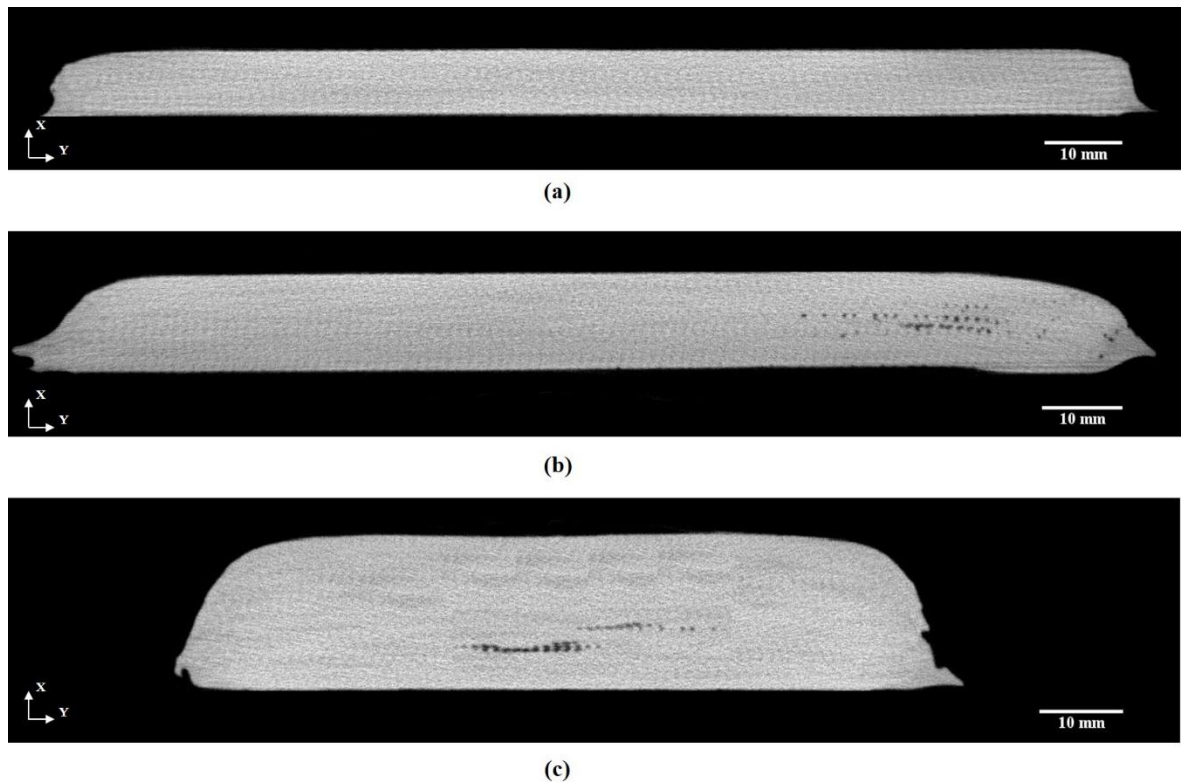


Figure 3.2: Typical XY slice images of a) T1 20 layers b) T2 30 layers c) T3 50 layers.

After demoulding, the flat composite panels were scanned using X-ray CT to observe voids. The initial attempt was to scan the panels at full size so they were not trimmed or cut at this stage. Some typical cross-sectional 2-D slice images for different panels are shown in Figure 3.2. As shown in Figure 3.2a, the internal structure in the 20-layered specimen T1 is uniform

and flat, and resin has wetted out the fabrics thoroughly without forming any visible voids. Figure 3.2b shows a cross-section of the specimen T2 that has 35 layers of aramid fabric, where some voids are visible, and these voids are concentrated on one side of the specimen. In the 50-layered specimen T3 many elongated voids have formed, similar to those in T2, but most of the voids now are centred in the middle layers of the specimen, as shown in Figure 3.2c. It is also found that such voids are continuous in the XY view, and localised in one or more layers. In addition, some distributed small voids have been observed.

From the tests conducted so far, no voids have been observed in the 20-layer panel, though this might be limited by the fact that the resolution of the scan is still not fine enough to capture smaller-sized voids. For the next stage of the project, studies will be focused on composite panels with more than 30 layers of fabric to investigate the features and distribution of voids in thick composite panels.

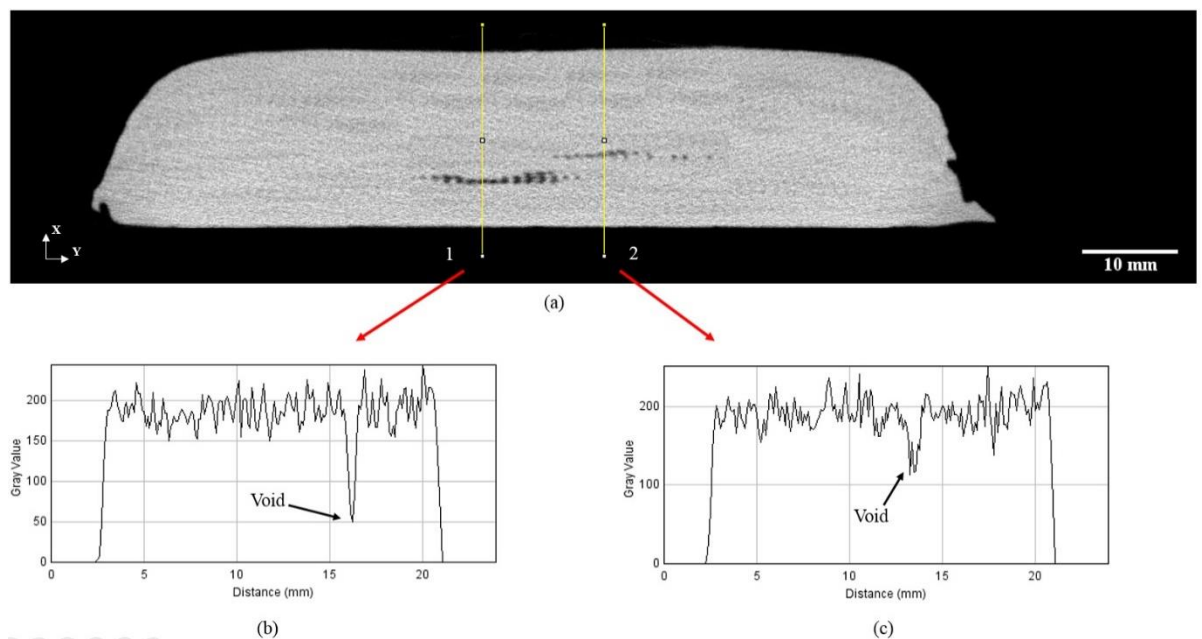


Figure 3.3: The difficulty in identifying void regions by differences in grayscale value. (a) XY slice image of T3 with two highlighted lines, (b) grayscale value change along the first line, and (c) grayscale value change along the second line.

When analysing the X-ray CT data, voids have been segmented by thresholding the grayscale range, so the threshold range will affect the determination of void volumes. In the

first scans, it was found that low contrast and large levels of interference noise affected the segmentation of voids and led to large errors in the quantification analysis. Figure 3.3a shows a slice image of T3, where two lines have been plotted passing through two different void regions. The line profiles corresponding to these two lines are shown in Figures 3.3b and 3.3c. It has been observed that the void area, where the first line passes, can be easily segmented; whereas the segmentation in the second void region is relatively difficult because of the similarity in the grayscale value of voids with the bulk composite and the large levels of noise. Therefore, in the later stage of the project, the segmentation of features in CT data should be further studied.

By improving the contrast and reducing the noise in the imaging data, the segmentation will be easier and the quantification analysis will be more precise. Therefore, before the set-up of the scan, trial scans should be carried out adjusting the setting parameters in order to obtain datasets with better contrast and lower noise. Moreover, it has been found that the untrimmed edges should not be considered in the quantification of voids. This is because the conditions at the edges are not representative of the quality of the composite panel, and in industries such edges will be cut off and will not be used for making composite parts. Therefore, in the following studies, all the panel edges will be trimmed. In addition, the study of smaller voids can be established by reducing the voxel size that is inversely proportional to the sample size. It is therefore essential to properly control these two parameters, and the preliminary study provides guidance to the sample size in later scans.

3.4. Chapter Summary

In the preliminary study, firstly the processing techniques in the manufacture of thick composite materials have been studied. X-ray CT proves to be an advanced NDT technique to assess the voids in thick aramid-epoxy composite panels. From the CT results, a preliminary understanding of voids in the 3-D volume has been obtained. In addition, considering the processing techniques together with the characterisation results, this study has provided ideas and support for the modifications in manufacturing process to improve the quality of thick composite panels.

4. Experimental

In this Chapter, the raw materials used, the manufacturing process for composite materials and the material characterisation methods employed in this project are described in detail.

4.1. Selection of Materials

4.1.1. Fabrics

In this research, Twaron[®] aramid fibres were used as the reinforcement of the composite material. Yarns with two different linear densities, 93Tex and 168Tex respectively, were used to weave the fabrics. The 93Tex and 168Tex fabrics were plain-woven with thread densities of 11.5 and 8.5 ends (threads) per cm, respectively, in the warp and the weft directions.

In plain weave fabrics, the warp tightness equals the weft tightness. The warp tightness can be calculated using the following equation,

Equation 4.1

$$E_1 = E_2 = \frac{d_1 \times n_1}{10}$$

where E_1 is the warp tightness, E_2 is weft tightness, d_1 is the estimated warp yarn diameter and n_1 is the warp thread density.

The diameter of the warp yarn can be estimated by assuming the yarn cross-section to be circular. Based on the definition of yarn linear density, the relationship between yarn diameter and linear density can be derived as follows,

Equation 4.2

$$T_1 = \left(\frac{d_1}{2}\right)^2 \times \pi \times \rho \times 10^3$$

or

Equation 4.3

$$d_1 = \sqrt{\frac{T_1}{\pi \times \rho \times 10^{-3}}} \times 2$$

where T_1 is the warp yarn linear density and ρ is the density of Twaron fibre, which is 1.44g/cm^3 . Then Equation (4.1) can be interpreted as follows.

Equation 4.4

$$E_1 = \sqrt{\frac{40T_1}{\pi \times \rho}} \times n_1 \times 10^{-3}$$

In plain weave fabrics, the weft tightness $E_2 = E_1$

4.1.2. Resin System

Epoxy resin is a thermosetting polymer. With the advantages of having a low thermal expansion coefficient, good adhesion and high mechanical properties, it has been extensively used as the matrix material in bullet-proof and engineering composite materials. Here epoxy resin Araldite[®] LY 564 and hardener Aradur[®] 3486 supplied by Huntsman were selected as the polymer matrix system. Some important parameters are listed in Table 4.1.

Table 4.1: Properties of Araldite® LY 564 epoxy resin and Aradur® 3486 hardener.

	Araldite LY 564		Hardener XB 3486
Aspect	clear liquid		clear colourless to slightly yellow
Viscosity (at 25 °C)	1200 - 1400 mPa s		10 - 20 mPa s
Density (at 25 °C)	1.1 - 1.2 g/cm ³		0.94 - 0.95 g/cm ³
Initial mix viscosity (at 25 °C)	200 - 300 mPa s		
	components	Parts by weight	Parts by Volume
Mix ratio	Araldite LY 564	100	100
	Hardener XB 3486	34	41

4.2. Fabrication of Thick Composite Panels

All the composite panels were manufactured using conventional or modified VARI methods. The manufacturing processes are detailed in the following sections.

4.2.1. Conventional Vacuuming Bagging Resin Infusion Method

4.2.1.1. Preparation of the Mould

The first step of the composite manufacturing process was to select a stainless tool plate with an appropriate size as the solid mould, where any marks and impurities on the mould surface should be thoroughly cleaned, since they will affect the smoothness and appearance of the composite panel. Nevertheless, the existence of impurities will influence the properties of the panel. It is important to choose appropriate tools to clean the mould surface to avoid scratches, especially when eliminating the cured resin left on the mould after demoulding the last panel. Plastic tool and laboratory tissues were used together for cleaning. Firstly acetone or mould cleaner was applied to the plate with tissues, then a plastic tool was used to remove the debris. In some regions, the mould needed to be cleaned repeatedly until the plate surface was clean and smooth enough. Then release agent

was applied to the cleaned mould following certain routes, and the mould was left untouched until the release agent dried out. The procedure was repeated several times to ensure that the mould was fully covered with release agent.

4.2.1.2. Lay-up of the Fabrics

Fabrics were cut into 20cm x 18cm pieces which were then placed layer by layer on the cleaned mould. The aramid fabrics can be cut electronic scissors or by an automatic ply cutter according to the size requirement of the composite panels to be made. Markers were used to mark the cutting guidelines on the fabrics, and the alignment of yarns was maintained during cutting. The fabrics were then laid up sequentially in the designed direction, during which process the flatness of the fabrics was carefully maintained. After placing each layer, the fabrics was evenly pressed with a plate in order to avoid fabric waviness, which otherwise would cause nests entrapping air. Therefore the formation of voids in the panel can be constrained.

4.2.1.3. Setting-up the Vacuum Bagging System

The VARI method was used to make the panels. The vacuum bagging system was made using a variety of materials, including plastic film (bagging material), peel ply, mesh, tacky tape, blue tape, plastic tubes, spiral tubes, cotton pads and a vacuum valve. As shown in Figure 4.1, reinforcing fabrics and other materials were placed on the mould according to the sequence and sealed in a vacuum bag. The main steps were: 1. Firstly, the top and bottom surfaces of the fabrics were covered by the peel ply and placed at the centre of the mould. The use of peel ply made it easier to separate the panel and the mould in the demoulding process. 2. Figure 4.2 shows a schematic diagram of the top view of the VARI method, plastic tubes and spiral tubes were wrapped by the peel ply and fixed on the mould as the resin inlet and outlet, which enabled the uniform and fast distribution of resin in the infusion process. 3. One layer of mesh was placed on the top of the peel-ply to aid resin flow, followed by the vacuum bagging covering all the layers. At the resin outlet, a sealed bag filled with cotton pads was connected before the vacuum valve, so that any extra resin can be

absorbed without damaging the valve and vacuum pump. After the vacuum bag was sealed, the bag was evacuated with a vacuum pump. A vacuum meter was used to check whether there is was leakage in the bag. This was usually repeated several times until the bag was completely air-tight. The vacuum meter was left connected with the panel for at least 4 hours or overnight to stabilise the vacuum condition. This is because any small leakage will result in the failure of resin infusion and curing of the panel.

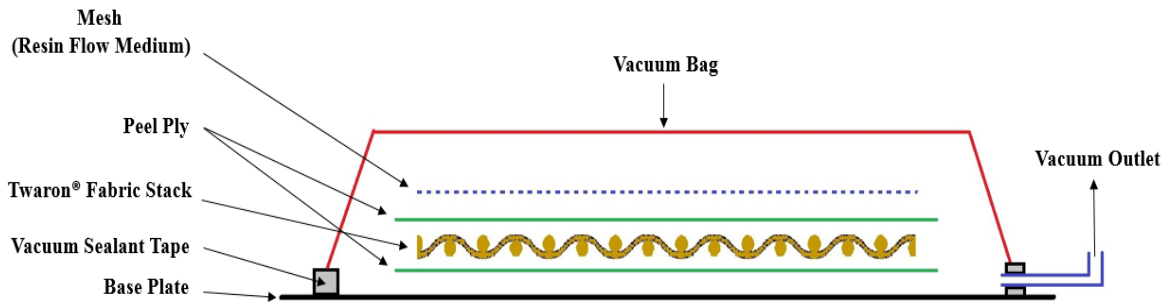


Figure 4.1: Schematic diagram of the vacuum bagging system in the VARI method (side view).

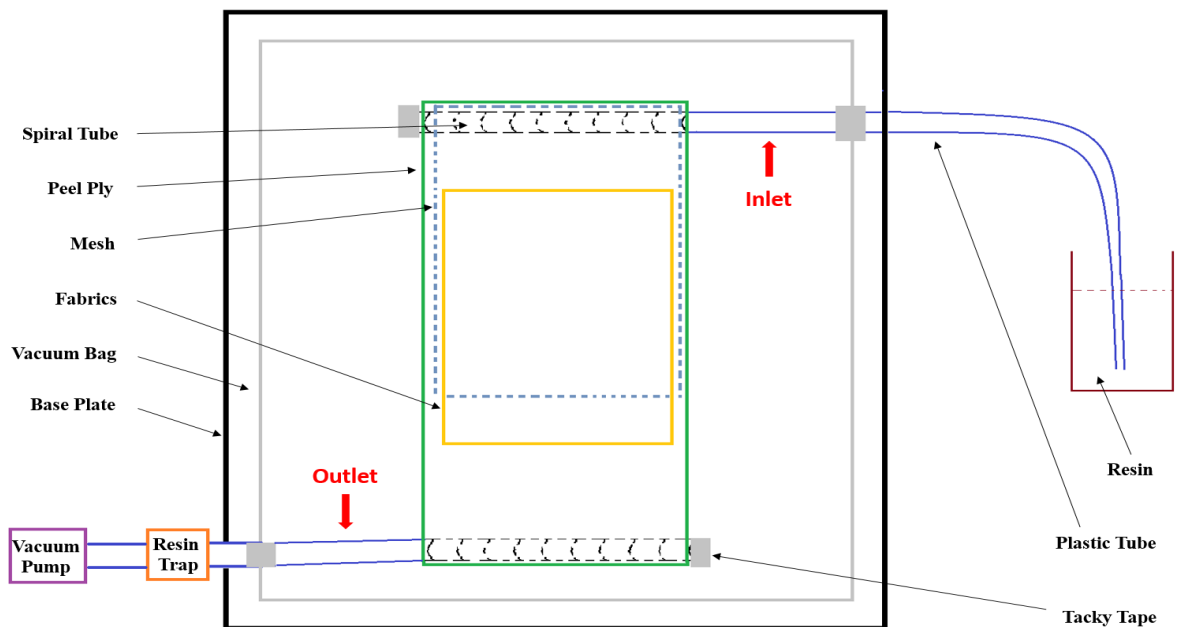


Figure 4.2: Schematic diagram of the set-up of the conventional VARI method (top view).

The following issues should also be addressed during the preparation of the vacuum bag system. As shown in Figure 4.2, the bottom edge of the mesh was several centimetres away

from the bottom edge of the fabrics. This gap was left to slow down the resin flow speed at the surface, so that there would be enough time for resin to permeate in the thickness direction and flow in the sub-surface planes until the resin front arrived at the bottom edge. The dimensions of the vacuum bag should be larger than the fabrics, and bumps should be made using tacky tape to leave extra space in the bag in order to accommodate the large thickness of the fabrics and avoid wrinkles on the panel top surface.

4.2.1.4. Resin Infusion

The resin should be prepared prior to the resin infusion process. The amount of resin to be used was estimated empirically by assuming that the fibre volume fraction in the composite is 50-60%. Then the weight of resin in the manufactured composite can be calculated using the following equations,

Equation 4.5

$$\begin{cases} V_f + V_r = 1 \\ M_f + M_r = M_c \end{cases}$$

Equation 4.6

$$M_r = \frac{(1-60\%) \times M_f \times \rho_r}{60\% \times \rho_f}$$

where V_f is the fibre volume fraction, V_r is the resin system volume fraction, M_f is the mass of the fabrics, M_r is the mass of the resin system, M_c is the mass of the composite, ρ_f is the fibre density and ρ_r is the density of the resin system. These parameters used in this dissertation are listed in Table 4.2. Considering the resin in the inlet and outlet plastic tubes and what remained in the resin cup, the total amount of resin system for infusion was estimated by adding 150g to M_r . Then the weight of epoxy resin and that of hardener were computed according to the mixing weight ratio 100:34 recommended in the datasheet:

Equation 4.7

$$\begin{cases} M_E = (M_r + 150) \times \frac{100}{(100 + 34)} \\ M_H = (M_r + 150) \times \frac{34}{(100 + 34)} \end{cases}$$

Where M_E is the weight mass of the epoxy resin, M_H is the mass of the hardener.

Table 4.2: Parameters used for calculating the amount of the resin system.

Fibre density	1.44 g/cm ³	
Resin density	1.15g/cm ³	
Fabric type	93Tex	168Tex
Weight of one layer	6.8±0.5g	9.5±0.6g

After the correct proportion of epoxy resin and hardener were weighed using an electronic scale, the two parts were mixed thoroughly using a tongue depressor. The stirring speed should be controlled, as if it is too fast more air will be introduced to the resin system. Then the cup with the mixed resin system was placed in a vacuum oven for degassing. It should be noted that if the degassing time is too short many air bubbles will remain in the resin, while if it is too long the resin system will start to gel. The resin cup was taken out from the vacuum oven when no air bubbles were visible.

Infusion was started immediately after degassing was finished. The vacuum pump was connected to the valve at the outlet of the vacuum bag and sealed by tacky tape. Then the vacuum pump was switched on before the resin inlet was placed into the resin cup underneath the resin surface. Then the clamp closing the resin inlet tube was removed and the infusion process began. The resin injection speed should be controlled properly during infusion. When resin started to flow into the plastic outlet tube, the inlet tube was clamped and sealed with tacky tape while the vacuum pump was still working. After resin became saturated in the fabrics, and continuous resin flowed into the outlet tube, the outlet tube was

clamped and sealed at the end.

4.2.1.5. Curing Cycle

After infusion, the panel was placed in an oven to be cured. As the curing mechanism varies for different resin systems, the curing cycle should be set according to the datasheet. For this resin system, the curing cycle consisted of three steps: 1. The oven temperature was raised to 80°C in 1 hour from room temperature; 2. The oven temperature was kept at 80°C for 8 hours; 3. The oven was cooled naturally.

4.2.1.6. Demoulding and Trimming of the Panel

Demoulding was started from one side of the panel, the materials were peeled off layer by layer with the help of scissors and knives without damaging the panel. If release agent was not applied appropriately, it would be difficult to demould the panel. After the panel was demoulded, the resin-rich edges of the panel were trimmed off using a diamond saw. Then each panel was numbered and labelled.

4.2.2. Modified Vacuuming Bagging Resin Infusion Method

Combining the X-ray CT results obtained from the preliminary study with the literature review study on the mechanisms of void formation, modifications to the vacuum bagging infusion process have been proposed. Three modifying methods were raised with focus on the different stages of resin infusion, including before the resin enters the vacuum bag, during the flow of resin in the reinforcement and when extracting the entrapped air from the vacuum bag.

4.2.2.1. Inlet Tube Position in Resin

The first amendment was cutting the inlet tube under the resin surface, which eliminated the air left in the tube before infusion and reduced the air entering the vacuum bagging system. In this case, the probability of void formation decreased at the beginning and the quality of the composite material should be improved. Figure 4.3 shows schematic diagrams of the conditions before and after modification. In the schematics, the black cross presents the clamp used to close the tube after the bag is evacuated, and the red region indicates the air. In the conventional manufacturing process shown in Figure 4.3a, the resin inlet tube is closed by a clamp and then the tube is placed into the degassed resin in the cup. The vacuum pump at the outlet is switched on, followed by opening the clamp at the inlet when the bag is fully evacuated and resin flows into the bag. When the inlet tube is put into the resin cup, the air between the clamp and the tube end will be trapped inside the tube and when infusion starts the air will be driven into the bag. The enclosed air will quickly pass through the channels in the reinforcement and most of the air will be discharged from the bag. However, the inclusion of this amount of air will affect the pressure and vacuum inside the bag to a certain extent, which will increase the uncertainty of the infusion process.

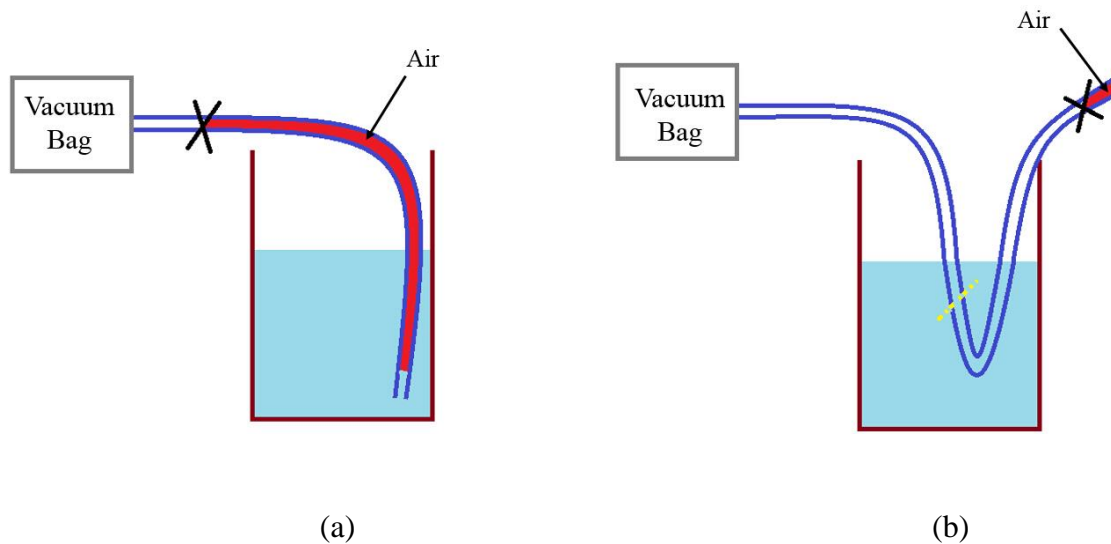


Figure 4.3: (a) Schematic diagram of the inlet tube position in conventional VARI method. (b) Schematic diagram of the modified inlet tube position. The tube was cut under the resin surface, so that no air remained in the tube when infusion started.

A modification has been made to the traditional processing procedure in order to eliminate the remaining air in the tube. Figure 4.3b shows the modified schematic diagram. As can be seen, a longer plastic tube was used between the clamp and the vacuum bag. As the bag was evacuated after the lay-up process, the tube between the clamp and the bag was also in the vacuum status. After curving this length of the tube, the tube was placed into the resin carefully, and tape was used to fix the position. Then the tube was cut under the resin surface carefully, followed by resin flowing into the bag as in the conventional resin infusion process. Therefore, the volume of air introduced to the vacuum bag was reduced, and the change in porosity conditions using this method will be detailed in Section 5.3.3.

4.2.2.2. Double Meshes

In the conventional VARI method of manufacturing composite panels, a single mesh is commonly used as the resin flow media, which is placed on top of the fabrics and the peel ply layer and below the vacuum bag. In the resin infusion process, the use of mesh aids the resin to distribute uniformly and rapidly on the surface of the reinforcement, which contributes to the even resin flow in the thickness direction. In the manufacturing of thick

composite panels, resin needs to flow through more layers through the thickness of the panel, so the flow rate is relatively low and non-uniform at the bottom layers. It has been found in the preliminary study that in the 50-layer thick composite, the voids are concentrated near the bottom surface of the panel as illustrated in Figure 3.2c. Therefore, a second layer of mesh was introduced to the bagging system as the second modification method. The extra layer of mesh was placed between the steel mould and the bottom peel ply, as shown in Figure 4.4. The bottom mesh was used to guide resin to flow from bottom to top, which was expected to aid the through thickness penetration of resin and improve the wetting condition. It should be noted that the two layers of mesh were connected at the top inlet spiral tube and actually were one piece of the mesh material folded into a U-shape. In this case, resin would flow evenly to the top and bottom layers of the mesh. This method has not been introduced in any manufacturing standards, and there is no identified paper or thesis discussing this technique. Therefore, in this dissertation the difference in material quality using single mesh or double meshes was studied and the results will be discussed in Section 5.3.1.

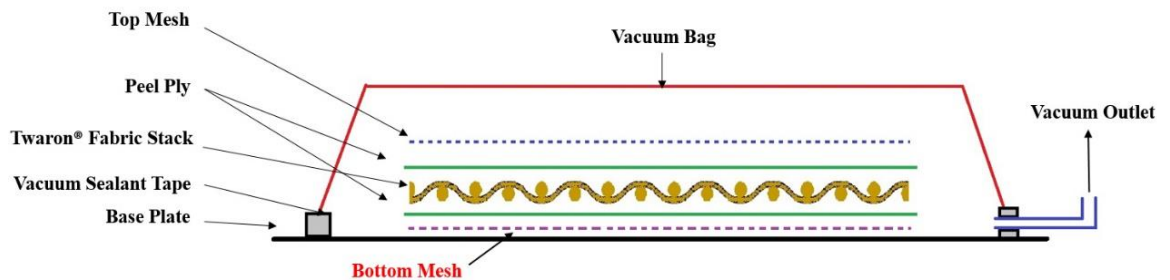


Figure 4.4: Schematic diagram of the modified VARI method with a second layer of mesh under the bottom peel ply.

4.2.2.3. Double Outlets

Other than the above two modifications, another improvement was proposed in the step when resin was discharged from the vacuum bag in order to reduce voids in the manufactured thick composite panel. In the original VARI method, a single inlet and a single outlet were used. The diagonal position to the resin inlet was usually chosen as the outlet

position. The resin outlet tube was connected with a spiral tube in the bag, guiding resin flow similarly to the outlet. During several infusion processes, an interesting phenomenon was noticed. Observing the panel from the top, when the resin flowed in the bag, although aided by the mesh and the spiral tube, the resin flow rates at the left and right of the panel were relatively balanced but the flow front was not parallel to the bottom edge. The flow front near the outlet position was more advanced than the other side, and with the progress of infusion this lead became even greater. The resin near the outlet was the first to be discharged to the spiral tube and the outlet tube.

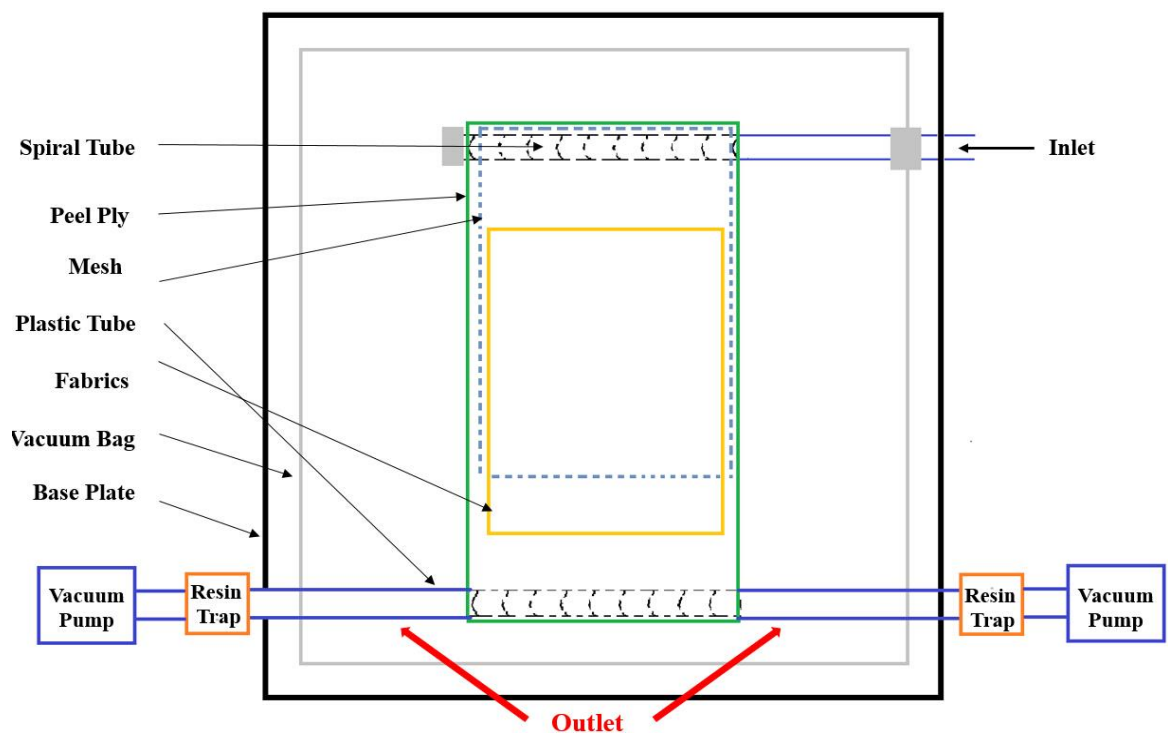


Figure 4.5: Schematic diagram of the modified VARI method with a second resin outlet positioned symmetrically to the first outlet.

Based on this, a new method was proposed. As shown in Figure 4.5, a second outlet tube was added symmetrically with respect to the original outlet. The connection to the vacuum pump provided the same pressure and the two outlets can not only speed up the discharging of voids (the resin started to gel progressively when mixed, so the infusion time was limited), but also provide an extra exit choice of voids. This method is expected to have certain effect on the reduction of voids in thick composite panels. The results will be discussed in section 5.2.2.

4.2.3. Overview of the Panels Manufactured

A summary of the details of the panels made in this project is shown in Table 4.3. Eight panels were manufactured for comparison studies. The changing parameters are the number of fabric layers, the yarn linear density, the number of outlets, the number of meshes and the inlet tube position in the resin.

Table 4.3: Summary of the panels manufactured using different processing parameters (in red).

Sample	20	35	50	93	168	SO	DO	SM	DM	CR
A										
B										
C										
D										
E										
F										
G										
H										

20, 35 and 50 – Number of fabric layers

93 and 168 – Tex

SO – Single outlet

DO – Double outlets

SM – Single mesh

DM – Double meshes

CR – Cut in resin

4.3. Characterisation Techniques

4.3.1. Specimen Preparation

Before characterisation, each panel was cut into nine squares using a diamond saw, as illustrated in Figure 4.6. Strips about 2.5mm wide were missing between each sample because the cutting wheel was 2mm thick.

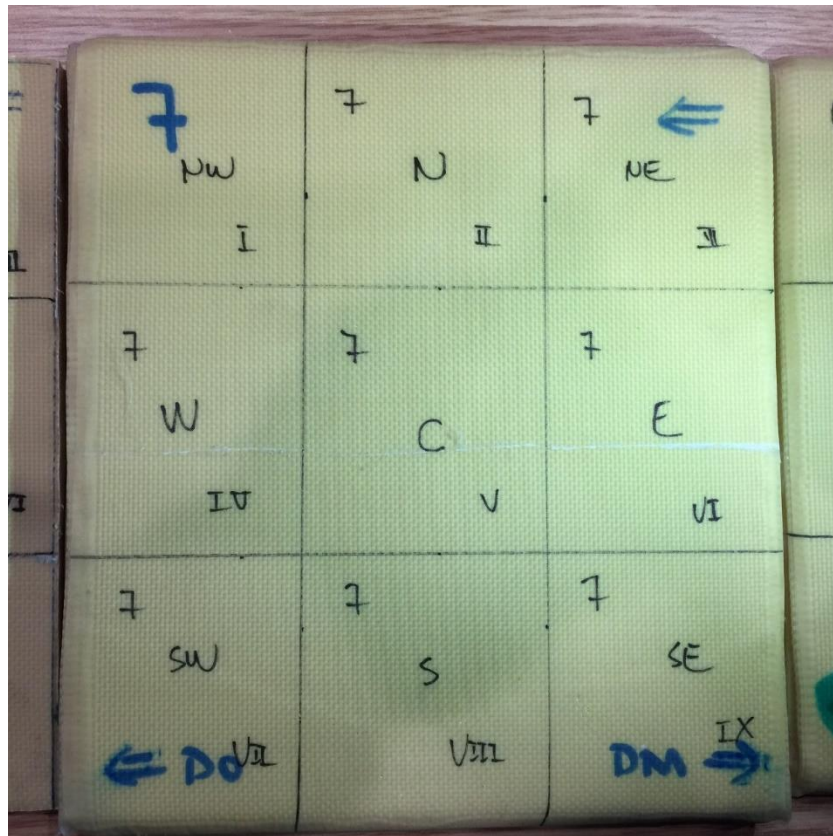


Figure 4.6: Image of a full panel with markers labelling the cutting guidelines. The full panel was cut into 9 small squares using a diamond saw. The cutting wheel was 2.5mm thick, so the panel cannot be perfectly recovered after cutting.

4.3.2. Ultrasonic C-Scan

As mentioned in Section 2.3.2.1, the ultrasonic inspection technique is a standard NDT method to characterise the internal defects and damage in composite materials, such as impact induced delamination and voids. The ultrasonic inspection results can be generally presented in three ways, which are termed as A-, B- and C-scan. The A-scan result is a raw

display of the wave pattern of the returning echoes as a function of time (or the equivalent penetration depth). The B-scan result is displayed as a side view of the object, which results from the combination of the A-scan and the movement of the probe. The C-scan result presents the projection of the top view of the object, which is perpendicular to the ultrasound travelling direction. The in-plane position and distribution of defects can be indicated in the C-scan result, but the extent of the defects and their position in the thickness direction cannot be assessed (Adams and Cawley, 1988). Figure 4.7 shows a schematic diagram of the results from the B- and C-scans. In this project, the ultrasonic C-scan was used to characterise the planar distribution of voids in thick composite laminates.

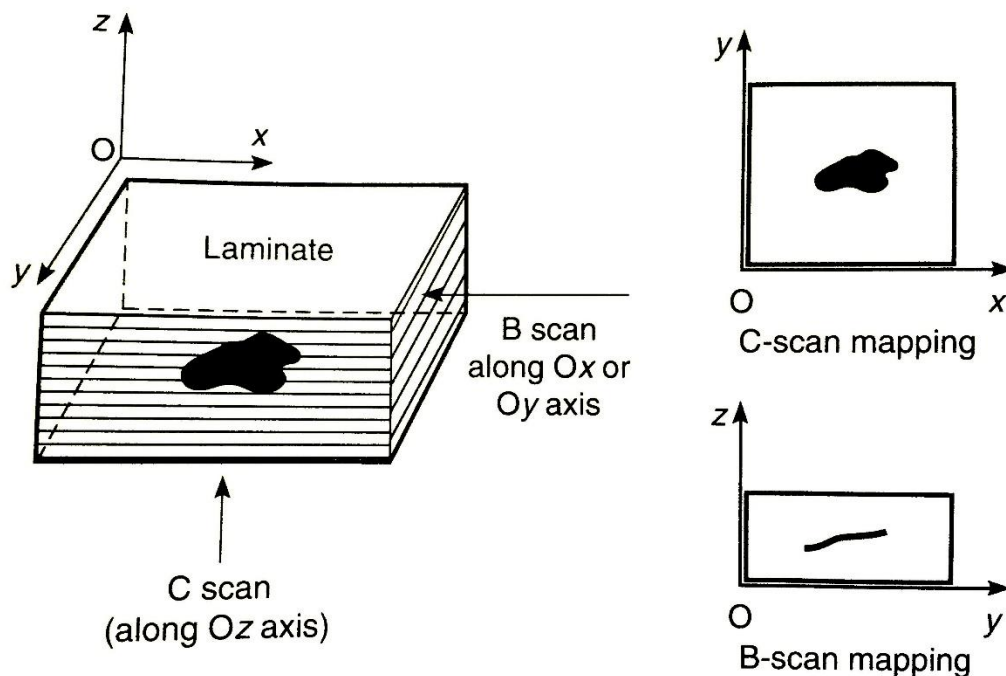


Figure 4.7: Schematic diagram of ultrasonic B- and C-scans of an internal defect. (Geier, 1994)

Ultrasonic C-scan tests of all the samples were performed on the Midas NDT C-scan system equipped with the Zeus V3.0 software. In the scan, an ultrasound wave with a certain frequency was emitted from the transmitter continuously and was received by the receiver. The frequency of the ultrasound should be selected according to the thickness of the sample, so that the sample thickness is larger than the ultrasound wavelength. In this experiment, the frequency employed was 0.5MHz. After the transducers were determined, the transmitter

and receiver were fixed at the two sides of the scanner. Then the two water jets were switched on and the water pressure was adjusted so that the water spouts were straight. The height of the transducers was adjusted in order to make the two water spouts aligned and stable. Calibration was performed to stabilise the transmitting and receiving of ultrasonic signals before scanning the samples.

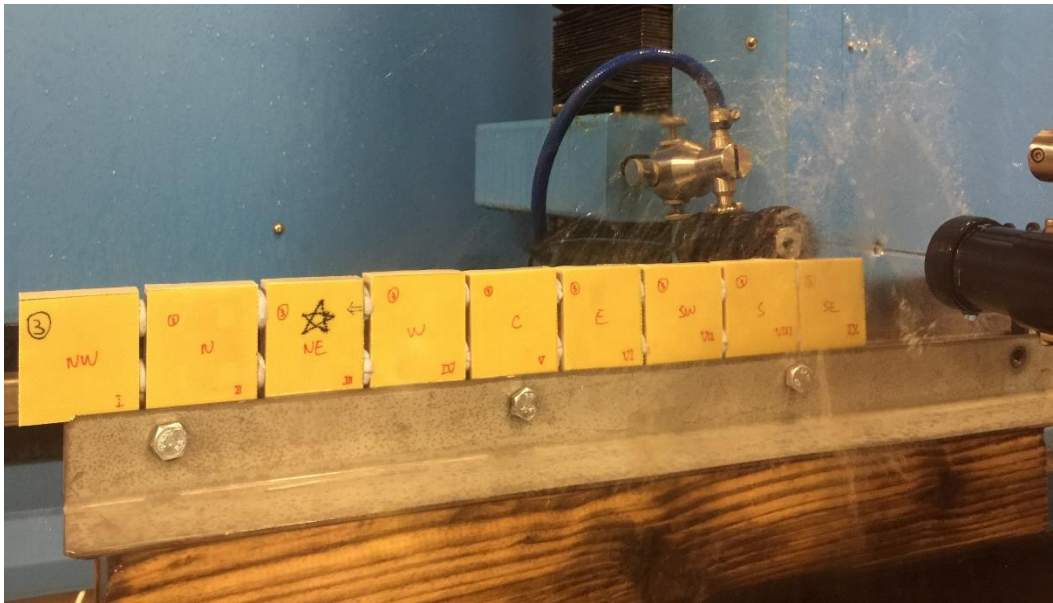


Figure 4.8: The sample set-up for ultrasonic C-scan testing.

After calibration, the sample was fixed on the stage with supporting tools, as shown in Figure 4.8. It is important to make sure that the panel surface is perpendicular to the ultrasound path between the two transducers. In addition, as shown in Figure 4.9 the grid size and index step for probe movement need to be set, which will affect the precision of the scan. Higher accuracy can be obtained using a smaller grid size and index step. In scanning these samples, the probe was set to move at 100mm/s with a grid size of 100 μ m and an index size of 100 μ m.

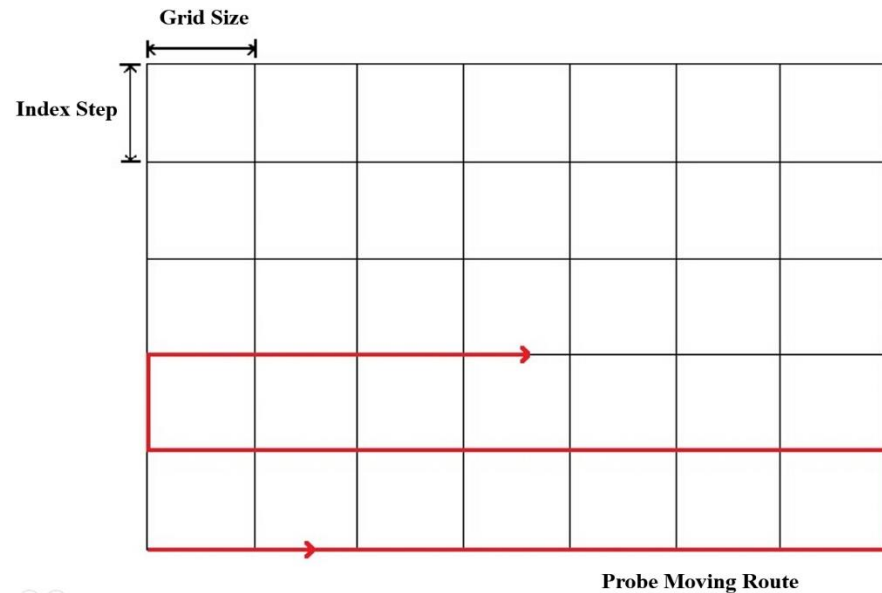


Figure 4.9: Schematic diagram of the moving route of the probe in ultrasonic C-scan. The grid size and index step are defined as the width and height of the grid, respectively.

In the C-scan images, the attenuation of ultrasonic signals was translated into different grayscale values. The result can be displayed in a grayscale, with darker regions indicating higher attenuation; or the result can be displayed as a colour map, with different colours representing attenuation ranging from 0-100 %. It should be noted that the C-scan result can only be employed to perform a qualitative study of the distribution of voids in flat composite laminates, not for the quantitative study of porosity. The C-scan results will be presented and discussed in Section 5.4.

4.3.3. X-ray CT

4.3.3.1. X-ray System Overview

The CT imaging of the samples was conducted in HMXIF. The scanning was carried out on the Nikon Metrology XT H 225 machine, which consists of a micro-focus X-ray source with a minimum focal spot size of $5\mu\text{m}$, a maximum accelerating voltage of 225 kV, a 5-axis manipulator to rotate the sample through 360° , and a flat panel detector. Figure 4.10 shows the Nikon XT H 225 CT imaging system. The system was operated using the Nikon Metrology Inspect-X software.

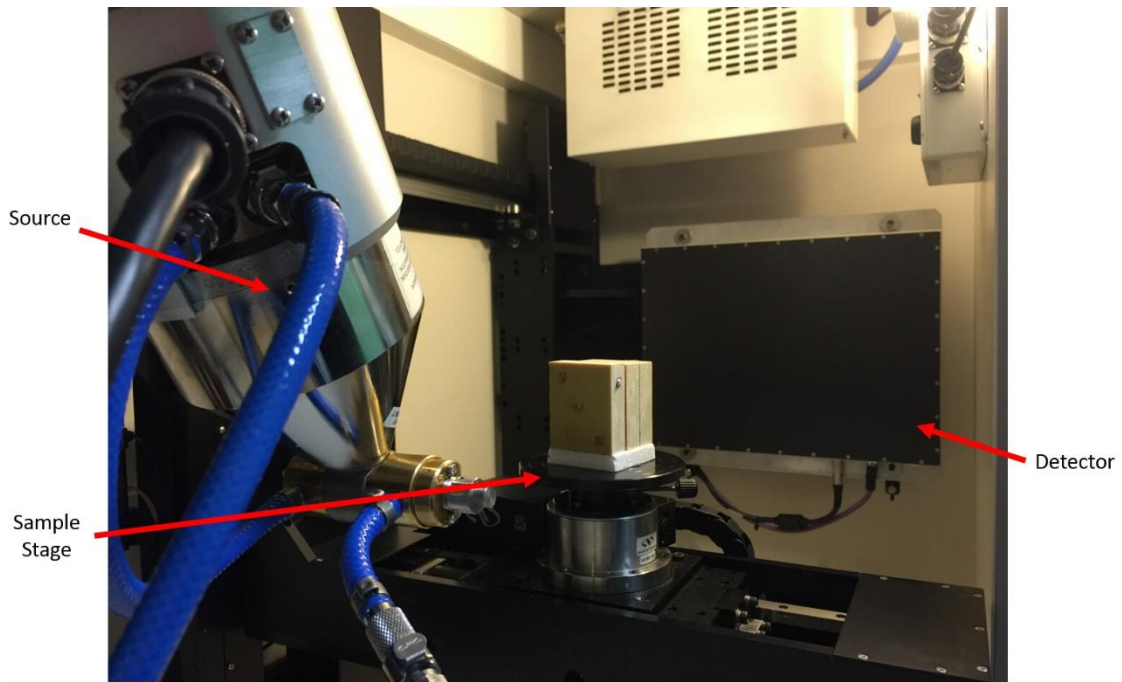


Figure 4.10: The Nikon XT H 225 X-ray CT imaging system. The source, sample stage and detector are highlighted.

4.3.3.2. Sample Set-up

As mentioned in Chapter 3, the initial scanning aimed to study the full extent of the panels; however, the image quality was limited by the panel size and quantitative study of voids could not be achieved. Therefore, the imaging specimens were downsized by cutting the panels into smaller parts. Although the dimensions of the specimens were smaller after cutting, the large aspect ratio (width to thickness ratio) can cause artefacts because of variation in the beam transmission distance while the sample rotates. In order to minimise the artefacts, a stack of 3-7 specimens were scanned at one time, and the number of specimens was determined according to the thickness of the panel. Putty-like adhesives (Blu-Tack™) were used as the spacing material to separate and position the specimens. Figure 4.11 shows a schematic diagram of the sample set-up.

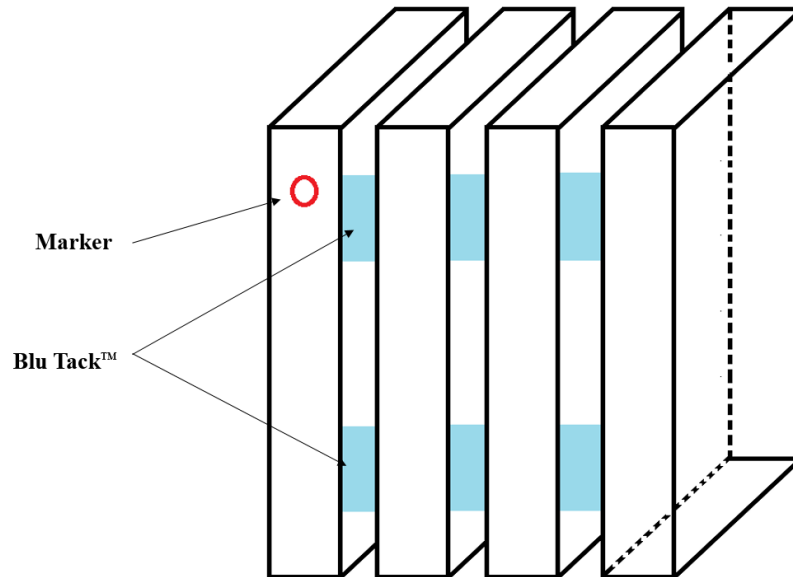


Figure 4.11: Schematic diagram of the sample set-up for the CT scan. A stack of specimens were scanned at one time. Blu-Tack™ was used between the specimens, holding them stable during the scan. A piece of tacky tape was used as the marker to identify the specimens in the CT data.

4.3.3.3. X-ray CT Machine Set-up and Data Acquisition

The accelerating voltage should be conditioned by selecting the ‘automatic conditioning’ option and setting the voltage to the maximum 225kV. The voltage should be kept at 225kV for half an hour prior to the first scan, assuring the stability of the X-ray beam energy. The focus of the beam should be checked using a circuit board with fine features, and adjusted using the ‘focus’ slide bar.

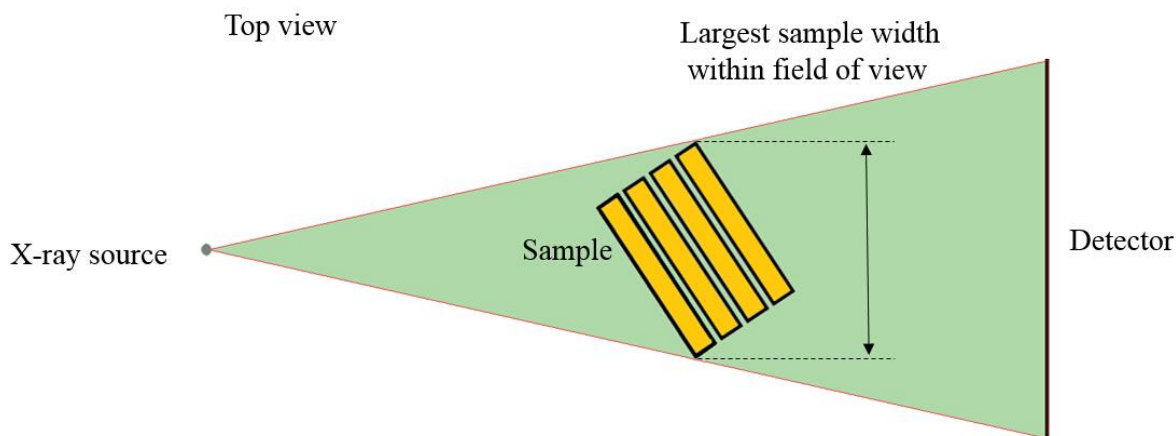


Figure 4.12: Schematic diagram of the scan set-up to make sure the sample is in the field of view during the scan. The source-sample and sample-detector distance are limited by the sample size.

It is important to make sure that all of the specimens were within the field of view during the 360° rotation, as illustrated in Figure 4.12. Table 4.4 shows the setting parameters used to scan the samples. The settings were optimised by balancing the contrast, voxel size, field of view and scan time. After the imaging parameters were set the sample was removed, and black (X-ray off) and white (X-ray on) shading correction reference images were taken using the same settings for the data acquisition in order to correct for variations of detector pixels. The scan time for each stack of specimens is around 1.5 hours. In total, 72 specimens cut from the 8 panels were imaged in 14 scans.

Table 4.4: Scanning parameters of the downsized aramid fibre-epoxy composite panels.

Target material	Tungsten
Filter	Cu 0.25mm
Voltage	125kV
Current	150 μ A
Exposure time	708ms
Number of projections	5000
Voxel size	34 μ m

4.3.3.4. X-ray CT Data Reconstruction

The CT data were reconstructed using the Nikon Metrology software CT-Pro®. The procedures are outlined below.

- A slight misalignment of the sample centre from the system designated centre will cause centre-of-rotation artefacts as described in Section 2.4.4. The correct centre of rotation needs to be determined before reconstruction in order to eliminate the artefacts. The centre of rotation was determined using the ‘automatic’ function in dual slices that were chosen at the top and bottom of the sample. Then the centre of rotation along the length of the sample can be automatically interpolated according to these two values.
- As mentioned in Section 2.4.4, the beam hardening artefact is a common artefact in X-ray CT scans, which will result in brighter edges. Beam hardening correction was performed by using the ‘reconstruct all presets’ function, and the correction value was chosen from 1 to 6 according to the effect of eliminating the intensity peaks at the sample edges. Figure 4.13 shows the change in line profile after the beam hardening correction was applied.

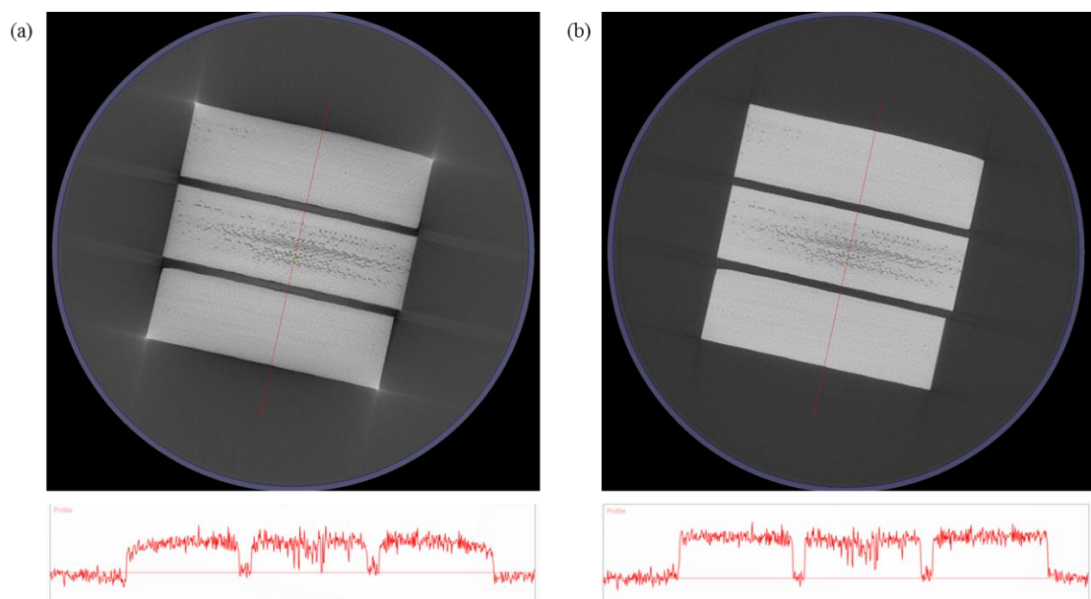


Figure 4.13: A typical previewed cross-sectional slice image of the sample. (a) before beam

hardening correction and the line profile, and (b) after beam hardening correction and the line profile.

- The volume was then reconstructed at 100% quality with the dimensions of $2000 \times 2000 \times 2000$ voxels. In this thesis, the X, Y and Z directions are the thickness direction, the width direction and the length direction of the panel, respectively, see Figure 4.14.

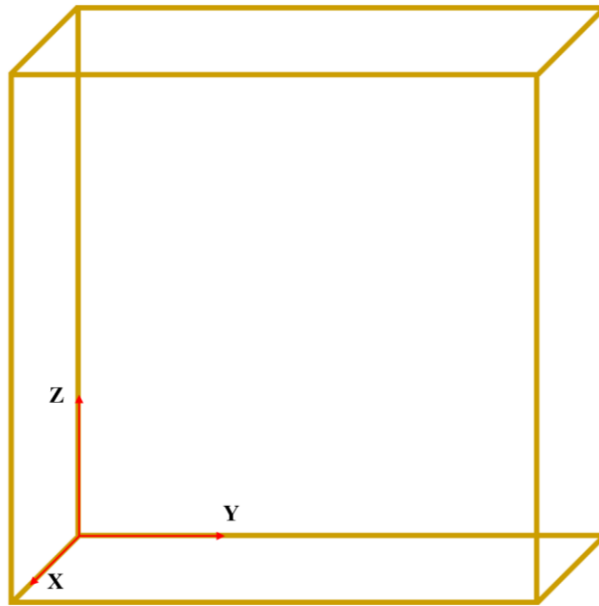


Figure 4.14: Schematic diagram showing the axes of specimens in the reconstructed CT data. The X direction points to the top surface of the panel.

- The reconstructed data were in 32-bit floating point format, and were then converted to 8 bit format, which will reduce the size of the file and remap the grayscale. In this case, the data processing becomes faster and the image contrast can also be improved.

4.3.3.5. Segmentation and Visualisation of the X-ray CT Data

The 3-D X-ray CT volumes were visualised and analysed in the Avizo® 8.0 software (Visualisation Science Group). The content, morphology and distribution of voids were studied. All the data were smoothed with the ‘anisotropic diffusion’ filter before segmentation, so most of the interference noise in the images was eliminated and the data

can be segmented using automatic tools. Figure 4.15 shows the slice images before and after filtering was applied. Then, the bulk aramid fibre-epoxy composite and the voids were segmented according to the variations in the grayscale, and labelled as different materials. Voids are darker than the composite in the reconstructed images. Figure 4.16 shows the histogram of a typical volume, with three distinguishable peaks for the voids, the bulk composite material and the Blu-tack™ adhesive, respectively.

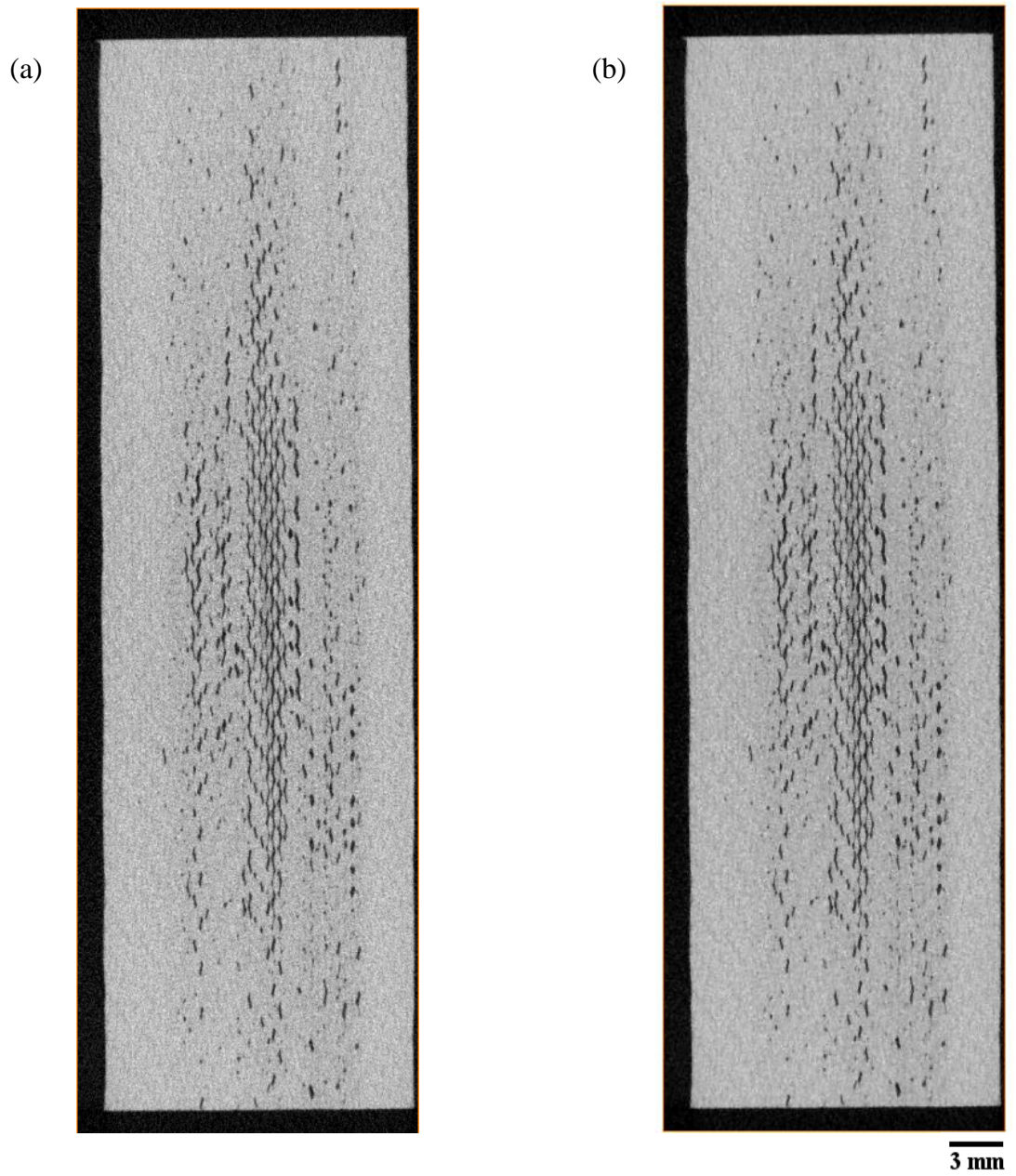


Figure 4.15: A typical slice image (a) before filtering, and (b) after smoothing using the anisotropic diffusion filter.

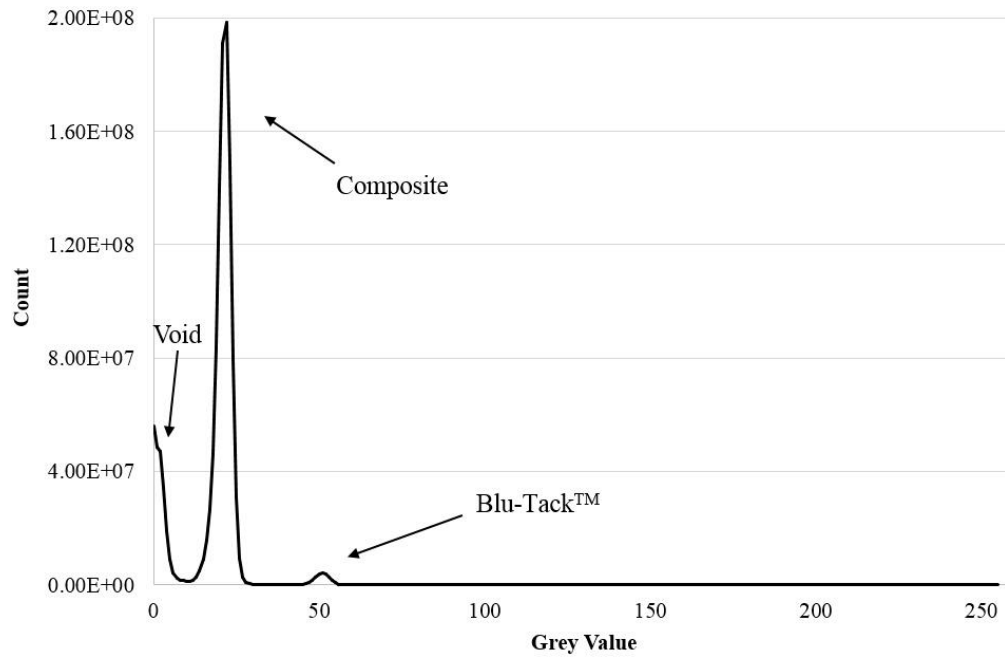


Figure 4.16: Histogram of a typical X-ray CT volume, with three peaks representing voids, composite material and Blu-Tack™, respectively.

The semi-automatic local thresholding and region-growing tool ‘magic wand’ was used to segment composites and voids. Different values were tried as the upper and bottom limits for thresholding the voids and the composite, and different ranges were determined for different datasets. Manual modification using the tool ‘brush’ was required in regions with ring artefacts. The ‘remove island’ function was then used, and dark regions less than 3 voxels in size were eliminated. The effect of removing islands will be discussed in Section 5.1.1.

All the datasets were segmented following the same procedure to keep the segmentation consistent throughout the data analysing process. However, the accuracy of segmentation was limited by the image quality and the voxel size of the datasets. The segmented volumes, labelled as composite and voids, can be visualised in 3-D by generating the surface of the volume, so the morphology and distribution of voids can be analysed. In addition, the volume of each label can be automatically calculated; therefore, the void content can be computed.

4.3.3.6. Data Analysis Using MATLAB®

The local density of voids cannot be directly demonstrated from the 3-D surface view in Avizo®, thus in order to obtain the porosity map of the specimens, the labels of the composite and the voids were imported into MATLAB® for further analysis. The labels were projected in the X, Y and Z directions, so that the number of void voxels was summed up along each direction and colour mapped. The porosity maps (a colour map of porosity) in YZ, XY and XZ views were then analysed, in these low porosity was coloured in blue while higher porosity was coloured in green and red, so that the localisation of voids can be demonstrated. The programming code is attached in the Appendix.

5. Results and Discussion

5.1. Voids in Composite Panels

The X-ray CT results of the panels, showing the morphology, content and distribution of voids, are shown and discussed in this section.

5.1.1. Effect of Thresholding on the Determination of Voids

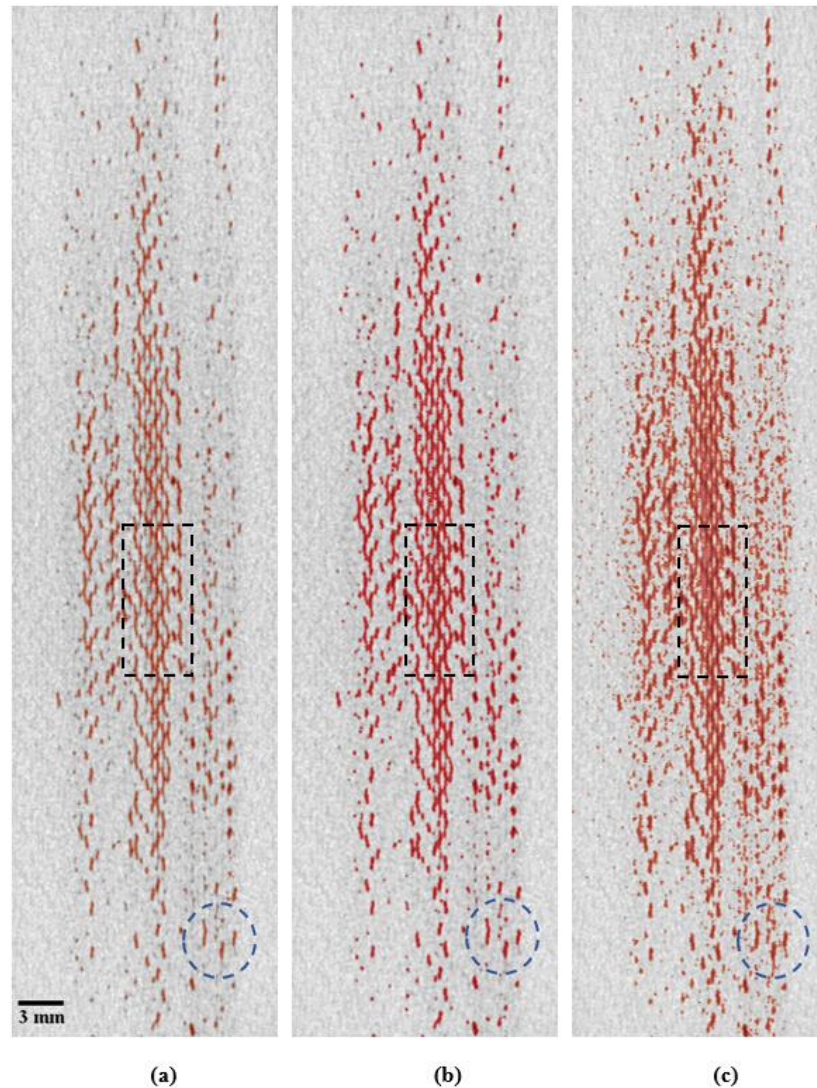


Figure 5.1: A typical XY slice image of the composite specimen with voids. The void region is segmented using three different threshold ranges and highlighted in red. The grey value range is (a) 0 to 12, (b) 0 to 15 and (c) 0 to 18, respectively.

In the characterisation of voids using X-ray CT, the determination of thresholding values is of great importance. This is because the choice of thresholding values will directly affect the

segmentation of voids, which will influence the determination of the amount and morphology of the voids inside the composite materials. In this work, the segmentation in all the datasets strictly follows the chosen thresholding range. Figure 5.1 shows a typical slice image with voids segmented using different thresholding values.

As mentioned in the literature review in section 2.4, the X-ray absorption capabilities of different materials are varied. In the X-ray CT data after reconstruction, the region that absorbs fewer X-rays appears darker. In the composite panels air and volatiles are entrapped in the regions where resin has not wetted out, thus in these void regions the X-ray absorption is less than the other parts of the composite. In the X-ray CT scans, the voids appear to be black and dark grey. In the 8-bit slice images, the grayscale value is from 0 to 255, so void regions are determined by the range 0 to x , where x needs to be determined in different samples. As shown in Figure 5.1, three different thresholding values have been used and the differences in the results show the effect of thresholding range on the segmentation of voids. The threshold ranges used in Figure 5.1a, b and c are 0 to 12, 0 to 15 and 0 to 18, respectively. A region with continuous voids is highlighted in a rectangular area in each of the images. As can be seen in Figure 5.1a some features in grey have not been selected and the width of the selected region is less than the observable width of the long voids. In Figure 5.1c some regions which are the bulk composite material have been selected and the segmented area is much larger than the void region. The same phenomenon has been observed in regions with distributed voids, highlighted in a circle. Using the range 0 to 12 as the threshold, the small dotted voids cannot be selected, while using the range 0 to 18 noisy voxels with interference signal have been selected. As shown in Figure 5.1b, the void area has been precisely selected using the range 0 to 15. After the comparison of the results using these three different thresholding ranges, it is found that the range 0 to 15 is the most appropriate thresholding range in this dataset to segment void regions.

Although the same settings were used in all the scans, the grayscale values in different scans vary. This is because the conditions of the CT machine are not perfectly stable and the dimensions of the samples are not exactly the same. Therefore, in each CT dataset, the grayscale range used to segment voids needs to be determined separately to ensure that the

segmentation result is reliable and comparable. On the other hand, although the semi-automatic thresholding works well in most of the volume, in the regions with strong ring artefacts and near the surfaces of the specimens, manual correction is required to remove extra bulk composite that has been selected and to add void regions that are missing. The segmentation of all the datasets was performed strictly following the same procedures and efforts have been made to eliminate the effect of subjective judgement in order to maintain the consistency in segmentation and obtain comparable results in different panels.

As mentioned in Section 4.3.3.5, after thresholding the 'remove islands' function has been used to eliminate noisy regions with a size smaller than three voxels. The number three was chosen for two reasons. Firstly, the smallest feature detectable in X-ray CT is at least 2 to 2.5 times the voxel size (Taina *et al.*, 2008). This is because in one voxel containing two materials with different attenuation coefficients the attenuation value for this voxel is the averaged value and is not representative of the feature in this voxel, which is known as the partial volume effect (Ketcham and Carlson, 2001). Thus considering the image quality of the CT data in this project, features smaller than 3 voxels were considered not truly representative of the real structure. Secondly, as mentioned before, it has been found that the existence of spherical or irregular voids with a size larger than $100\mu\text{m}$ (≈ 3 voxels) will substantially affect the mechanical properties of the composite materials (Kas and Kaynak, 2005). Therefore, in this project, dark regions with more than three voxels are classified as voids and attention has been focused on these voids in composite panels. The study of these voids is significant as they affect the performance of the composite in structural applications.

5.1.2. Morphology of Voids

It has been found that the shapes of voids in three dimensions are critical to the mechanical performance of composite structures (Lambert *et al.*, 2012). Although the morphology of voids has been studied by many researchers using optical microscopy, the size and shape of the voids can only be observed in the plane that was sectioned for observation. The advantage of using X-ray CT imaging is that the 3-D morphology of voids can be visualised. It has been found that there are two types of void in the aramid fibre-epoxy composite panels as manufactured; spherical voids and elongated voids.

5.1.2.1. Spherical Voids

Spherical voids with diameters as large as around 500 μm have been observed in the panels and the voids are not uniformly distributed in the panels. As the volume consists of cubic voxels, the voids cannot be segmented as perfect spheres and most of the voids are spheroids. Figure 5.2 shows a small region of extracted void volume in sample A, where an individual void is highlighted in blue and visualised in three directions. Figure 5.2 a, b and c show the views in the XY, XZ and YZ planes, respectively, where such highlighted voids are of spheroidal shape. In CFRP composites, voids with diameters of 5 to 20 μm have been observed by Stone and Clarke (1975) and when the voids become larger they found that the typical shape becomes elongated and flat. Schilling *et al.* observed spherical voids with diameters ranging from 250 to 500 μm between yarns in S-2 glass fibre composites. Compared with their results, the spherical voids in the aramid composite have a relatively larger diameter than those in carbon fibre reinforced plastics (CFRP), and similar to those in glass fibre reinforced plastics (GFRP). It should be noted that spherical voids with smaller diameters might also exist in the panel, but were not detectable due to the voxel size.

The individual aramid fibre yarn in the composite panel is about 3 to 4 voxels thick. As the contrast between yarns and the matrix is very low, it is difficult to determine whether the voids are located inside the matrix or within the yarns from these datasets. Therefore, it is

believed that the spherical voids observed in this project are located between yarns. Long (2005) suggested that small voids are formed within yarns, while larger voids are formed in between the inter-tow gaps. As the VARI manufacturing method involves impregnating dry fabrics during the infusion process, the flows at macro-scale and micro-scale move simultaneously in the fabric in an unstable way. In this case, air and other gases tend to be trapped inter-tow and intra-tow during infusion and form spherical voids that are distributed loosely in the panel.

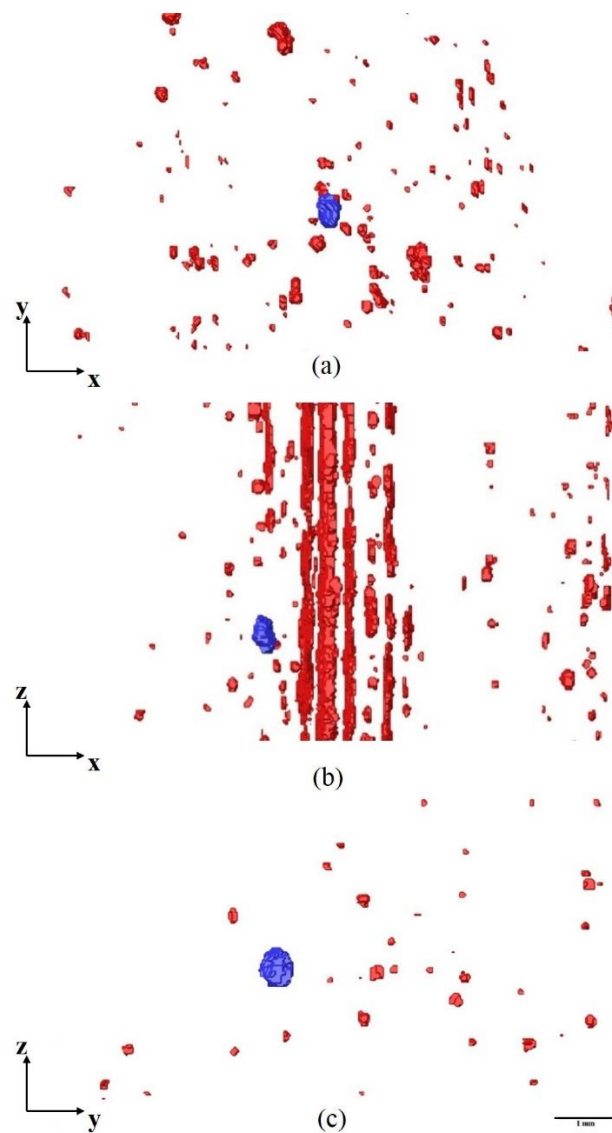


Figure 5.2: Extracted volume of the typical segmented voids. One spherical void is highlighted in blue, and the other surrounding voids are shown in red. Views of (a) XY, (b) XZ, and (c) YZ planes are shown.

5.1.2.2. Elongated Voids

Other than the distributed spherical voids, elongated and connected voids have been observed. Figure 5.3 shows typical extracted volumes of elongated voids. On the macro-scale, the observed elongated voids lie in three different directions, i.e. the horizontal direction as in Figure 5.3a, the vertical direction as in Figure 5.3b and at 45 °to the horizontal

direction as in figure 5.3c. As shown in Figure 5.3c, on the micro-scale the voids along the 45° direction are formed by the connection of short segments of voids, about 1mm long, along the vertical and horizontal directions.

These elongated voids are mostly connected in the YZ plane, which is the plane of the fabric layers, and sometimes connected in the through-thickness direction. Thus the void planes are overlapped in some regions. The continuous voids like these are concentrated in one (without through-thickness connection) or more layers (with through-thickness connection) in the panel. As discussed in Section 2.2.2.2, there are two competing driving forces for resin flow, the pressure gradient and the capillary effect. In regions where the capillary effect dominates, the resin flows faster in the yarns than in the channels between yarns. When the resin flow front in the yarns arrives at a junction, the resin percolates in the transverse direction. If the transverse flows meet each other, relatively easy resin path forms. Therefore, the following resin will tend to pass via the same route, and the channel in between might be enclosed at the two ends, forming elongated voids. It is believed that these connected voids are mostly located between layers. In these regions, the in-plane flow is faster than the through-thickness flow, so continuous dry areas have been enclosed between layers.

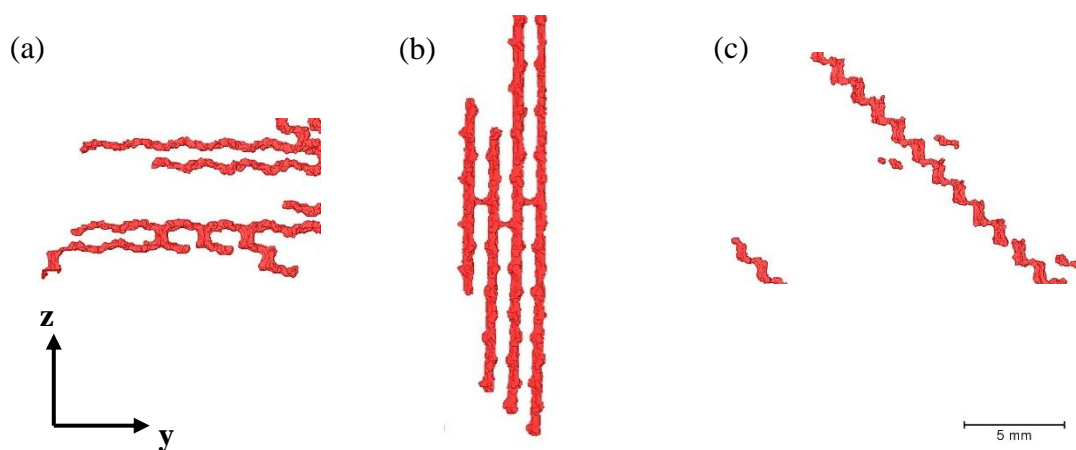


Figure 5.3: XY view of extracted volumes of the typical segmented voids. The elongated voids are highlighted in red, lying in (a) the Y direction, (b) the Z direction and (c) at 45° to the Y direction.

5.1.3. Void Content in the Composite Panels

Each voxel in the X-ray CT data can be segmented and assigned into one label, so the internal void region once labelled as a void cannot be added to the composite label. Therefore, the total volume of the composite panel is the sum of the volumes of composite labels and void labels. The void content can then be calculated by dividing the void volume by the total composite volume. For each panel, the void and composite volumes in all of the nine specimens have been summed for calculation.

Table 5.1: Void content of the composite panels measured using the CT data.

Sample	20	35	50	93	168	SO	DO	SM	DM	CR	Void Content
A											0.84%
B											0.39%
C											0.97%
D											0.65%
E											0.71%
F											1.62%
G											0.91%
H											1.75%

Table 5.1 shows the void content for each panel. It can be seen that the void content here is less than the values in published literature. This is because that the void content here is the volume fraction of the voids with a size larger than 3 voxels. Smaller voids that cannot be detected due to the relatively large voxel size restricted by the size of the samples and this accounts for the difference in the void content obtained. The effect on void content of panel thickness, fabric properties and different manufacturing techniques will be discussed in the following sections.

5.1.4. Void Distribution in the Composite Panels

In order to study the distribution of voids in the panel, the 3-D X-ray CT data have been presented in 2-D porosity maps using MATLAB[®]. Figures 5.4 to 11 show the top view of the porosity maps of sample A-H. Each panel includes nine parts, numbered from 1 to 9.

In general in all the panels, continuous elongated voids are concentrated in part 8. Spherical voids are observed to be distributed in the upper parts of the panels. Vila *et al.* (2014) measured the local pressure in the panel during resin infusion, and they found that the fluid pressure decreases with increasing distance from the inlet tube. At a certain position in the panel, the pressure gradient driving force competes with the capillary effect (Rudd *et al.*, 1997). In regions where the pressure is less, the capillary effect dominates. Therefore, the observation of large voids near the outlet side can be due to the enclosed voids within inter-tow gaps and between layers induced by the locally overwhelming capillary effect.

The void distribution in each panel will be discussed in detail along with the fabric properties and the manufacturing techniques in latter sections.

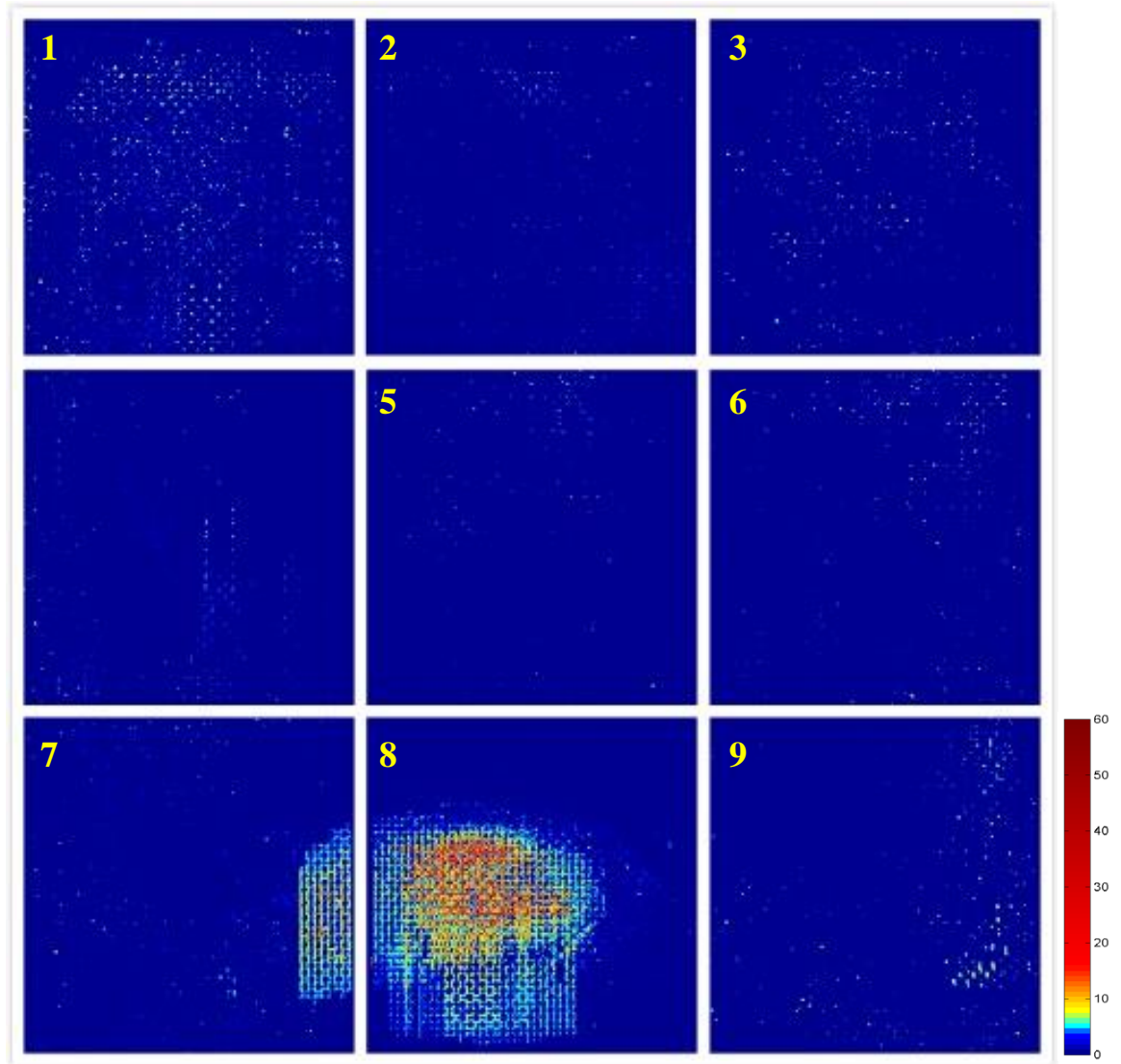


Figure 5.4: The YZ view porosity map of sample A.

Sample	20	35	50	93	168	SO	DO	SM	DM	CR	Void Content
A											0.84%

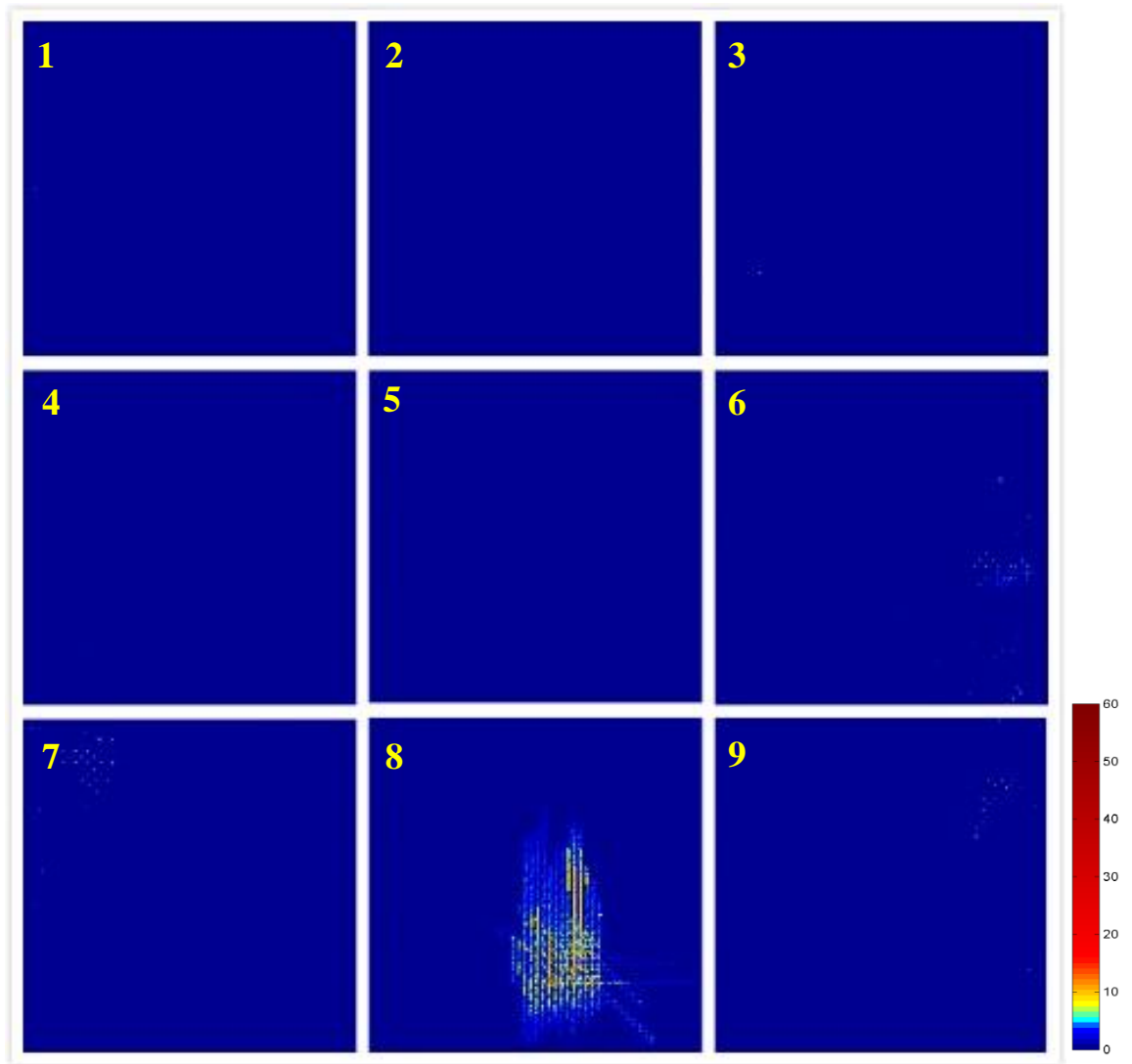


Figure 5.5: The YZ view porosity map of sample B.

Sample	20	35	50	93	168	SO	DO	SM	DM	CR	Void Content
B											0.39%

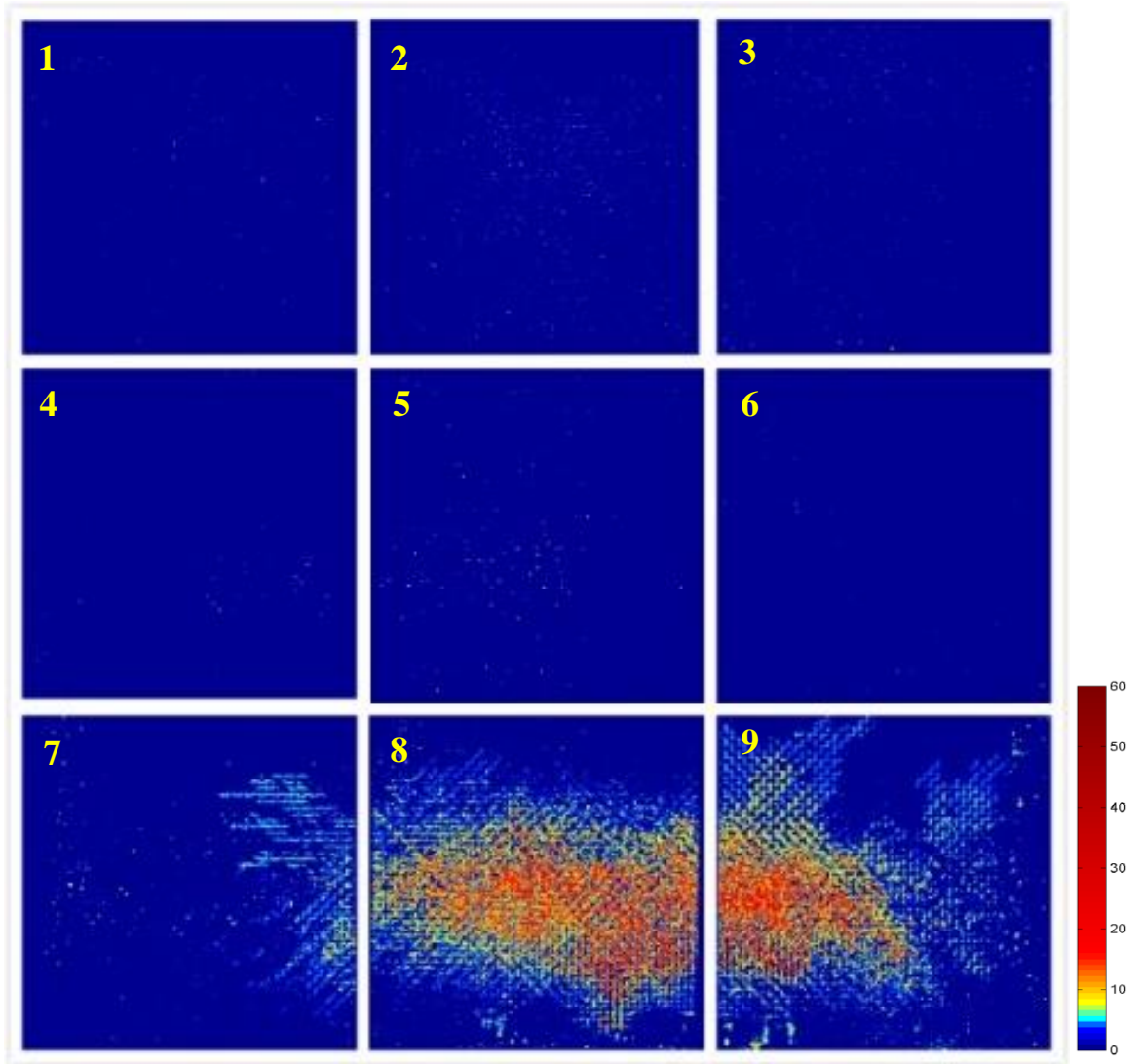


Figure 5.6: The YZ view porosity map of sample C.

Sample	20	35	50	93	168	SO	DO	SM	DM	CR	Void Cont
C											0.97%

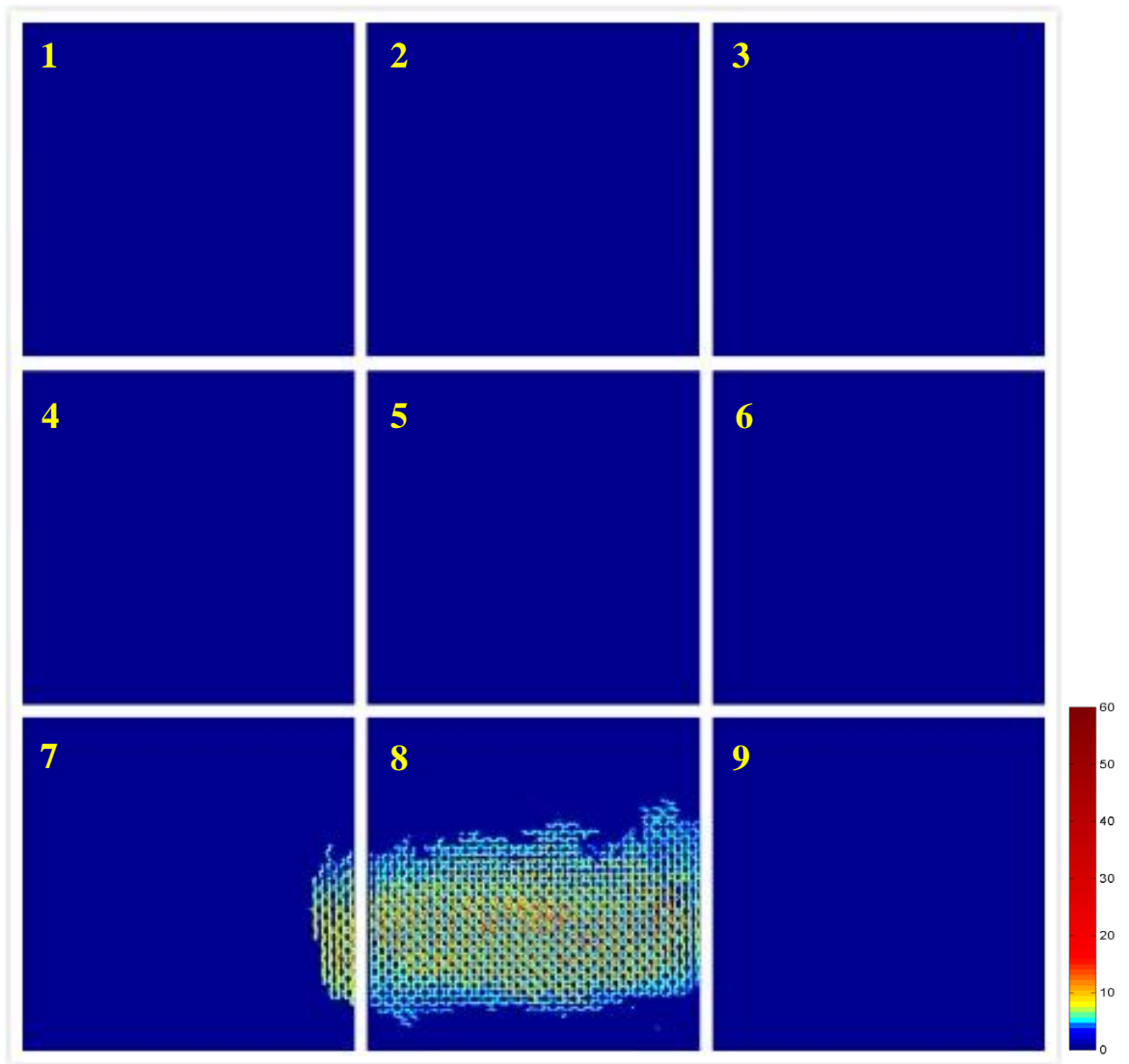


Figure 5.7: The YZ view porosity map of sample D.

Sample	20	35	50	93	168	SO	DO	SM	DM	CR	Void Content
D											0.65%

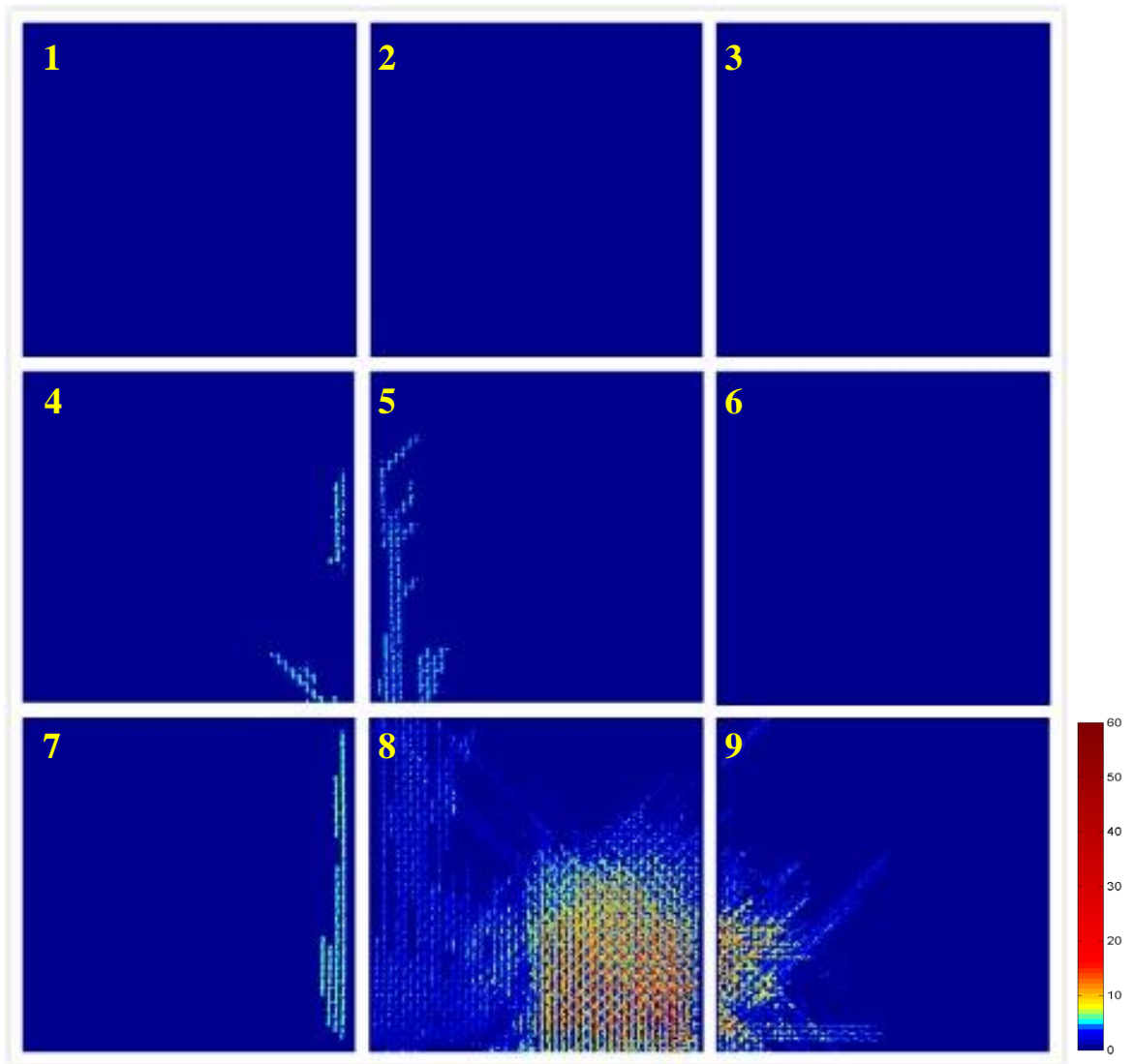


Figure 5.8: The YZ view porosity map of sample E.

Sample	20	35	50	93	168	SO	DO	SM	DM	CR	Void Content
E											0.71%

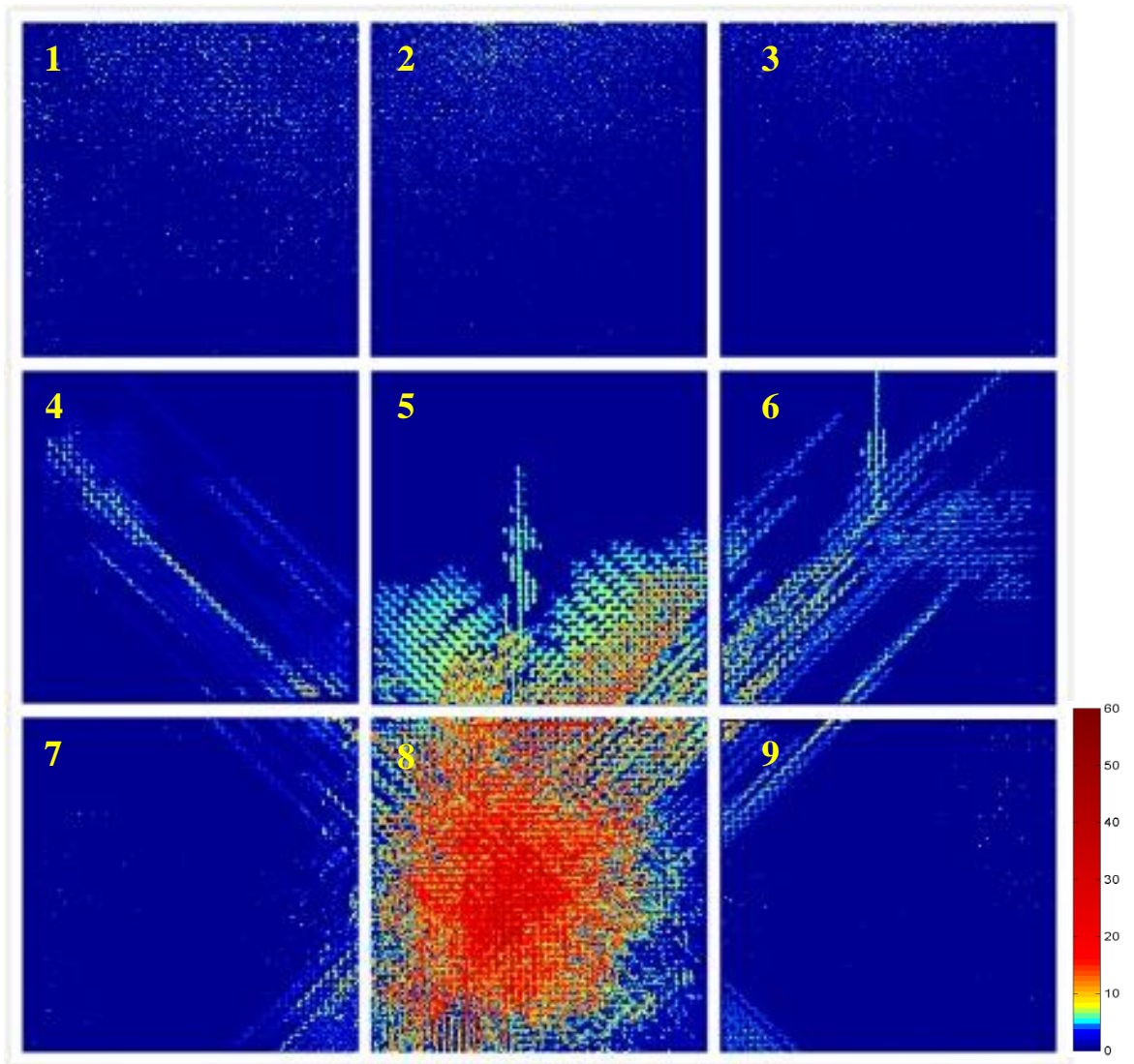


Figure 5.9: The YZ view porosity map of sample F.

Sample	20	35	50	93	168	SO	DO	SM	DM	CR	Void Content
F											1.62%

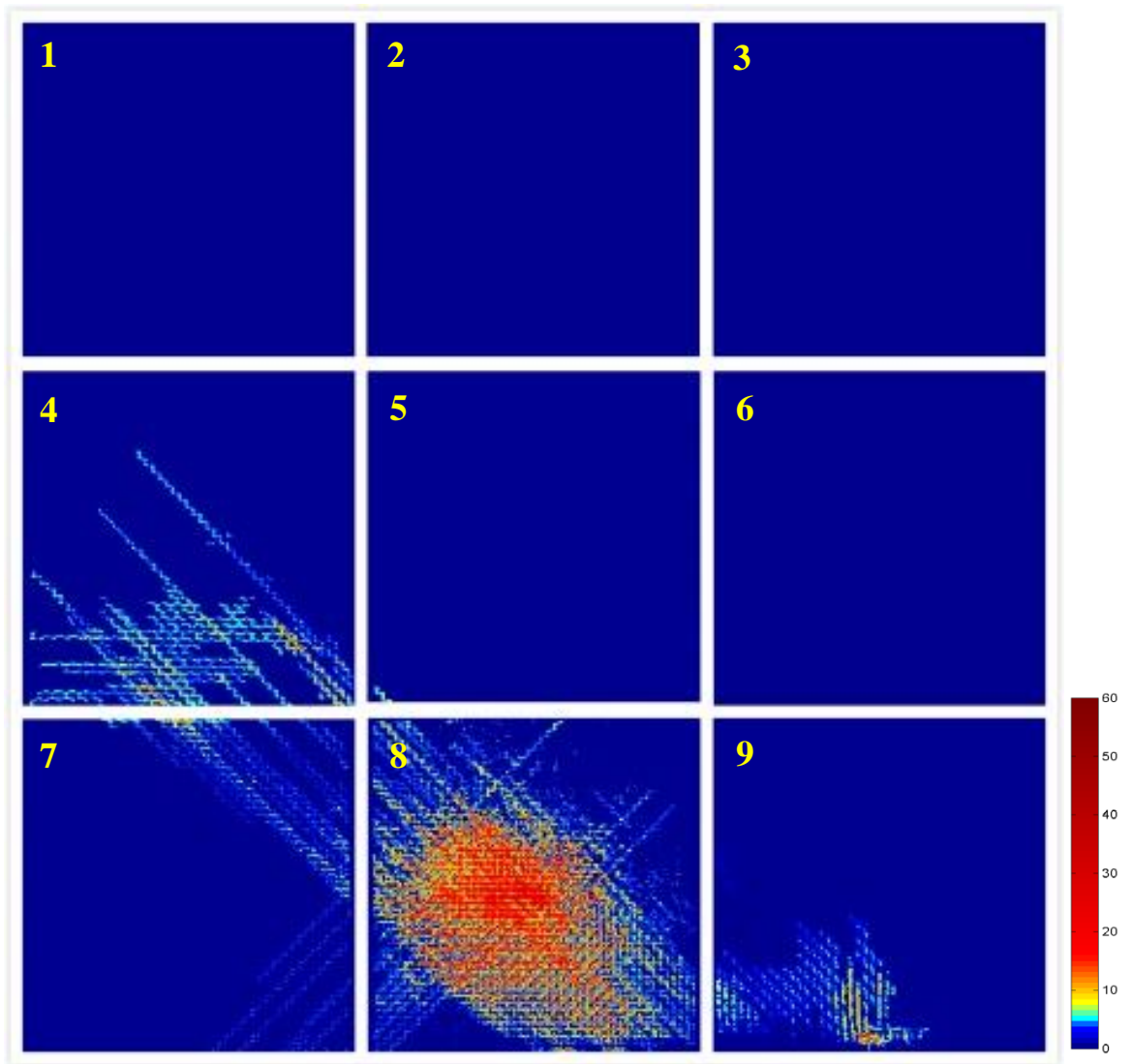


Figure 5.10: The YZ view porosity map of sample G.

Sample	20	35	50	93	168	SO	DO	SM	DM	CR	Void Content
G											0.91%

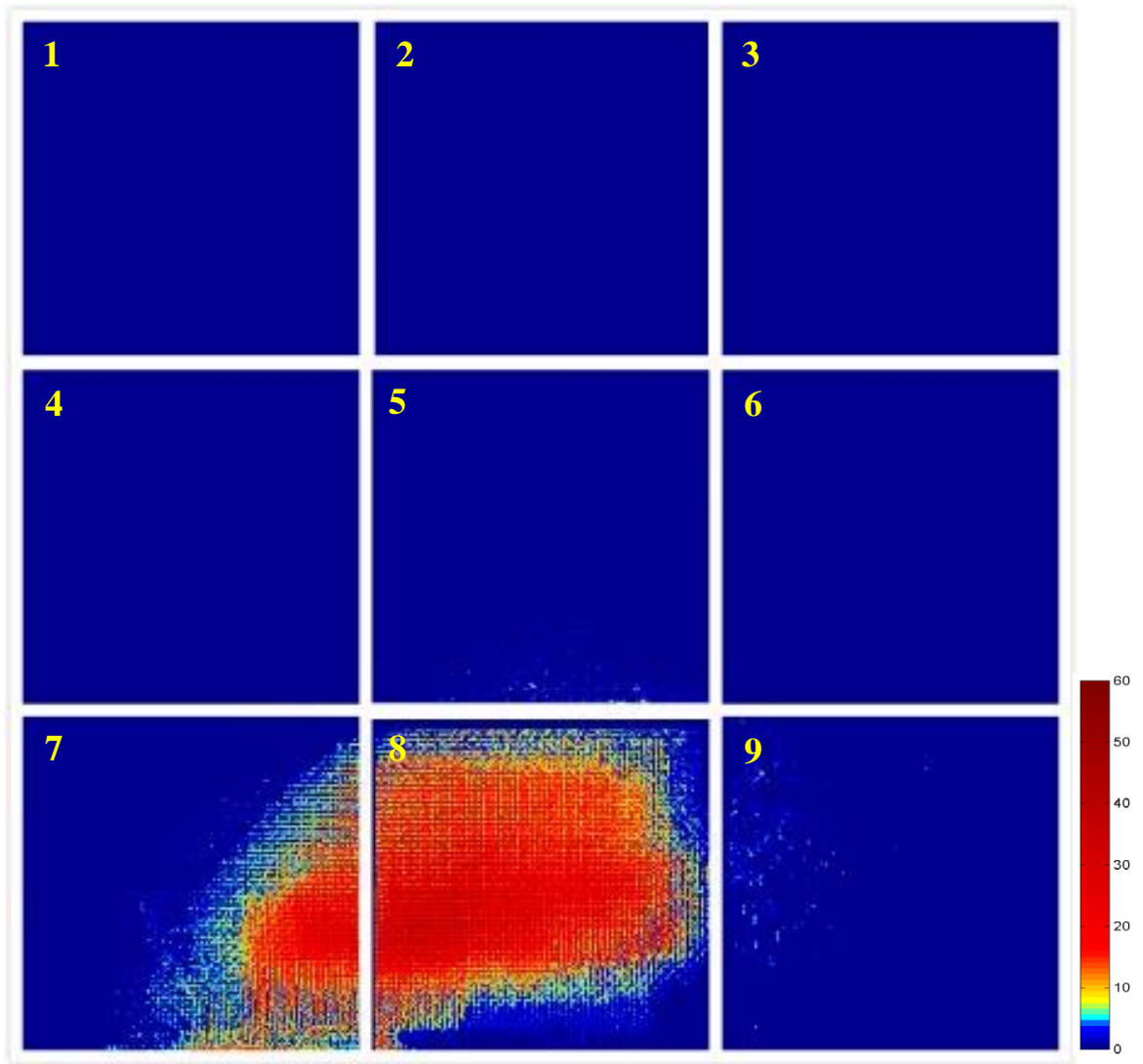


Figure 5.11: The YZ view porosity map of sample H.

Sample	20	35	50	93	168	SO	DO	SM	DM	CR	Void Content
H											1.75%

5.2. Effect of Textile Reinforcement on Composite Panel Quality

Based on the X-ray CT results of the panels, the effect of the structure and property of the reinforcement has been investigated.

5.2.1. Effect of the Number of Fabric Layers

The first comparative study is to reveal the effect of the number of fabric layers on the panel quality. Table 5.2 shows the properties of the samples for comparison. Samples D, E and F consist of 20, 35 and 50 layers of fabrics, respectively, with the other processing parameters kept unchanged. As can be observed in the X-ray CT projected images, the majority of the voids in the three panels exist in the elongated form and some distributed spherical voids have been found in the 50-layer panel. The projected void area increases with increasing numbers of fabric layers. From the quantitative point of view, the void content increases with additional layers of fabric. Based on the calculation using segmented X-ray CT volumes, the void contents in the panels are 0.65%, 0.71% and 1.62%, respectively. The difference in porosity in 20-layer and 35-layer panels is relatively small, but the increase in porosity value in the 50-layer panel is rather significant. Similar observations can be obtained in the other sample group – samples B and C.

Table 5.2: Properties of samples for the study of the effect of the number of fabric layers.

Group	Sample	Number of fabric layers	Void content
Group 1	D	20	0.65%
	E	35	0.71%
	F	50	1.62%
Group 2	B	35	0.39%
	C	50	0.97%

With the increase of the number of fabric layers, the number of nests formed between yarns will increase, thus more air tends to be trapped in these nests. The rise in the number of layers can also give rise to a more complex fabric architecture, which makes the expelling of air more difficult. In addition, with the increase in the number of layers, the tendency for non-uniform stacking is increased. Long (2005) suggested that in regions where the stacking of fabrics is not uniform and the compaction between layers is relatively low, resin flow is favourable in-plane and the transverse permeability is relatively low. Therefore, the more continuous elongated voids observed in 50-layer panels are induced by the low transverse permeability. Furthermore, in this project the fabrics used are all plain woven and there is no yarn in the Z direction to accelerate the resin flow, thus the increase in thickness will make the flow in the through-thickness direction more difficult.

5.2.2. Effect of Fabric Linear Density

Two yarns with different linear densities have been used to weave the reinforcing fabrics. The effect of yarn linear density has been studied by analysing the X-ray CT data, as shown in Table 5.3. The tightness of the two fabrics has been calculated according to Equation 4.4. The warp tightness (equal to weft tightness in plain weave fabric) of the 168Tex fabric is 0.3275, and that of the 93Tex fabric is 0.3297. The void content of the 93Tex panel (sample H) is 1.75%, while for the 168Tex panel (sample F) it is 1.62%. When it comes to the void distribution condition, the projected void area in sample F is relatively large while in sample H voids are more localised. The causes of the difference in distribution will be presented later when discussing the manufacturing techniques.

Table 5.3: Properties of samples for the study of the effect of fabric properties.

Sample	Linear density (Tex)	Thread density (ends/cm)	Warp (weft) tightness	Void content
F	168	8.5	0.3275	1.62%
H	93	11.5	0.3297	1.75%

There is not much difference in the void content of these two panels, and the 168Tex panel

has slightly fewer voids. It is found that the tightness of these two fabrics is very similar. With similar tightness, the 168Tex fabric with thread density of 11.5 ends/cm is finer, while the 93Tex with a thread density of 8.5 ends/cm is coarser. In the finer fabrics there are more junction points where the weft and warp yarns cross, therefore the main resin flow will be diverted into more sub-flows, which will slow down the main flow rate and void expelling rate and might result in more voids in the final panel. These observations are similar to the modelling work done by Amico (2000). He found that the distance between junctions affects the resin flow rate. In addition, the increase in thread density will result in more nests, thus increases the chances for air to be trapped, which is similar to the condition of increasing the number of fabric layers.

As the infusion process is affected by many factors, and a little distortion of the fabrics will result in local permeability changes, thus the observed trends need to be confirmed with more experiments in the future.

5.3. Effect of Modified VARI Methods on Thick Composite Panel Quality

In this section, the effect of the three modifications in the manufacturing process will be presented. The panel quality, before and after modification, will be discussed according to the void content and distribution.

5.3.1. Effect of Top and Bottom Meshes

It is found that the use of double meshes is effective. As shown in Table 5.4, the void content of sample A is 0.84%, while in sample B it is 0.39%. The decrease in porosity is obvious. As shown in Figure 5.4, other than many continuous voids in part 8, there are small distributed voids in the other parts of sample A. However, in sample B the voids concentrate in part 8 and the projected area is relatively small as seen in Figure 5.5.

Figure 5.12 shows the XZ view porosity maps of part 8 in these two panels. It can be observed that in sample A, voids are located close to the bottom surface of the panel. In contrast, in sample B, the voids are lying in the middle of the panel thickness, which indicates the similar effect of the top and bottom meshes. Resin can be quickly distributed on both surfaces of the panel, and percolates in the thickness direction simultaneously, resulting in more effective wetting out of the fabrics. Therefore, it has been observed that the addition of resin flow media at the bottom surface of the panel moves the void region closer to the centre of the panel thickness and reduces the amount of voids.

Table 5.4: Properties of samples for the study of the effect of additional mesh.

Sample	Mesh	Void content
A	Single	0.84%
B	Double	0.39%

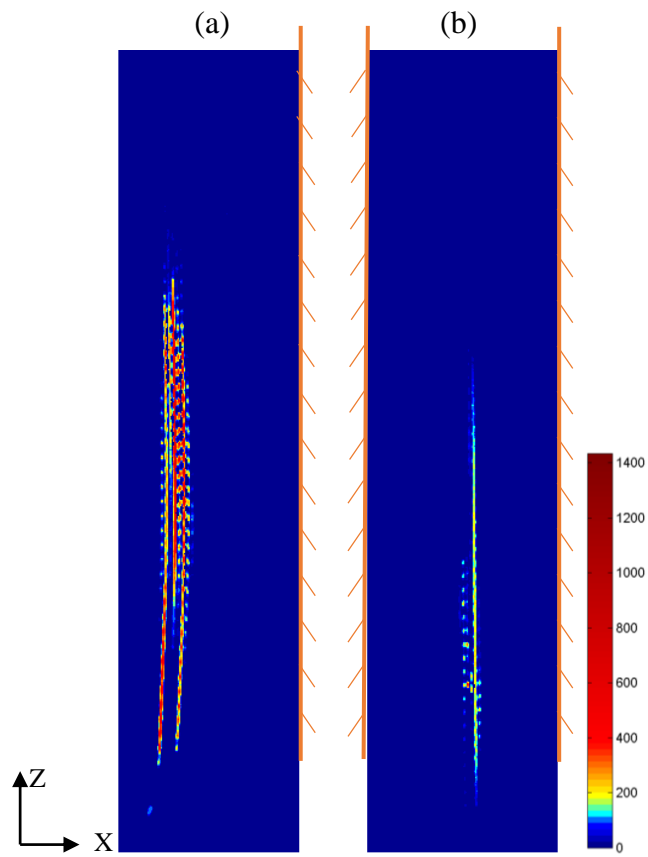


Figure 5.12: XZ view porosity maps of part 8 in (a) sample A and (b) sample B, showing the void distribution through the panel thickness. Meshes are demonstrated as the orange layer on the sample surfaces.

5.3.2. Effect of Two Outlets

The influence of double outlets on the quality of panels has been investigated by adding a second outlet tube symmetrical to the initial one relative to the centre of the bottom edge. In the composite panels manufactured in this project, samples E seen in Figure 5.8 and B seen in Figure 5.5, and samples F seen in Figure 5.9 and C seen in Figure 5.6 can be compared to reveal the effect of double outlets. Sample E and sample F were infused using one outlet,

while sample B and sample C were infused using two outlets.

Table 5.5: Properties of samples for the study of the effect of additional outlet.

Group	Sample	Outlet	Void content
Group 1	E	Single	0.71%
	B	Double	0.39%
Group 2	F	Single	1.62%
	C	Double	0.97%

Table 5.5 shows the properties of these samples. It can be concluded that the void content of single outlet (SO) panels is less than that of double outlet (DO) panels. As can be seen in the porosity maps, part 8 is the region with the majority of the voids in all of the four panels. It has been found that the projected void area in the YZ plane in the SO panels is smaller. In addition, the connected void region is constrained in the bottom row in the the DO panels, whereas in SO panels these voids have extended to the centre row.

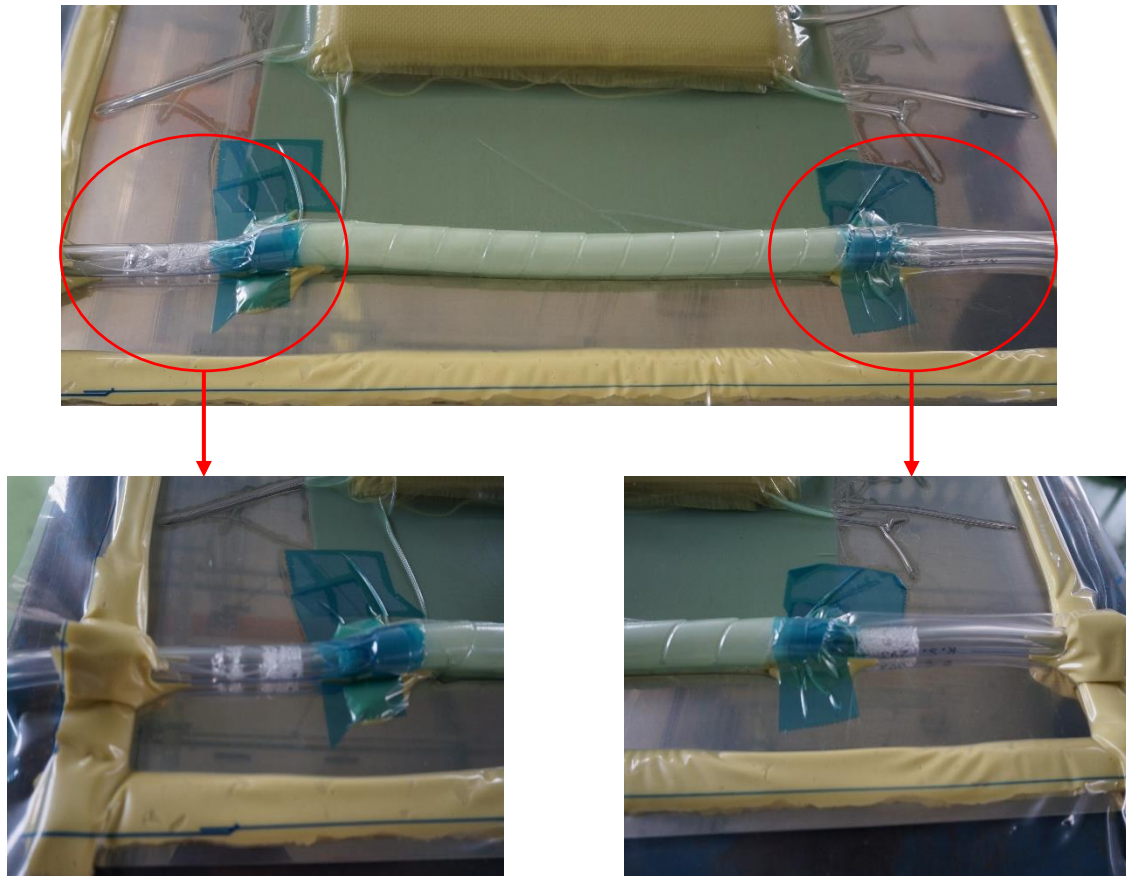


Figure 5.13: The image of the panel and the outlet tubes in the infusion stage. Air bubbles came out of the two outlet tubes simultaneously.

With the addition of another outlet, the resin flow front is found to be more parallel to the panel bottom edge and the resin and voids came out of the two outlets evenly and simultaneously, as shown in Figure 5.13. The extra outlet provides another exit for voids to be expelled, so that it becomes easier for entrapped gas to be driven out. This might account for the smaller void content and area. As the entrapped air is driven to move from the top to the bottom edge of the panel progressively and more voids can be expelled in DO panels during a certain time due to the extra exit, the void area has moved closer to the bottom in DO panels than in SO panels. Therefore, the addition of an outlet tube can improve the quality of panels to a certain extent.

5.3.3. Effect of Resin Level in the Inlet Tube

The effect of eliminating the air left in the inlet tube before infusion has been investigated. In the infusion process of sample F the clamp closing the inlet tube was opened when resin infusion started, so that the air left in the inlet tube between the clamp and the tube end was drawn into the vacuum bag before resin. In contrast, in the infusion process of sample G of which the inlet tube was carefully cut in the resin, thus there should be no extra air drawn into the vacuum bagging system when resin infusion begins. As shown in Table 5.6, it is found that the void content of sample G is less than that of sample F, which is due to the elimination of the air in the inlet tube.

Table 5.6: Properties of samples for the study of the effect of cutting the inlet tube in resin.

Sample	Inlet tube	Void content
F	Normal	1.62%
G	Cut in resin cup	0.91%

Figure 5.9 and 5.10 show the porosity maps of sample F and sample G. As can be seen, in sample G, the voids are formed in part 4, 7, 8 and 9, and concentrate in part 8. Compared with sample F, in sample G the void area in the YZ plane is smaller and closer to the bottom edge, and the major difference is in part 5 and 6 where little voidage has been observed. Considering the changes in void content and distribution, it seems that the reduction of the amount of air introduced into the vacuum bag at the beginning of infusion reduces the final void content in the panel and shrinks the flawed region.

5.4. Validation of the CT Results by Ultrasonic C-Scan

As ultrasonic C-scan is a widely used NDT technique, it can be used to assess the internal defects in composite materials (Geier, 1994). In this project, ultrasonic C-Scan has been employed as a non-destructive method to analyse voids, and the scan results have been compared with the X-ray CT results. Typical ultrasonic C-scan images are shown in Figure 5.14.

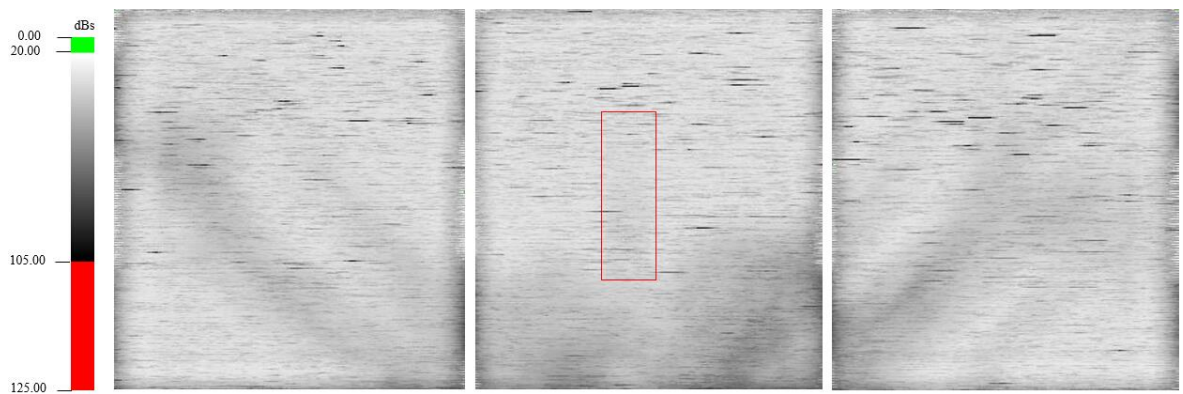


Figure 5.14: Ultrasonic C-scan images of three specimens from sample F and the colour spectrum of the dB losses. The set range is 20-105dB.

Three specimens are all cut from the sample F composite panel as described in Section 4.3.1. In the ultrasonic C-scan experiment, these specimens were scanned at one time with the same setting parameters. In these images the extent of ultrasonic attenuation is demonstrated in different colours, and the black and dark coloured regions are determined as voids. It should be noted that, the horizontal short lines in black are “noisy” pixels. From the ultrasonic C-scan images, the existence and the approximate position of voids can be observed. However, the result can only demonstrate the superimposed effect of voids in the cross-sections, and cannot provide sufficient information to characterise the location of voids in the thickness direction.

In the X-ray CT experiment, the information in the YZ planes throughout the composite panel can be projected into a 2-D plane so that the void voxels can be calculated and imaged.

This is realised by analysing the segmented X-ray CT volume in MATLAB[®]. The detailed code will be presented in the Appendix. The typical projected porosity maps are shown in Figure 5.15.

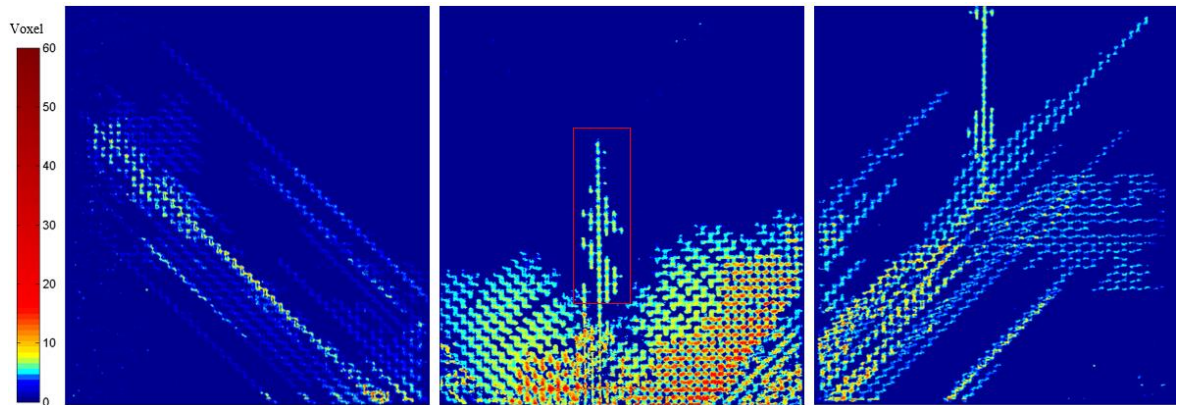


Figure 5.15: The projected porosity map calculated based on segmented X-ray CT volumes. The number of void voxels is displayed in different colours.

The three specimens demonstrated in Figure 5.15 are exactly the same specimens in the ultrasonic C-scan images in Figure 5.14. Similar in-plane void distribution has been observed. The different colours represent the total number of void voxels in this position along the X direction. As the 3-D X-ray CT volumes consist of a stack of 2-D slice images, the number of voids can be calculated by summing the information in these slices. In most of the area, voids occur in around 0 to 10 slices through the specimen thickness, in the dark red area in the centre voids exist in dozens of slices.

The results from the two characterisation techniques can be compared in the highlighted rectangular region. As can be seen, the relatively narrow and elongated voids have not been shown in the ultrasonic C-scan image and only light grey a little darker than the background can be seen. In addition, the borders of the void area can hardly be distinguished. In contrast, the X-ray CT result is more detailed. In the C-scan imaging, the probe with the smallest frequency is used and the finest grid size is set, the change of void volume superimposed along the thickness direction still cannot be demonstrated. Only void regions with good continuity and large area can be observed. This might be because that the void region is relatively small and the ultrasonic attenuation is not very obvious. Kastner *et al.* (2010)

have found that the ultrasonic testing of voids can not only be affected by the experimental settings but also be influenced by the size, shape and distribution of voids in the sample. Although ultrasonic C-scan can approximately represent the superimposed distribution of voids in the YZ planes, compared with the capability of assessing other internal defects (such as delamination and impact induced damage) the assessment of small voids is not very effective. To assess voids in composite materials, the result obtained from ultrasonic C-scan itself is not reliable, it is thus necessary to use alternative techniques.

The assessment of voids using ultrasonic C-scan and X-ray CT techniques has been compared. It is found from the images that good correlation can be observed in the general distribution of the majority of the voids. The ultrasonic C-scan result can confirm the X-ray CT result to some extent. These two methods can both be used as qualitative characterisation techniques and the X-ray CT result is relatively better. Nevertheless, X-ray CT can not only be employed to assess voids qualitatively but also demonstrates a good capability for quantitative analysis.

6. Conclusions and Future Work Recommendations

6.1. Conclusions

In this research, military-use thick Twaron®-epoxy composite materials have been studied with the aim of improving their quality by reducing voids formed in the manufacturing process.

The comparison experiments have been designed for two purposes. Firstly, the influence of reinforcement on voids has been investigated. It shows that the increase of the number of layers brings in greater uncertainties in the stacking arrangement between layers, whilst more resistance occurs in the through-thickness resin flow. This will inevitably lead to a rise in void content and broader void distributions in the panel. It is also found that, when the tightness of two fabrics are similar, the void content is inversely proportional to the threading density, which might be because it is easier for air to be trapped in finer structures.

Secondly in the work, the effect of different modifications to the VARI manufacturing process has been comparatively studied. The change to the inlet tube position in the resin has been able to eliminate the air sucked into the vacuum bag, therefore the formation of voids has been controlled effectively at the beginning of the infusion process. It is found that the void content using this method is lower than that using the conventional method. The use of double meshes also proves to be effective in void reduction. With the aid of infusion from both top and bottom meshes, the void distribution in the thickness direction becomes more centralised into the middle layers. Another modification proposed is the use of double outlets. The test results show that in the panels that are made with this method, along with the reduction in porosity, there is a trend for voids to move closer to the bottom edge, near the outlet spiral tube.

In this project, the X-ray CT technique shows promising capabilities for 3-D characterisation, which has been used as a major method for qualitatively and quantitatively assessing the voids in the composite panels. Meanwhile, ultrasonic C-scan

technique has been used for studying the 2-D void distribution.

In summary, from this study the voids in thick Twaron®-epoxy composite panels have been comprehensively studied and modifications to the VARI manufacturing process have been proposed and confirmed to be effective in constraining the amount and distribution of voids.

6.2. Future Work Recommendations

This study has made a contribution to the understanding of distribution and morphology of voids formed in the VARI process, but the number of samples is limited to summarise the trend. This is partly because of the time-consuming X-ray CT data analysis. It is necessary to conduct repeated experiments to minimise the influence of sample variations. Moreover, as the formation of voids is affected by many factors, such as the properties of the fibre, the structure of the reinforcement, and the properties and curing conditions of the resin system, future studies on voids should consider such factors more broadly. Several suggestions are proposed for future work, including:

- Modelling of the resin infusion process

The resin infusion process should be simulated using software such as ANSYS or RTM-worx based on the experimental results, so that the resin flow process can be monitored and analysed. In thick composite panels, the complex stacking arrangement of fabrics should be discussed. It is of importance to establish stacking models for different fabrics and study the resin flow behaviour in different structures.

- Experimental study on different fabric architecture

It is also an interesting subject to study the resin infusion process by changing the type and architecture of the fabrics. The difference in the resin infusion process in 2-D and 3-D woven fabrics needs to be studied, as the use of 3-D fabrics will significantly increase the

through-thickness permeability.

- Experimental study on different shapes of composites

In this project, the study of voids is based on the simply-shaped flat composite panels. However, one of the advantages of the VARI method is its good adaptability to complex structures, thus it is of great importance to study the voids in complex structured composite components.

These recommendations for future work are proposed to achieve the ultimate goal of improving the quality and reliability of composite materials by reducing voids based on the study on void formation mechanisms and distribution. The improvement in composite quality is of great importance to the wider application of composite materials.

References

Adams, R. and Cawley, P. 1988. A review of defect types and nondestructive testing techniques for composites and bonded joints. *NDT international*, 21 (4), 208-222.

Amico, S. C. 2000. *Permeability and capillary pressure in the infiltration of fibrous porous media in resin transfer moulding*. University of Surrey.

ASTM D3171 Methods for Constituent Content of Composite Materials.

Baker, A., Gunnion, A. J. and Wang, J. 2015. On the Certification of Bonded Repairs to Primary Composite Aircraft Components. *The Journal of Adhesion*, 91 (1-2), 4-38.

Baruchel, J., Buffiere, J.-Y. and Maire, E. 2000. *X-ray tomography in material science*.

Birt, E. and Smith, R. 2004. A review of NDE methods for porosity measurement in fibre-reinforced polymer composites. *Insight-Non-Destructive Testing and Condition Monitoring*, 46 (11), 681-686.

Boh, J., Louca, L., Choo, Y. and Mouring, S. 2005. Damage modelling of SCRIMP woven roving laminated beams subjected to transverse shear. *Composites Part B: Engineering*, 36 (5), 427-438.

Bowles, K. J. and Frimpong, S. 1992. Void effects on the interlaminar shear strength of unidirectional graphite-fiber-reinforced composites. *Journal of Composite Materials*, 26 (10), 1487-1509.

Br éard, J., Henzel, Y., Trochu, F. and Gauvin, R. 2003. Analysis of dynamic flows through porous media. Part I: Comparison between saturated and unsaturated flows in fibrous reinforcements. *Polymer composites*, 24 (3), 391-408.

Brooks, R. A. and Di Chiro, G. 1976. Beam hardening in x-ray reconstructive tomography. *Physics in medicine and biology*, 21 (3), 390.

Centea, T. and Hubert, P. 2011. Measuring the impregnation of an out-of-autoclave prepreg by micro-CT. *Composites Science and Technology*, 71 (5), 593-599.

Chambers, A., Earl, J., Squires, C. and Suhot, M. 2006. The effect of voids on the flexural fatigue performance of unidirectional carbon fibre composites developed for wind turbine applications. *International Journal of Fatigue*, 28 (10), 1389-1398.

Cilley, E., Roylance, D. and Schneider, N. Methods of fiber and void measurement in graphite/epoxy composites. Composite Materials: Testing and Design (Third Conference), ASTM STP, 1974. 237-249.

- Correia, N., Robitaille, F., Long, A., Rudd, C., Simacek, P. and Advani, S. G. 2004. Use of resin transfer molding simulation to predict flow, saturation, and compaction in the VARTM process. *Journal of fluids engineering*, 126 (2), 210-215.
- Costa, M. L., De Almeida, S. F. M. and Rezende, M. C. 2001. The influence of porosity on the interlaminar shear strength of carbon/epoxy and carbon/bismaleimide fabric laminates. *Composites Science and Technology*, 61 (14), 2101-2108.
- Darcy, H. P. G. 1856. *D ètermination des lois d'écoulement de l'eau à travers le sable. Fontaines publiques de la ville de Dijon.*
- Davis, G. and Elliott, J. 2006. Artefacts in X-ray microtomography of materials. *Materials science and technology*, 22 (9), 1011-1018.
- De Almeida, S. F. M. and Neto, Z. d. S. N. 1994. Effect of void content on the strength of composite laminates. *Composite structures*, 28 (2), 139-148.
- Douarche, N., Rouby, D., Peix, G. and Jouin, J. 2001. Relations between X-ray tomography, density and mechanical properties in carbon-carbon composites. *Carbon*, 39 (10), 1455-1465.
- Feldkamp, L., Davis, L. and Kress, J. 1984. Practical cone-beam algorithm. *JOSA A*, 1 (6), 612-619.
- Gay, D. 2014. *Composite materials: design and applications*, CRC press.
- Geier, M. H. 1994. *Quality handbook for composite materials*, Chapman and Hall.
- Gloria, A., Ronca, D., Russo, T., D'Amora, U., Chierchia, M., De Santis, R., Nicolais, L. and Ambrosio, L. 2010. Technical features and criteria in designing fiber-reinforced composite materials: from the aerospace and aeronautical field to biomedical applications. *Journal of applied biomaterials & biomechanics: JABB*, 9 (2), 151-163.
- Goodwin, A., Howe, C. and Paton, R. The role of voids in reducing the interlaminar shear strength in RTM laminates. Proceedings of the 11th International Conference on Composite Materials: Composite Processing and Microstructure, 1997. Woodhead Publishing, 11.
- Goren, A. and Atas, C. 2008. Manufacturing of polymer matrix composites using vacuum assisted resin infusion molding. *Archives of materials Science and Engineering*, 34 (2), 117-120.
- Gourichon, B., Binetruy, C. and Krawczak, P. 2006. A new numerical procedure to predict dynamic void content in liquid composite molding. *Composites Part A: applied science and manufacturing*, 37 (11), 1961-1969.

- Gourichon, B., Deléglise, M., Binetruy, C. and Krawczak, P. 2008. Dynamic void content prediction during radial injection in liquid composite molding. *Composites Part A: applied science and manufacturing*, 39 (1), 46-55.
- Hahn, H. T. and Tsai, S. W. 1980. *Introduction to composite materials*, CRC Press.
- Herman, G. T. 1979. Image reconstruction from projections. *Image Reconstruction from Projections: Implementation and Applications*, 1.
- Hounsfield, G. N. 1973. Computerized transverse axial scanning (tomography): Part 1. Description of system. *The British journal of radiology*, 46 (552), 1016-1022.
- Hull, D. and Clyne, T. 1996. *An introduction to composite materials*.
- ISO 1172:2002 Textile-glass-reinforced plastic, prepregs, moulding compounds and laminates - Determination of the textile-glass and mineral-filler content - Calcination methods.
- ISO 7822:1990 Textile glass reinforced plastics -- Determination of void content -- Loss on ignition, mechanical disintegration and statistical counting methods.
- Johnson, R. and Pitchumani, R. 2008. Active control of reactive resin flow in a vacuum assisted resin transfer molding (VARTM) process. *Journal of composite materials*, 42 (12), 1205-1229.
- Judd, N. C. 1978. Voids and their effects on the mechanical properties of composites--an appraisal.
- Kak, A. C. and Slaney, M. 1988. *Principles of computerized tomographic imaging*, Siam.
- Kang, M. K., Jung, J. J. and Lee, W. I. 2000. Analysis of resin transfer moulding process with controlled multiple gates resin injection. *Composites Part A: Applied Science and Manufacturing*, 31 (5), 407-422.
- Kas, Y. O. and Kaynak, C. 2005. Ultrasonic (C-scan) and microscopic evaluation of resin transfer molded epoxy composite plates. *Polymer Testing*, 24 (1), 114-120.
- Kastner, J., Plank, B., Salaberger, D. and Sekelja, J. Defect and porosity determination of fibre reinforced polymers by X-ray computed tomography. 2nd International Symposium on NDT in Aerospace, 2010. 1-12.
- Ketcham, R. A. and Carlson, W. D. 2001. Acquisition, optimization and interpretation of X-ray computed tomographic imagery: applications to the geosciences. *Computers & Geosciences*, 27 (4), 381-400.
- Khattab, A. 2006. Exploratory development of VARIM process for manufacturing high

temperature polymer matrix composites. *2005 Freely available dissertations (MU)*.

Kikuchi, A., Higuerey, E. and Coulter, J. 1995. An experimental investigation of resin flow sensing during molding processes. *Journal of engineering materials and technology*, 117 (1), 86-93.

Koefoed, M. 2003. *Modeling and simulation of the VARTM Process for Wind Turbine Blades*.

Kosaka, T., Kurimoto, H., Osaka, K., Nakai, A., Osada, T., Hamada, H. and Fukuda, T. 2004. Strain monitoring of braided composites by using embedded fiber-optic strain sensors. *Advanced Composite Materials*, 13 (3-4), 157-170.

Kuentzer, N., Simacek, P., Advani, S. G. and Walsh, S. 2007. Correlation of void distribution to VARTM manufacturing techniques. *Composites Part A: applied science and manufacturing*, 38 (3), 802-813.

Lambert, J., Chambers, A., Sinclair, I. and Spearing, S. 2012. 3D damage characterisation and the role of voids in the fatigue of wind turbine blade materials. *Composites Science and Technology*, 72 (2), 337-343.

Landis, E. N. and Keane, D. T. 2010. X-ray microtomography. *Materials characterization*, 61 (12), 1305-1316.

Leclerc, J. S. and Ruiz, E. 2008. Porosity reduction using optimized flow velocity in Resin Transfer Molding. *Composites Part A: Applied Science and Manufacturing*, 39 (12), 1859-1868.

Leonard, S. 2008. The crossover from RTM to resin infusion. *Reinforced Plastics*, 52 (10), 28-29.

Little, J., Yuan, X. and Jones, M. Voids characterisation in carbon fibre/epoxy composite laminates. 18th International conference on composite materials, Edinburgh, Scotland, 2009.

Long, A. C. 2005. *Design and manufacture of textile composites*, Elsevier.

Martin-Herrero, J. and Germain, C. 2007. Microstructure reconstruction of fibrous C/C composites from X-ray microtomography. *Carbon*, 45 (6), 1242-1253.

Moffat, A., Wright, P., Buffière, J.-Y., Sinclair, I. and Spearing, S. M. 2008. Micromechanisms of damage in 0 splits in a [90/0] s composite material using synchrotron radiation computed tomography. *Scripta Materialia*, 59 (10), 1043-1046.

Mouritz, A. 2012. *Introduction to aerospace materials*, Elsevier.

- Nesterets, Y. I. and Gureyev, T. High-performance tomographic reconstruction using graphics processing units. Proc. 18th World IMACS/MODSIM Congress Modeling and Simulation (MODSIM'08), 2009.
- NFT 57 109:1979 Textile Glass Reinforced Plastics - Determination Of The Proportion Of Voids By The Statistical Count Method.
- Nikishkov, Y., Airoidi, L. and Makeev, A. 2013. Measurement of voids in composites by X-ray Computed Tomography. *Composites Science and Technology*, 89, 89-97.
- Olster, E. F. 1972. Effect of voids on graphite fiber reinforced composites. DTIC Document.
- Pan, X., Sidky, E. Y. and Vannier, M. 2009. Why do commercial CT scanners still employ traditional, filtered back-projection for image reconstruction? *Inverse problems*, 25 (12), 123009.
- Patel, N. and Lee, L. J. 1996. Modeling of void formation and removal in liquid composite molding. Part II: Model development and implementation. *Polymer Composites*, 17 (1), 104-114.
- Radon, J. 1917. On determination of functions by their integral values along certain multiplicities. *Ber. der Sachische Akademie der Wissenschaften Leipzig,(Germany)*, 69, 262-277.
- Ragondet, A. 2005. *Experimental characterisation of the vacuum infusion process*. University of Nottingham.
- Reh, A., Plank, B., Kastner, J., Gröller, E. and Heinzl, C. Porosity Maps–Interactive Exploration and Visual Analysis of Porosity in Carbon Fiber Reinforced Polymers. Computer Graphics Forum, 2012. Blackwell Publishing Ltd, 1185-1194.
- Rudd, C., Long, A., Kendall, K. and Mangin, C. 1997. *Liquid moulding technologies*, Woodhead, Cambridge.
- Saidpour, S. H. 1991. *The effect of fibre/matrix interfacial interactions on the mechanical properties of unidirectional E-glass reinforced vinyl ester composites*. © Seyed Hossein Saidpour.
- Schell, J., Siegrist, M. and Ermanni, P. 2007. Experimental determination of the transversal and longitudinal fibre bundle permeability. *Applied Composite Materials*, 14 (2), 117-128.
- Shepp, L. and Stein, J. 1977. Simulated reconstruction artifacts in computerized X-ray tomography. *Reconstruction Tomography in Diagnostic Radiology and Nuclear Medicine*, 33-48.
- Shim, S. B., Ahn, K., Seferis, J. C., Berg, A. J. and Hudson, W. 1994. Flow and void

- characterization of stitched structural composites using resin film infusion process (RFIP). *Polymer composites*, 15 (6), 453-463.
- Stock, S. 1999. X-ray microtomography of materials. *International Materials Reviews*, 44 (4), 141-164.
- Stone, D. and Clarke, B. 1975. Ultrasonic attenuation as a measure of void content in carbon-fibre reinforced plastics. *Non-Destructive Testing*, 8 (3), 137-145.
- Stover, D. 1990. Resin-transfer molding for advanced composites. *Advanced Composites*, 5 (2), 60.
- Streeter, M., Blake, J., Quinn, S., Mavrogordato, M. and Spooner, J. 2007. Liquid Composite Moulding Flow Front Characterisation by Micro-CT.
- Taina, I., Heck, R. and Elliot, T. 2008. Application of X-ray computed tomography to soil science: A literature review. *Canadian Journal of Soil Science*, 88 (1), 1-19.
- Tiseanu, I., Tsitrone, E., Kreter, A., Craciunescu, T., Loarer, T., Pégourié B. and Dittmar, T. 2011. X-ray micro-tomography studies on carbon based composite materials for porosity network characterization. *Fusion Engineering and Design*, 86 (9), 1646-1651.
- Tzetzis, D. and Hogg, P. 2008. Experimental and finite element analysis on the performance of vacuum-assisted resin infused single scarf repairs. *Materials & Design*, 29 (2), 436-449.
- Vila, J., González, C. and LLorca, J. 2014. A level set approach for the analysis of flow and compaction during resin infusion in composite materials. *Composites Part A: Applied Science and Manufacturing*, 67, 299-307.
- Weber, E., Fernandez, M., Wapner, P. and Hoffman, W. 2010. Comparison of X-ray micro-tomography measurements of densities and porosity principally to values measured by mercury porosimetry for carbon-carbon composites. *Carbon*, 48 (8), 2151-2158.
- Wright, P., Fu, X., Sinclair, I. and Spearing, S. 2008. Ultra High Resolution Computed Tomography of Damage in Notched Carbon Fiber—Epoxy Composites. *Journal of Composite Materials*, 42 (19), 1993-2002.

Appendix

MATLAB codes for imaging process as follows:

Find local max

```
function [max1, max2, max3] = find_local_max(blockid)
max_proj1 = zeros(1,9);
```

```
max_proj2 = zeros(1,9);
max_proj3 = zeros(1,9);
```

```
for numid = 1:9
```

```
    filepath = 'G:\Yuan CHAI\Mat\';
    filename = strcat(filepath, 'Result\');
    filename = strcat(filename, sprintf('S%iNo%i-Ro.result.mat', blockid, numid));
```

```
%    fprintf('processing file = %s\n', filename);
    load(filename);
```

```
    max_proj1(numid) = max(max(proj1));
    max_proj2(numid) = max(max(proj2));
    max_proj3(numid) = max(max(proj3));
```

```
    out_max_file = fopen('data_max_file.csv', 'a+');
    fprintf(out_max_file, '%s, yz_max=%i, xz_max=%i, xy_max=%i\n', filename,
max_proj1(numid), max_proj2(numid), max_proj3(numid));
    fclose(out_max_file);
```

```
end
```

```
max1 = max(max_proj1(:));
```

```
max2 = max(max_proj2(:));
```

```
max3 = max(max_proj3(:));
```

```
out_max_file = fopen('data_max_file.csv', 'a+');
```

```
fprintf(out_max_file, 'S%i-Ro.result.mat, yz_max=%i, xz_max=%i, xy_max=%i\n',
blockid, max1, max2, max3);
```

```
fclose(out_max_file);
```

```
end
```

Edit colourmap

```
function [new_colormap] = edit_colormap()
```

```
clolor0 = [ 0 0 0.5625]; % dark blue jet(1,:)
color1 = [ 0 0 1.0000]; %jet(8,:)
color2 = [ 0 1.0000 1.0000]; %jet(24,:)
```

```

color3 = [1.0000 1.0000 0.0000]; %jet(40,:)
color4 = [1.0000 0.0000 0.0000]; %jet(56,:)
color5 = [0.5000 0 0]; % red %jet(64,:)
color_r = [color0(1) color1(1) color2(1) color3(1) color4(1) color5(1)];
color_g = [color0(2) color1(2) color2(2) color3(2) color4(2) color5(2)];
color_b = [color0(3) color1(3) color2(3) color3(3) color4(3) color5(3)];

loc = [1, 3, 6, 9, 14.5, 64]; % do not modify 1 and 64th row of jet colormap
% loc = [1, 8, 24, 40, 56, 64]; % as default
new_colormap = zeros(64,3);

for i = 1:length(loc)-1
    x = [loc(i), loc(i+1)];

    y_r = [color_r(i), color_r(i+1)];
    y_g = [color_g(i), color_g(i+1)];
    y_b = [color_b(i), color_b(i+1)];

    r = interp1(x,y_r, x(1):x(2));
    g = interp1(x,y_g, x(1):x(2));
    b = interp1(x,y_b, x(1):x(2));
    new_colormap(x(1):x(2), 1) = r;
    new_colormap(x(1):x(2), 2) = g;
    new_colormap(x(1):x(2), 3) = b;
end
end

```

Figures

```

d1 = zeros(9,1)
d2 = zeros(9,1)
d3 = zeros(9,1)

for i = 9:9
    [d1(i,1), d2(i,1), d3(i,1)] = find_local_max(i);
end

max1 = max(d1(:))
max2 = max(d2(:))
max3 = max(d3(:))

for i = 9:9
    for j = 1:9

```

```
        blockid = i;  
        numid = j;  
  
        make_individual_figure(blockid, numid, max1, max2, max3);  
    end  
end
```